Multi-responsive calixarene hosts for the detection of drug molecules

by

Juan Pablo Diaz Duran
B.Sc., Universidad de los Andes, 2019

A Thesis Submitted in Partial Fulfillment of the
Requirements for the Degree of

MASTER OF SCIENCE

in the Department of Chemistry

University of Victoria

Multi-responsive calixarene hosts for the detection of drug molecules

by

Juan Pablo Diaz Duran

B.Sc., Universidad de los Andes, 2019

Supervisory Committee

Dr. Fraser Hof, Department of Chemistry

Supervisor

Dr. David Leitch, Department of Chemistry

Departmental Member

Abstract

The field of host-guest systems is advancing toward a wide variety of biologically relevant applications such as drug delivery, encapsulating agents, sensing target molecules of interest, and acting as therapeutics themselves. Calixarenes are a family of macrocyclic hosts that have been able to fill many of these roles, including novel systems that can act as therapeutic drug reversal agents and powerful chemosensors. In this work we present a new series of Stilbene-calix[4]arene (StiCx) molecules that can act as fluorescent sensors for small cationic drug molecules. The reaction by which these are constructed was optimized to synthesize a small library of compounds, by introducing a phenylacetylene "arm" with different substituents onto the calixarene scaffold, followed by *in situ* semi-reduction to obtain the corresponding stilbene. We also studied the ability of these molecules to bind and detect small drug molecules, with detection based on the change of fluorescent intensity of the host upon binding. We find that the new StiCx system can have either a turn-on or turn-off response depending on the identity of the target, which has the advantage of giving information-rich outputs of a mixture. This system is also capable of differentiating different analytes based on the fluorescence response using multivariate statistical treatment of the data. The mechanisms of guest binding and sensing by StiCx sensors were studied using different NMR and optical spectroscopy techniques. This work provides novel chemo-sensors for future use in drug detection, as well as providing insight into their mechanisms of action.

Table of Contents

List of Figures

Supporting information

List of Schemes

List of Tables

Supporting Information

List of abbreviations

DNA - Deoxyribonucleic acid

RNA - Ribonucleic acid

H-bonding - Hydrogen bonding

IDA - Indicator Displacement Assay

PET - Photoinduced electron Transfer

HOMO - Highest Occupied Molecular Orbital

LUMO - Lowest Unoccupied Molecular Orbital

ICT - Intramolecular Charge Transfer

FRET - Fluorescence Resonance Energy Transfer

GBL - Gamma-butyrolactone

DD - DimerDye

LC - Liquid Chromatography

GC - Gas Chromatography

MS - Mass Spectrometry

NMR - Nuclear Magnetic Resonance

GHB - Gamma-hydroxybutyrate

UV - Ultraviolet

PCA - Principal Component Analysis

MDMA - 3,4-Methylenedioxymethamphetamine

MDA - 3,4-Methylenedioxyamphetamine

AIEE - Aggregation-Induced Emission Enhancement

DPA - Diphenylacetylene

NO - Nitric Oxide

DMC - Dichloromethane

NBS - N-Bromosuccinimide

DMF - Dimethylformamide

HPLC - High Performance Liquid Chromatography

TEA - Triethylamine

HRMS - High Resolution Mass Spectrometry

TFA - Trifluoroacetic Acid

FA - Formic Acid

IR - Infrared

UPLC - Ultra Performance Liquid Chromatography

RFU - Relative Fluorescence Unit

Abs - Absorbance

µM - Micromolar

mM - Millimolar

LOD - Limit of Detection

CAN - Acetonitrile

ATR - Attenuated Total Reflectance

MHz - Megahertz

THF - Tetrahydrofuran

TLC - Thin-Layer Chromatography

FTIR - Fourier-Transform Infrared

DAD - Diode Array Detector

NOESY - Nuclear Overhauser Effect Spectroscopy

NOE - Nuclear Overhauser Effect

DOSY - Diffusion-ordered spectroscopy

COSY - Correlated Spectroscopy

Å - Armstrongs

ESPT - Excited State Proton Transfer

Acknowledgements

This thesis took a lot of time and dedication, and I would like to first thank my supervisor and the person who led me through it all, Dr. Fraser Hof. This wouldn't have been possible without your guidance and support. Also, to my co-supervisor and committee member, Dr. David Leitch, for additional support, guidance and the use of his equipment. I'd also like to thank Dr. Cornelia Bohne, for all the input given during our joint group meetings and help with interpreting fluorescence data.

Aside from the professors, there are a lot of people at UVic who have helped me on a day-to-day basis. I'd like to thank Chris Barr for his infinite patience with all the NMR experiments. Ori Granot and Tyler Trefz for help with UPLC-MS experiments and troubleshooting. And Becky Hof for all the immeasurable amount of work she does to help the lab and solve our problems in moments of crisis. I've also had incredible support from my fellow lab members, I'd like to give special thanks to Allison Selinger and Chelsea Wilson for all the help they've given me throughout the run of this project. To Cleo for all the coffees and Star Wars discussions to have a break from work. To Anton for letting me steal the chair every day. To Michelle for being my one undergrad and giving me the amazing experience of being a mentor. To Zoey for all the tasty pastries. And all current and past members who make this an amazing group to work in. I'd also like to thank Nahia, Jingjun,

Greg and the other members of the Leitch lab for help and support with all synthesis setup and training.

I'd also like to thank the friends from all around the world who I'm lucky to have supporting me through it all. To Santiago and Alejo for all the gaming/series streaming/zoom drinking nights which were of vital importance for the development of the plot. To David and Danna for all the salsa nights and being my home away from home in Victoria. To Eduardo and Rosa for all the board game nights. To Dan and Mario for keeping me fed through my thesis writing. To Miguel, Pedro, Vale and all the other friends back home who I miss every day.

And most importantly to my family who are the reason why I'm here in the first place. To my mom for always being there for me and giving me strength to push ahead. To my dad for everything he's given to get to where I am. Thank you to my sister, my aunt and uncles, and my cousins. This would not be possible without all of you, *muchas gracias a todos.*

Chapter 1: Supramolecular systems in water-soluble and biological media

1.1 Basics of supramolecular chemistry

Supramolecular chemistry is defined as a system with a discrete number of molecules or assemblies that interact or are held together reversibly by non-covalent interactions or effects (hydrogen bonding, van der Waals forces, hydrophobicity, etc.).[1] At a higher level, this concept has given rise to important advances in self-assembling systems, smart materials and molecular machinery. Taking inspiration from nature, this field of study is based upon the non-covalent forces that govern and are essential to nearly all biological processes such as enzymatic reactions, protein assemblies and DNA/RNA recognition and translation, giving rise to dynamic systems. The versatile way that these interactions govern so many different processes in nature through reversible interactions, that are also able to identify specific target molecules has put forward the challenge to understand and replicate these systems. The field itself encompasses many different concepts and applications, such as smart materials for biomimetics,[2] molecular machinery through interlocked molecules,[3] and drug delivery agents in medicinal and chemistry and chemical biology,[4] and the list goes on to nanoparticles, electronic devices, catalysts, and so on. The variety in structure and function has created a big playground from which to explore this branch of chemistry.

Like with biomolecules, 3-dimensional structure plays an important part in supramolecular chemistry. Macrocycles are a common theme here because of their structure which forms a cavity within which binding interactions will take place, as depicted in Figure 1.1. And just

like biological assemblies, these also come together through the sum of many reversible noncovalent interactions. Because these interactions are dynamic and reversible, supramolecular chemistry takes advantage of them to create systems that work in real-world complex systems. Some of the main forces that drive these systems are hydrogen bonding, electrostatic interactions, hydrophobic effect, π-π interactions and van der Waals forces[5]. Hydrogen bonding is an interaction between a polarized hydrogen atom and a highly electronegative electron donor and is a very common and crucial binding force in biological assemblies. Electrostatic interactions refer to favourable interaction between oppositely charged ionic species, these can be important if you insert charged groups in your systems. Hydrophobic association (or the hydrophobic effect) is the tendency of nonpolar substances to aggregate in an aqueous media to exclude water molecules, generating an energetically favoured environment as contact with the nonpolar molecules is reduced. Aromatic interactions or "π-π interactions" are the interactions between the π orbitals of a conjugated system that often occur during "π-stacking" between the two molecules. Since many supramolecular systems use aromatic rings, both in their assemblies and the analytes they work with, these interactions provide a significant contribution. Finally, van der Waals forces are the interactions arising between induced dipoles in molecules, which while being the weakest of them all as individual interactions can still provide a significant total driving force for assembly formation. All of these forces are significant, and most systems are designed to use many of them to create strongly bound assemblies. Knowing how to tune and use these binding equilibria makes for an exciting field of possibilities.

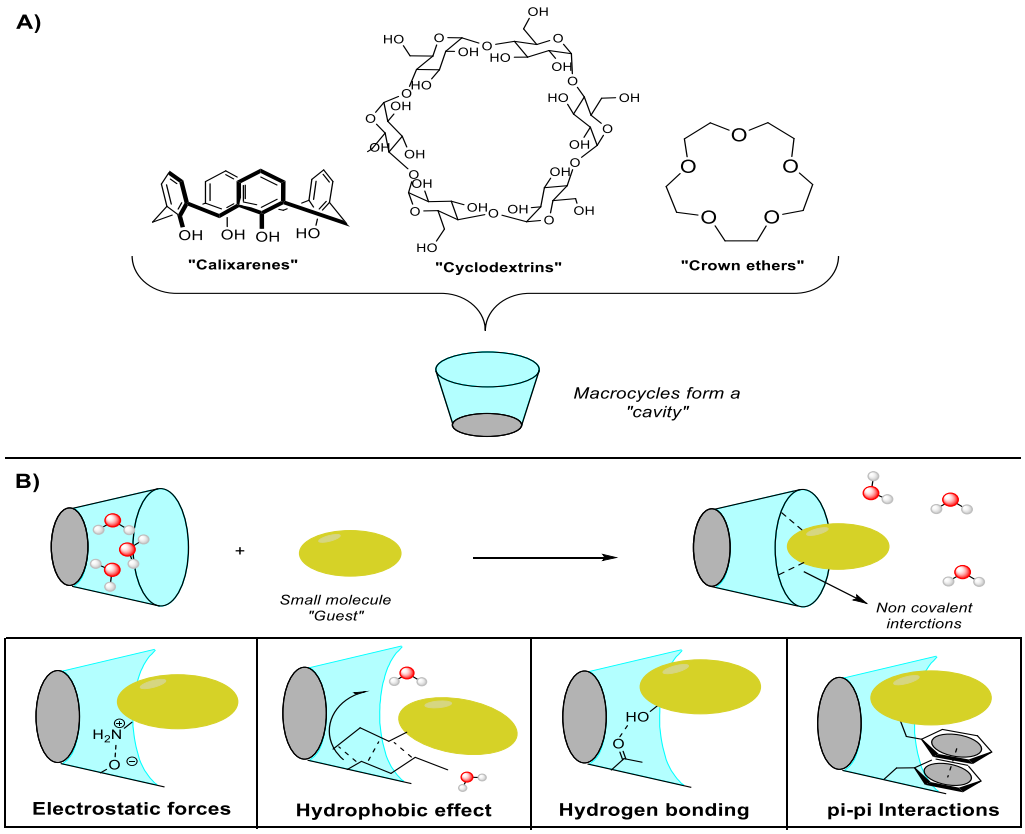

Figure 1.1: A) Examples of supramolecular macrocycles and cartoon representations of the cavity they form. B) Representation of host-guest complexes that form and the main non-covalent interactions responsible for it.

The one area of supramolecular chemistry that will be the focus of this thesis is host-guest chemistry. This consists of a large molecule called the "host" which has a three-dimensional structure with a cavity, called a binding "pocket", which can recognize and bind a smaller "guest" molecule inside the pocket. This binding will be guided by the previously discussed interactions, we can see a representation of them in Figure 1.1. One of the most significant applications, though not by far the only one, is in its use for pharmaceutical research,[6] as these pockets can increase drug stability, improve solubility in biological media, and control release in *in vivo* systems.[7] These pockets can encapsulate many types of different analytes which we can adjust for as the host can be tuned in different ways depending on the

application. The size and shape of the cavity can be changed to recognize specific targets, similar to the “lock-and-key” concept found in enzyme-substrate complexes. The chemical environment and nature of the host can be adjusted so the molecular interactions are different and the strength of binding to the guest can be tuned. Ionic groups are attached to favour electrostatic interactions, aromatic rings are used to favour π-stacking with analytes, and electronegative atoms can form H-bonding with polarized hydrogen atoms. Additionally, binding pockets tend to have a hydrophobic environment, so organic molecules can easily fit, and the hydrophobic effect will favour them being inside the cavity if we are working in an aqueous media.

The families of host molecules that exist are vast, and there are too many to discuss them all here. However, we will narrow down our focus to the most common host molecules with a container or cage shape in their structure. Normally these molecules consist of cyclic structures of a repeating unit to form a macrocyclic oligomer. An example of this is the Cucurbit[n]uril family, which consists of a macrocycle formed with ‘n’ repeating units of glycoluril monomers, creating a hydrophobic host cavity. Some of its main applications have been in binding positively charged organic molecules, as the dipolar carbonyls lining this host cavity participate in strong ion-dipole interactions. One drawback for many cucurbiturils has been low water solubility which limits usefulness for biologically compatible systems.[8] Another very popular family with many biomedical applications is cyclodextrins. These are macrocycles composed of oligosaccharide rings, which can contain 6, 7 or 8 repeating units in their structure. These compounds form a cavity with a cone shape, which acts as the

binding pocket. Though their pocket is somewhat less hydrophobic than other hosts, the formation of host-guest complexes with cyclodextrins is favourable and still has a significant contribution from hydrophobicity. This arises because water molecules in the hydrophobic cavity are displaced as the guest is inserted.[9] Calixarenes are another important family that will be discussed later as they are the main focus of this study. While they are some of the most studied, other structurally similar families like pillararenes and resorcinarenes also exist. These examples showcase the wide field that exists from the different types of cavitand molecules, how chemical interactions and the chemical groups involved can have an important effect on its applications, and how much these can still be explored.

1.2 Host-Guest systems as fluorescent sensors

One of the many applications of host-guest systems is as sensors. The concept of molecular sensors goes as back as 1967,[10] when it was defined as a molecular structure that interacts with an analyte generating a measurable response. Since then, a wide variety of different classes and types of sensor-type molecules exist and have been used in the detection of many kinds of analytes of interest, from contaminants and pollutants in environmental samples to biomolecules of interest in living systems.[11] Different mechanisms for different sensors exist, however, our focus and interest will be in fluorescent sensors that that can bind analytes through host-guest chemistry. These systems allow for the design of sensors that can report on the presence of an analyte of interest.

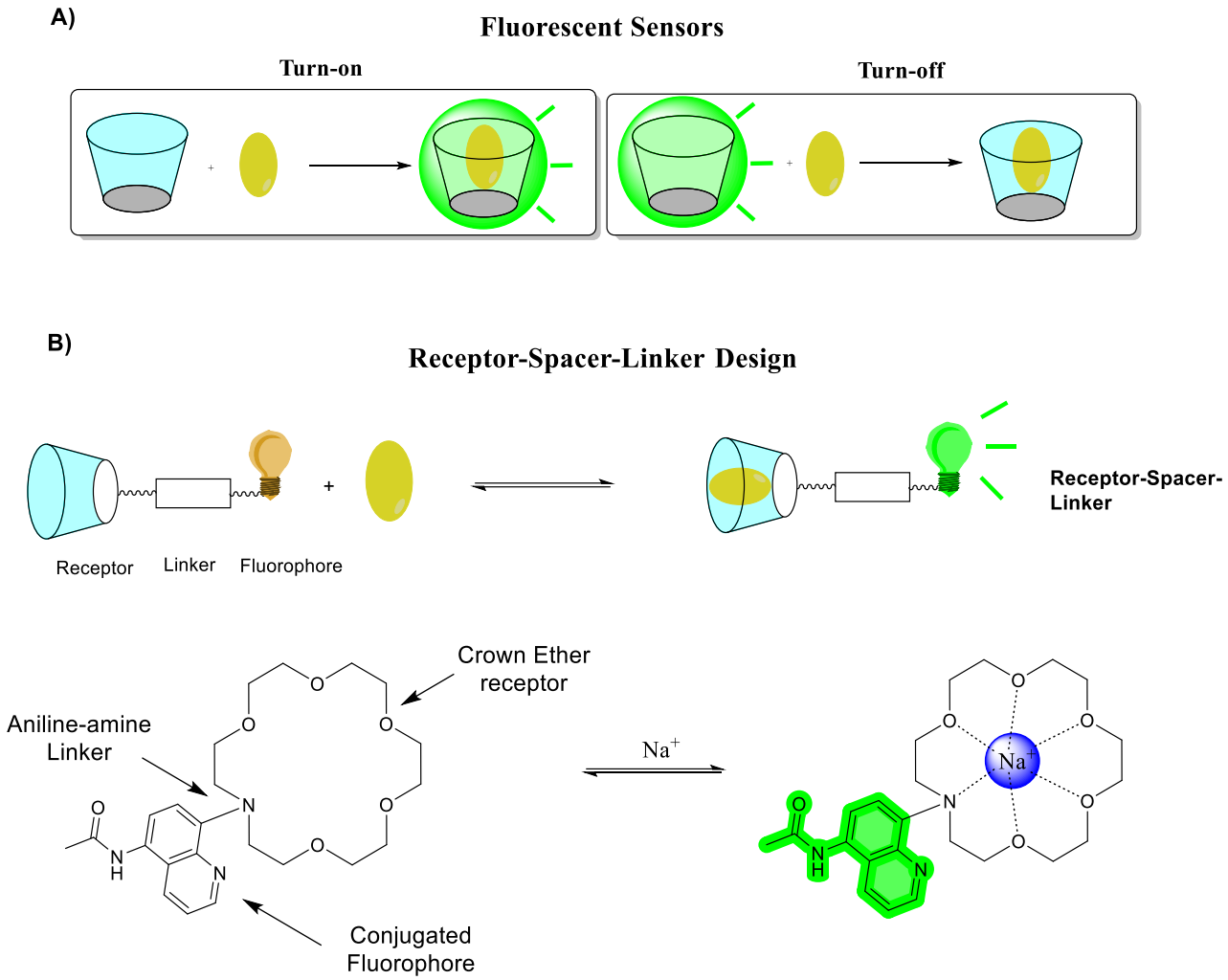

Figure 1.2: A) Depiction of a turn-on and turn-off fluorescence sensor system. B) Depiction of a receptor-spacer-linker design along with a structural example with a crown ether sensor reported by Tsien.[12]

With the increasing interest in monitoring drug concentrations and related biological analytes, the field of fluorescence reporters as monitoring systems has attracted many design and synthesis efforts. Such sensors must follow certain requirements to work properly. First, their brightness and absorbance properties must be high enough to measure distinctively. Fluorescence is an attractive mechanism for this as it is very sensitive and has a high signal-to-noise ratio, meaning there will be little interference from the matrix. If the sensor is to be

used in a biologically compatible system, then solubility in water and in salty solutions is also an important key factor. Many modern sensors are appended with polar or hydrophilic groups which make them water soluble, and additional modifications can be made to allow for the permeation of cell membranes. The type of fluorescence can also be tuned according to the design with sensors that exist with a "turn-on" or "turn-off" response, as shown in Figure 1.2a.

There are many ways to design host-type molecules that act as fluorescent sensors for their guests. Most follow a design that consists of three parts that form the structure of the host: a fluorophore, a spacer and a receptor. The receptor is a structural moiety that can recognize and bind the target guest or analyte, meaning this is the sub-structure that has an affinity for the target of interest. This can be the most variable moiety depending on the target in mind and can range from structures with a particular affinity for a given target, or macrocycles with a cavity that can encapsulate the target. The spacer (or "linker") connects the fluorophore and the receptor allowing the change in fluorescence to be directly affected by binding and formation of a host-guest complex. This linker is normally a permanent bond, but can also be a "cleavable" linker, that can be degraded in certain biological conditions when the application requires it. An example of this is a disulfide bond linker, where the disulfide bond can be cleaved by cellular thiols overexpressed in cancer cells, making such linkers attractive in theranostics research.[13] Other commonly used cleavable groups include hydrazones,[14] azo compounds,[15] esters,[16] among others.[17,18] Finally, the fluorophore (or reporter) is the part of the molecule that is capable of emitting light upon excitation and whose fluorescence changes upon binding so that we can detect the presence of the analyte.

Going back to a familiar structure, crown ether sensors have been reported that serve as an example to illustrate this concept. Tsien and Minta reported a system with a 1,7-diaza-4,10,13-trioxacyclopentadecane receptor, linked by its nitrogen to a conjugated fluorophore system (Figure 1.2b) which served as a sensor for cytosolic sodium.

Though many types of sensors follow this fluorophore-linker-receptor model, other methods exist to circumvent the challenges involved with their preparation. One of the most prominent linker-free sensing approaches is the Indicator Displacement Assay (IDA) (Figure 1.3). In this method, the receptor is complexed with a dye in a way such that it has a characteristic fluorescence emission, and in the presence of a guest there is a displacement of the dye as the host-guest complex formation causes the dye to be released resulting in the fluorescence changing in intensity or wavelength. The direct proximity of the dye and the host pocket means that a significant change in photophysical properties is often achieved upon dye release. An example illustrating this can be seen in Figure 1.3, where calix[4]pyrroles can be used with a nitrophenolate dye for halide ion sensing.[19] One of the drawbacks of this method, however, is that it depends strongly on the binding constants of two competing host-guest complexes, meaning the affinity for the dye must be low enough so it is easily displaced by the concentration of guests that are present in any given sample. This can sometimes lead both to low sensitivity and signal-to-noise ratios, and low specificity as other interferants could cause displacement and give false positives. Some novel approaches have tried to solve this in the form of intramolecular IDAs,[20] linking the dye to the receptor by a flexible tether that still allows for the dye to bind inside of the binding pocket. The concept was proved in

its use as a sensor for phosphate-type anions in herbicides and has now advanced to use in complex systems. An example of this is the family of Cucurbit[7]uril-based Intramolecular IDAs developed by Biedermann for drug detection and small-molecule sensing in biological systems.[21–23] However, this approach brings back the synthetic complexity of a dye-linker-receptor approach and it doesn't necessarily solve selectivity issues which in other studies have also persisted from this method.[24]

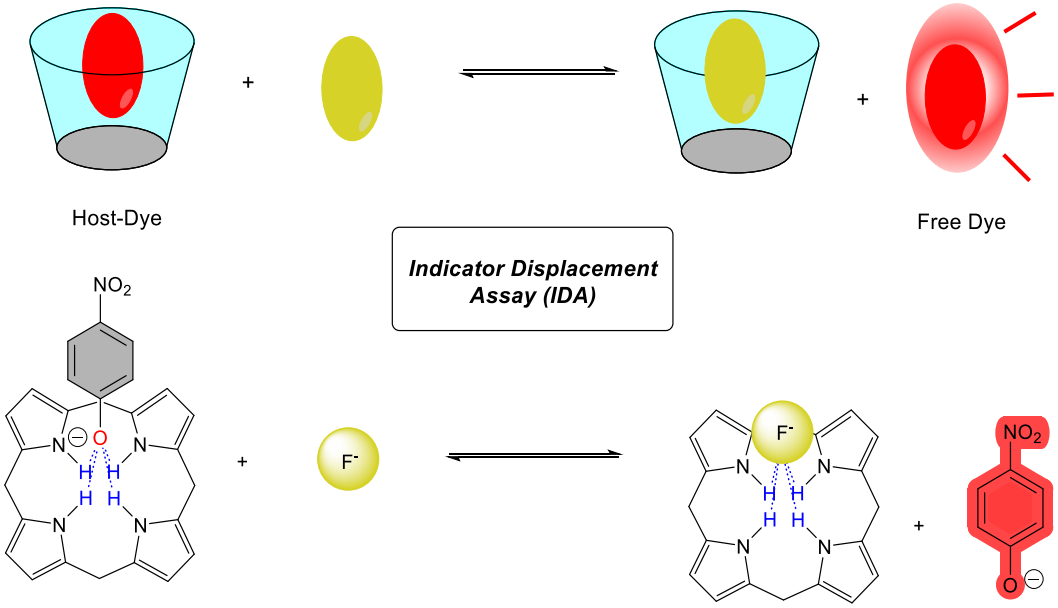

Figure 1.3: Fluorescence reporter structure moieties showing different approaches to the use of fluorescence with the use of a host-guest system.

Alternatively, we can have systems with a fluorescent moiety that is directly integrated into the binding pocket, as illustrated in Figure 1.4. This means host systems where the receptor is also a fluorophore and is directly bonded to the receptor or is embedded into the macrocyclic portion of the host, without any need for a linker unit. A good example is the use of a bis(cyanostyryl)pyrrolic anion receptor, that has a turn-on fluorescence when it binds

halide ions.[25] In this case the fluorescence is caused by the interactions causing a restraint in the torsion angle of the fluorophore, allowing for the turn-on fluorescence. Functionalized resorcin[4]arenes also proved to be useful sensors for the detection of amine and aldehyde vapours;[26] no linker was used and the luminescent properties were attributed to the receptor which in itself showed photophysical activity. Because of the versatility in substituting macrocyclic structures, and the inherent proximity in the binding pocket as the receptor, it is no surprise that many in this family of compounds find themselves following this route. Functionalized macrocycles are a common theme in the field of luminescent sensors. Functionalized cyclodextrins with an attached fluorophore unit proved to be useful sensors in the detection of a variety of organic analytes (alcohols, pesticides, polychlorinated biphenyls) and were even capable of discriminating between analyte isomers, or closely related analogues.[27] One of the advantages they highlight is the proximity of the fluorophore to the receptor due to being directly bonded to the cavity, and other such modifications can be introduced.

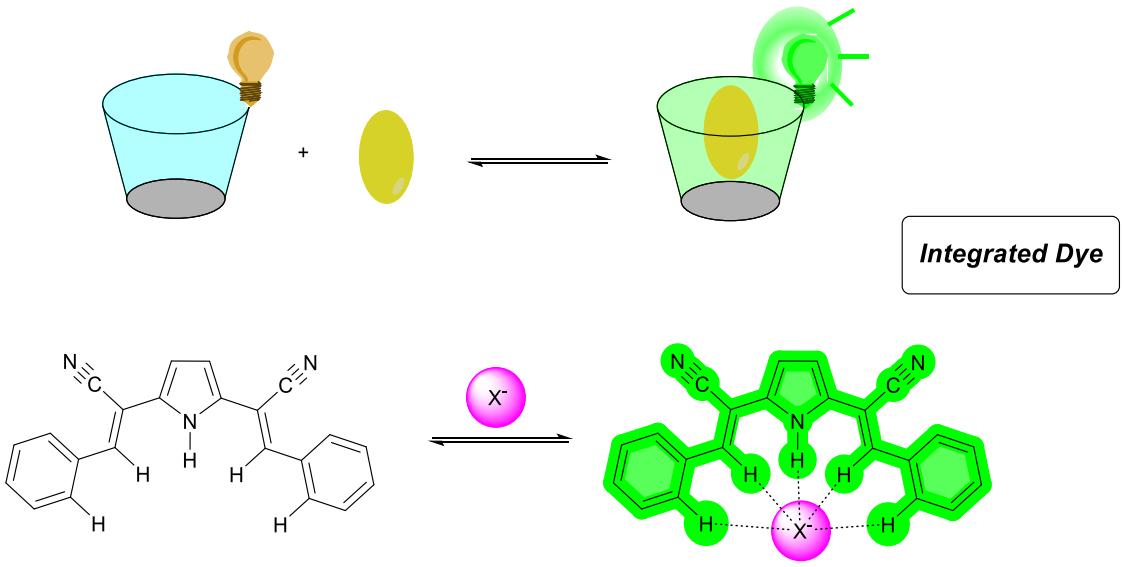

Figure 1.4: Representation of an integrated fluorophore sensor. An example of such a system is represented with a bis(cyanostyryl)pyrrolic anion sensor.

Various kinds of photo physics give rise to useful sensing responses in host-type sensors. The type of fluorescent response we can see can depend on the type of fluorophore we can have, and can either be "turn-on" in which case the fluorescence is enhanced upon binding or "turn-off" in which case the fluorescence is quenched (Figure 1.2). Generally speaking, "turn-on" sensors are preferred over "turn-off" as the latter can give false positives from environmental interference as well as lack of activity for analytes without active chemical sites.[28] This is usually controlled by the type of dye that we have, however, the molecular interactions within the system and with the analyte itself are also features that can determine the type of fluorescence changes that our system will have.

Most fluorescence changes are caused by one of a few different photophysical mechanisms, which have been exploited in different ways. The basis for the fluorophore reporter acting as a sensor is that its π-electron conjugated system changes or is perturbed upon analyte binding, thereby changing its photophysical properties. Turn-off fluorescent sensors commonly rely on mechanisms like photoinduced electron transfer (PET),[29] where the excited-state fluorophore is quenched as there is an electron transfer between the HOMO and LUMO of the dye and the analyte. PET is a type of dynamic quenching, where contact from the collision of the molecules makes the energy transfer possible, but another type of quenching mechanism can be static quenching where the fluorophore and analyte form a non-emissive complex. The two main mechanisms behind most turn-on fluorescent systems are intramolecular charge transfer (ICT) and Förster resonance energy transfer (FRET). ICT is a

widely studied phenomenon[30] and requires the presence of an electron-donor and an acceptor present in a conjugated system creating a polarized environment, which upon excitation or binding will drastically change the polarity of the molecule. The photophysical properties of these systems will be highly sensitive to analyte interactions, as this can change the polarity, the Stokes shift or even lead to quenching. Finally, FRET fluorescence is a phenomenon that relies on proximity between a donor and an acceptor fluorophore.[31] In this case there is a non-radiative energy transfer from an excited-state donor dye to an acceptor dye that occurs through dipole-dipole coupling. This is very commonly used in biological studies using fluorescent proteins, but small-molecule FRET systems also exist. FRET-based sensors can be challenging in their design because they require the synthetic attachment of two dyes on two different molecules or at two different attachment points. But when these conditions are met FRET-based sensors can be very powerful and sensitive tools.

The choice of the fluorophore, and therefore of the fluorescence mechanism that it works with, is an important decision in the overall design of the sensor. Several conjugated dye molecules exist that are commonly used as reporters or labels, and efforts are constantly being made to develop new ones while adding more innovative features. Among them, we find commonly used ones such as fluorescein and BODIPY dyes, which are attractive because of properties like high absorptivity and quantum yields, ideal wavelengths of emission at physiological pH and are easily connected to linkers. Fluorescein, for example, has been used to monitor drug release through a release from a cleavable linker, showing emission only in its free form once the drug is released.[16] BODIPY on the other hand also enjoys ample use

in biomedical applications, but can also work as a sensor for analytes such as illicit date rape drugs, showing an increasing fluorescence response to gamma-Butyrolactone (GBL) in spiked drink samples.[32] These examples are just a few of many that exist. In some such systems, there are shortcomings to this approach since the receptor unit is separated from the fluorophore. Because there is a distance between the dye and the site of binding that we want to measure, the readout is not always that strong or could give false readings from other interference events. An additional shortcoming is the synthesis required to functionalize the host, add a linker, and connect the fluorophore.

1.3 Calix[4]arenes

As we discussed before, macrocycles are a common theme in supramolecular fluorescent sensors, but one family that we haven't touched upon yet and the ones that will be the focus of this project are calixarenes. Calix[n]arenes are cyclic oligomers of "n" phenols linked together by "n" methylene bridges. Calixarenes were first synthesized by the condensation of *p-tert* butylphenol with formaldehyde in 1944.[33] Their name comes from the Greek word *calix* (chalice), in reference to the cavity that is formed by the cyclic tetramer calix[4]arene which was first characterized in detail by Gutsche.[34] Calix[n]arenes can be comprised of a different number of monomer units, but by far the most investigated and the main focus of the project will be calix[4]arenes. Their popularity comes from their ease of synthesis. While other higher order calix[n]arenes can be obtained (n=5, 6, 7,…), calix[4]arenes have the highest yields, are the thermodynamically favoured products during synthesis, and can be readily derivatized.[35] Their structure consists of a wide upper rim and a narrower lower rim,

both of which can be functionalized to control their structure, binding, conformation, shape, and solubility. This gives control over their functions and makes them quite versatile in tuning their physical and chemical properties for a specific goal.

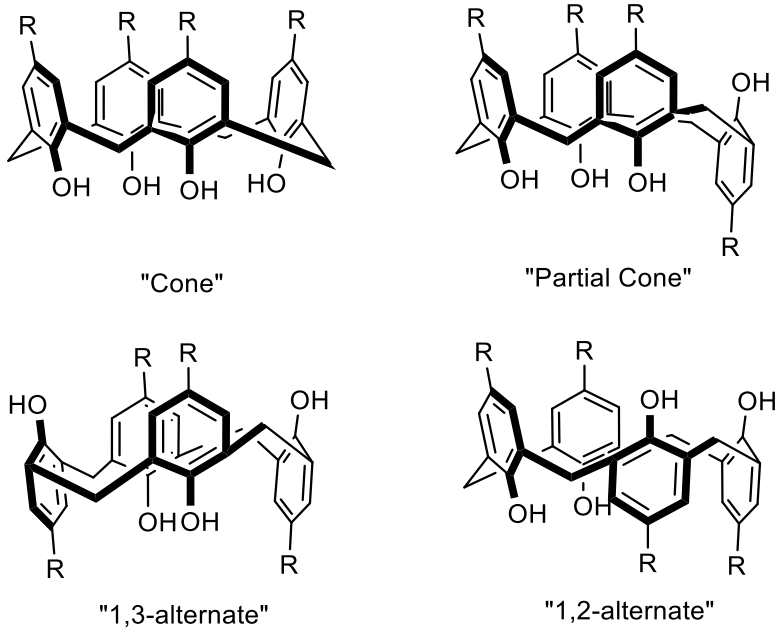

Figure 1.5: Molecular structure of calix[4]arene and its conformational isomers showing the different spatial distributions of the upper and lower rim.

One of the most interesting properties of calix[4]arenes is that they can adopt 4 different conformations as there can be rotation around the methylene bridges reverting the positions of the upper and lower substituents. The 4 possible conformations are shown in Figure 1.5, the “cone”, “partial cone”, “1,2-alternate” and “1,3-alternate. The “cone” conformation is the best suited for guest binding and is also the predominant conformation in solution because the hydroxyl groups of the phenols are attracted to each other through hydrogen bonds.[36] The dynamics of this conformation can change depending on various environmental factors, including the addition of substituents that can hinder conformational changes.[37] Introducing a substituent can cause the cavity to be “immobilized” as the functional groups can create

steric hindrance around the macro-ring inversion. For the most part, these changes in conformation don't affect the binding that we are interested in, and since the "cone" formation is the predominant form we can often ignore the other conformations during analysis. However, this change in conformation can cause peculiar behaviours during characterization, as the symmetry of the molecules can change upon changes in conformation.

Calixarenes have enjoyed great popularity with potential applications such as fluorescent drug sensors, receptors, delivery systems and fluorescent materials.[38] Because of the aromatic rings in the oligomer, the cavity has an electron-rich binding pocket that can bind via π-π interactions and hydrophobic effect. Positively charged targets have a great affinity for this electron-rich environment[39] and so they have been used for binding applications for many cationic targets. One of these examples is their use as sensors for metal ions, with the more predominant ones being Cu^{2+} and Hg^{2+} for their biological relevance.[40–43] Calixarene-based sensors have also been used in the detection of Zinc,[44] Cesium,[45] Iron,[46] Silver,[47] Lead[48] and many others. This variety in applications comes from the many functional derivatives that we create by modifying the host, including groups that encourage incorporation into nanoparticle and polymer systems as well as guest-binding groups and fluorophores.

One of the substituents that has generated a great deal of interest is the sulfonate group. The sulfonate groups give the calixarene several new features and advantages, some of which are illustrated on the *p*-sulfonatocalix[4]arene scaffold in Figure 1.6. First, they add water

solubility which makes them compatible with biological systems and aqueous media. Furthermore, the *in vivo* toxicity of sulfonated calixarenes has been tested and found to be low,[49] and they also have been found not to produce an immune response.[50] Second, they change the electron density of the rings and the ionic environment of the cavity. Because the sulfonate groups and one of the phenol units are deprotonated at physiological pH (7.4), their addition creates an even more electron-rich environment for binding cationic guests, complimenting the hydrophobic effect and π-cation interactions already present in the aromatic-lined cavity with ionic interactions from the anionic sulfonates. This increased affinity for cationic guests in sulfonated calixarenes has attracted much attention to its potential for biological and medicinal applications that include but are not limited to, monitoring enzymatic reactions, drug delivery and drug encapsulation.[51]

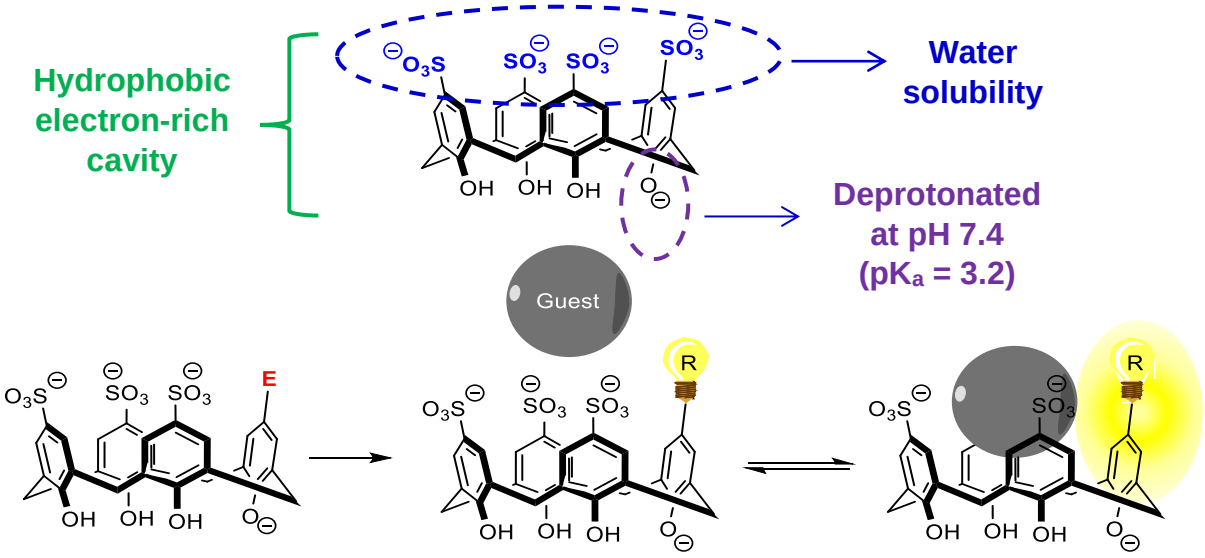

Figure 1.6: Structural representation of sulfonated calix[4]arene in solution with formal charges[52] highlighting some desirable properties and scheme showing fluorescence sensing mechanism as fluorophore groups are attached and guest inserts into the cavity.

As said before, one of the shortcomings of linkers is the distance put between the fluorophore and receptor, which can diminish the output size of the signal change upon binding. Having the fluorophores integrated directly into the binding pocket is an alternative to that approach. One of the most relevant systems that have been developed is a family of sensors called DimerDyes, which are hosts consisting of sulfonatocalix[4]arenes in which one of the four rings is an integral part of the merocyanine dye. In the absence of guests, DimerDyes can dimerize in solution quenching the dye´s fluorescence. As the guest binds into the cavity, it causes this dimer to dissociate and generate a turn-on fluorescence that has proven to be very useful in the detection of drugs in solution, in buffered water, and even in real biological fluids.[53] Through the creation of a small library of DimerDye host molecules, this system has even been expanded to find analogues that can discriminate drugs in a sample. When more than one DimerDye is used to analyze a given sample, the resulting "sensor array" eliminates problems with cross-detection and false positives, as each analyte generates a "fingerprint" of responses from the small array of sensor that can be processed through multivariate statistical analysis. This is a great advantage over previously developed sensors designed specifically for one analyte.

Like many other fluorescent systems, the DimerDye system unfortunately tends to create a single kind of response, which is generally a turn-on fluorescence with very little change in wavelength. This is a relatively information-poor kind of sensing response, especially when the binding of multiple similar analytes with relatively similar affinities and degrees of

response is considered. This lack of specific signal generation from each individual sensor and targeted analyte limits the amount of information generated by these sensors and remains a major drawback. To obtain more capable sensor systems, sensor systems that can generate information-rich outputs while still using a small number of sensors are required. In this context, information-rich means that the optical signals in some way indicate the identity of an analyte, rather than simply turning on or turning off to varying degrees in response to any given analyte.

Design of sensors that meet these criteria is a complex task,[54] and many approaches to this problem have arisen. Most modern sensing approaches can be split into two categories, very specific selective sensing systems that are designed for one particular target, or an array-based selective system like the DimerDyes we discussed. Selective sensors are useful when we wish to get information on a specific analyte, but interference from chemically similar structures in complex systems can easily render them impractical. A more interesting alternative is achieved with sensor systems, often called chemical noses because of the similarity in principle with human noses. Like human olfactory systems, which consist of hundreds of cross-reactive receptors, sensor arrays use many cross-reactive interactions to differentiate and get a unique pattern for any given analyte sample. Drug detection is an application we already discussed, but this approach is widely used in other sensing applications as well, such as sensing of carbohydrates or a family of enzymes using arrays of biomolecules with selective binding to these families, using multiple component analysis to create a "fingerprint" for specific analytes. [55] Because of this level of discrimination, a well-

engineered system can identify analytes in a mixture with a single experiment, creating an information-rich system and becoming a widely used concept for many modern sensors[56–58].

1.4 Use of supramolecular hosts for drug detection

One of the target applications of this work is the use of supramolecular calix[4]arene hosts as fluorescent drug sensors. The use of illicit drugs is a very serious social issue affecting well-being and mental health, creating addiction and eventually leading to health problems due to overconsumption. In Canada, the number of opioid-related deaths has increased dramatically in the last years,[59] leading to a health crisis as many people die from overdose from both legal and illegal opioid consumption. These often centre around the use of powerful opioids, such as fentanyl, where just a few milligrams of substance are enough to be lethal.

While many deaths are caused by overdose, many are also caused by the combination of substances found in street drugs. Opioids are the major contributor to the drug overdose crisis, but their use in a mixture without precise knowledge by the user is what makes them so dangerous. Fentanyl is widespread in the Canadian illicit drug supply[59], so an important social issue lies in giving users information about the presence, identity and amounts of other drugs that would make dangerous mixtures. Various combinations of opioids with benzodiazepines are examples of such dangerous mixtures.[60] Another example of a potentially harmful drug combination that is typically unknown to users is the presence of the anti-worm drug levamisole in cocaine.[61] For another example, even the combined use of alcohol and cocaine can lower the threshold of life-threatening concentrations when

compared to the use of cocaine alone.[62] This is because the mixed use of cocaine and ethanol leads to the formation of cocaethylene, a toxic metabolite that has even greater potency than cocaine. Another concern is the occurrence of "spiked drink" cases that involve drugs being administered without the knowledge of the consumer, causing scenarios where a person is unknowingly drugged to make more susceptible to situations of robbery or sexual assault. It is because of this that a great effort needs to be put into creating efficient ways to control and test for these illegal substances in samples that may otherwise be unsafe to consume.

By far the most commonly used method for the detection of drug samples and their respective analytes is Liquid Chromatography Mass Spectrometry (LCMS), a robust and sensitive technique which allows for the detection of even trace amounts of analyte in a highly complex matrix.[63] Other methodologies have also been used to detect drug consumption from biological samples such as the use of NMR for analysis of urine samples[64] or Raman spectroscopy in saliva samples.[65] While these methods are useful in diagnostic and therapeutic applications, the downside is that they need highly specialized equipment, long sample preparations and trained personnel to use.

To make drug testing more accessible, chemical sensors can serve as an alternative as they can provide quick on-site detection and real-time responses. Test strips that detect the presence of fentanyl as a yes/no result are widely available. These strips work on lateral flow assays, which are antibody-based methods commonly used to test for samples in biological fluids. These have good cutoff points of 10-20 ng/mL[66] for fentanyl and offer user-friendly

ways to test drug samples. However, the use of fentanyl test strips has not achieved the expected safety improvements in the Canadian public health setting because >90% of street drug samples contain at least some trace of fentanyl as reported by the Hore group,[67] and the test strips are unable to report on the amount of fentanyl or on the presence of other components that would make the drug sample more dangerous.

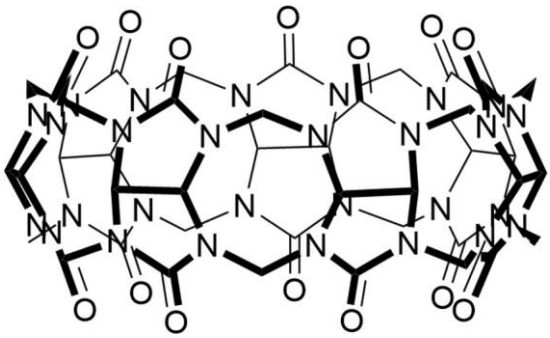

Figure 1.7: Chemical structure of Cucurbit[7]uril.[68]

The use of fluorescent supramolecular drug sensors shows the potential to become a new tool in the field of drug sensing. This approach shows several advantages when combined with sensor array analysis, however, there is still a lot of unexplored territory as there is a large of number of dyes, but very few that use host-guest systems.[69] As mentioned before, the versatility of fluorescence makes it a very attractive technique, because even though it is not as sensitive as GC/MS methods it is more readily available. It is no surprise then, that most point-of-care sensors rely on fluorogenic and colorimetric assays as an easier and less costly alternative. From the selection of macrocyclic fluorescent sensors, we have two main families that have been thoroughly studied in their applications for supramolecular drug sensing; cucurbit[n]urils and calix[n]arenes.

As a predominant family of supramolecular macrocycles, it's not unexpected to find that Cucurbit[n]urils (Figure 1.7) have found applications in drug sensing. The Biedermann group has done extensive research into developing chemosensors that can detect a wide variety of illicit drugs in biofluids.[21,70] They have also developed an electrochemical IDA which takes a step back from fluorescence, and instead functions with an electrochemical indicator, which proved to be very useful in the detection of muscle relaxants in urine samples.[23] Isaacs on the other hand, has used both traditional cyclic Cucurbit[n]urils and acyclic Cucurbit[n]uril analogues to test urine samples for antihistamines and analgesic overdoses, as well as opiates and their metabolites.[71,72] It should be noted that they also used multiple component analysis with three sensors to differentiate between analytes, yet again showing the power of this tool. Another example with a real-life application in mind for these macrocycles was done for the detection of GHB (Gamma-hydroxybutyrate). In this case, dyes have been developed for the detection of this drug in spiked drinks with a fluorescence change that can be seen even by the eye under a UV light.[73] Some of the supramolecular approaches that have been developed include the use of cucurbiturils complexed with a fluorescent dye for the encapsulation of GHB.[74] Many of these studies however do not include some of the more predominant drugs that have taken over the current overdose crisis.

The other family that has tacked the challenge in supramolecular drug sensors is the family that will be the main body of this work: Calix[n]arenes. The DimerDye family of compounds we discussed was first developed as a salt-tolerant alternative to IDA approaches or other hosts like Cucurbit[n]urils.[75] Although these systems show good bindings they are easily

affected by the presence of ions like Cl^- and Na^+ which can drastically change their binding constants.[76] They were found to be excellent hosts in salt-compatible media and were used as sensors for enzyme reaction monitoring. The compounds mentioned consist of a merocyanine arm directly hooked into one of the aromatic rings of the cavity. Upon dimerizing, the positively charged pyridinium ring has a favourable interaction with the anionic sulfonate groups of another calixarene. In Figure 1.8A we can see an example of dimerization where DimerDye DD1 can exist in an equilibrium with the monomeric state where primarily we will have the dimer complex. This equilibrium is reversible and can be perturbed by the addition of a competitive guest. The fluorescence is quenched when the dyes are complexed together, and dissociation of this dimer generates a turn-on fluorescent response when a guest enters the cavity. These systems already have shown very interesting sensing mechanics and good binding affinity for drugs such as opioids, amphetamines, and tropane alkaloids.[53,77] When used in combination with a sensor array, they were very effective in discriminating between closely related drug samples and their primary metabolites. The way this has been done is through the use of PCA (Principal Component Analysis) and with an array of 5 DimerDyes sensors, differentiation could be made between methamphetamine and its metabolite amphetamine, and MDMA from MDA (Figure 1.8B).

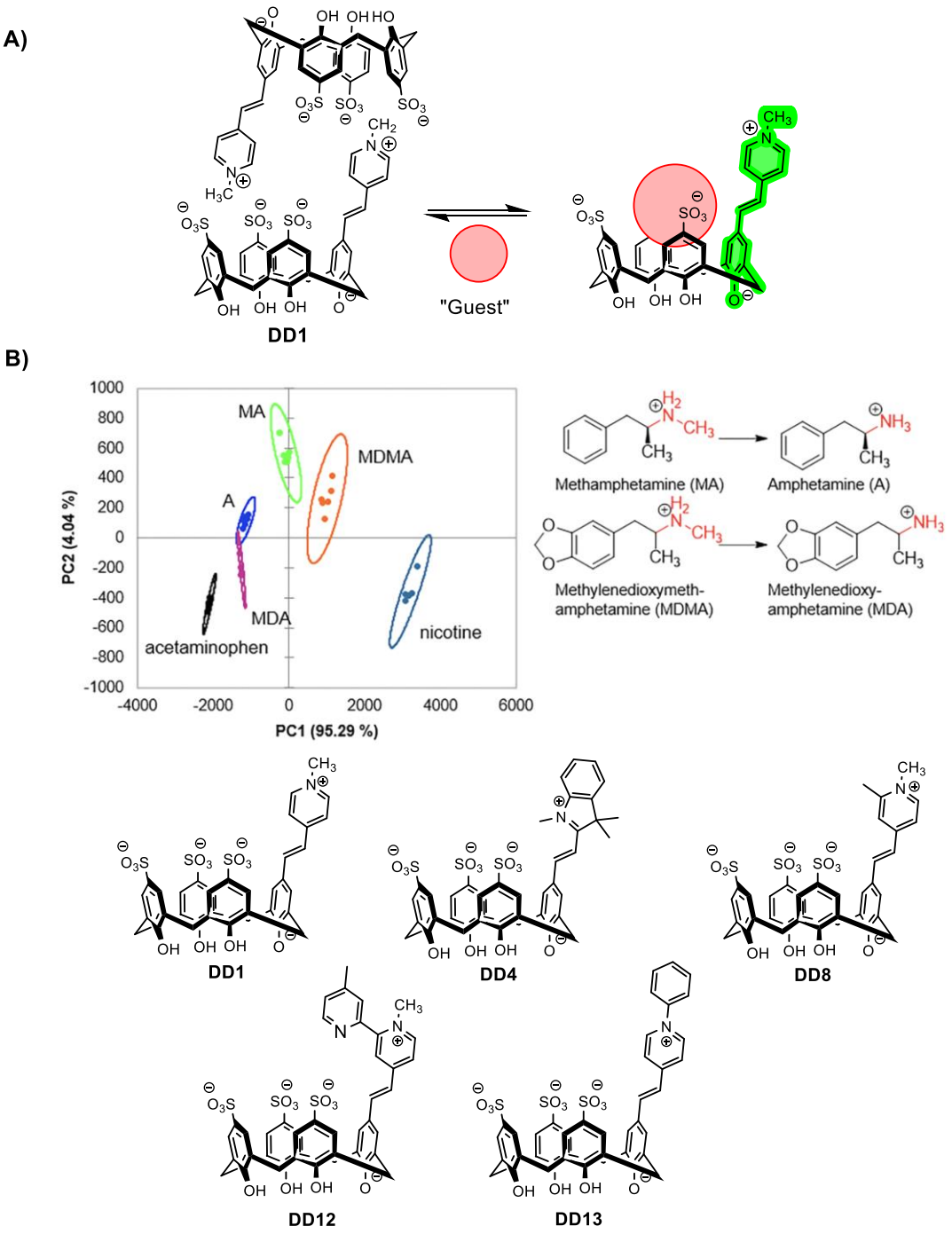

Figure 1.8: Chemical structure for DD1 (A) and B) Results for sensor array discrimination of different amphetamine analytes.[53]

As we mentioned the backbone of the conjugated system is made up of a merocyanine dye, which is a well-established dye in the literature with unique properties such as its change in

absorbance under different solvents.[78] However, one of the drawbacks is that to hook that merocyanine into the host a reactive handle is needed. For previous work, a condensation reaction from an aldehyde handle was used, but the synthesis of the aldehyde itself requires long synthesis routes (6-step synthesis) to obtain (Figure 1.9A) and because of this they are difficult to obtain in large quantities. The system is also limited in that we can only have a single type of fluorescent response, which is a turn-on for the DimerDye separation. This is illustrated in Figure 1.8B in which the response of the sensor will always be a turn-on regardless of the analyte. There will be slight differences in the intensity of those fluorescence changes, but they will be small which is why statistical methods like PCA are needed to help differentiate them. Moreover, changes in concentration can make the signal of an analyte with a weaker response overlap with a less concentrated analyte with a stronger response. This also means that while we can detect certain analytes, we can't get more details about their identities, as all responses are similar. So we are still limited in what information this system gives us, and fluorophores that have more distinct responses (color change, shifts in emission or turn-off responses) would be highly desirable.

One thing we can see is that the merocyanine group is very closely related to a stilbene group, which is a dye with very interesting optical properties.[79] This family of compounds has applications in the detection of nitrophenol in explosives,[80] metal ions[81,82] and even to quantify target proteins in biological systems.[83] An example of the structure and application can be seen in Figure 1.10 where a dye was synthesized with Aggregation-induced emission (AIEE) properties.[84] This dye showed a good quenching response to the addition of

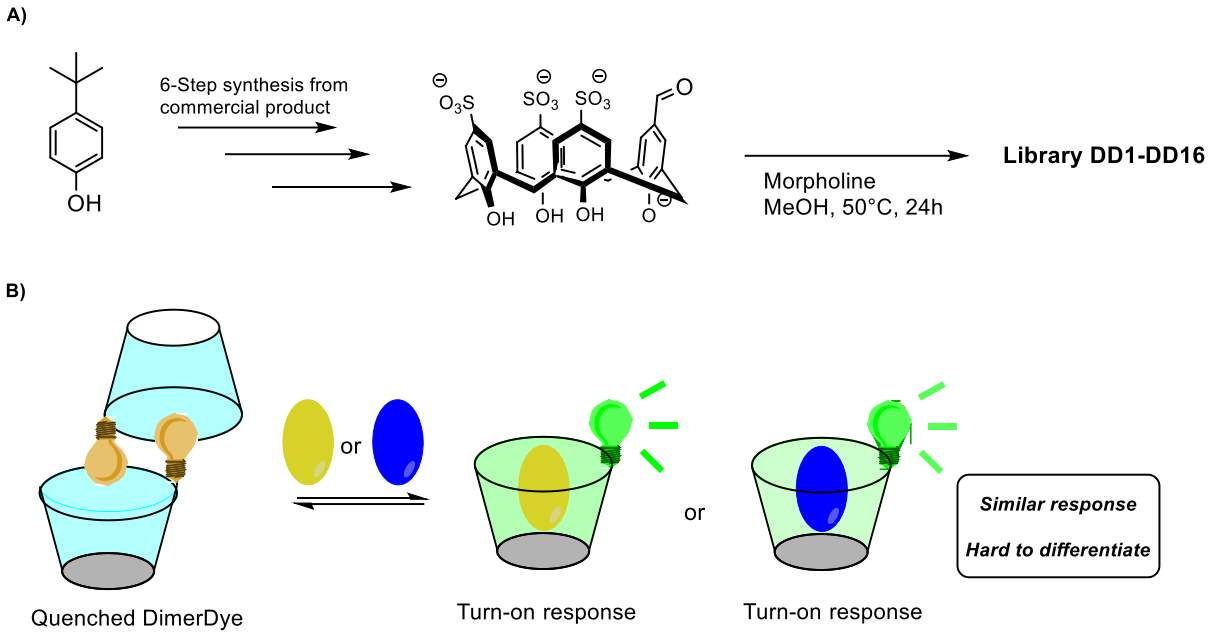

Figure 1.9: Current limitations in the DimerDye system. A) Synthesis route for a DimerDye library showing limitation in multi-step procedure to obtain aldehyde reactive handle. B) Cartoon representation of the DimderDye sensor system showing similar responses for different analytes.[53].

nitrobenzene and quenching and NMR studies confirmed interaction through π-π stacking. A test strip for gas phase detection was even developed and showed some promising results. This study showed the potential of stilbenes as fluorophore units and how they could be implemented into more advanced sensors. While some chemistry with calixarene-based stilbene scaffolds has been explored, they functioned as bifunctional units[85] or polymer-based systems,[86] and they are not aimed at use in water-soluble systems.

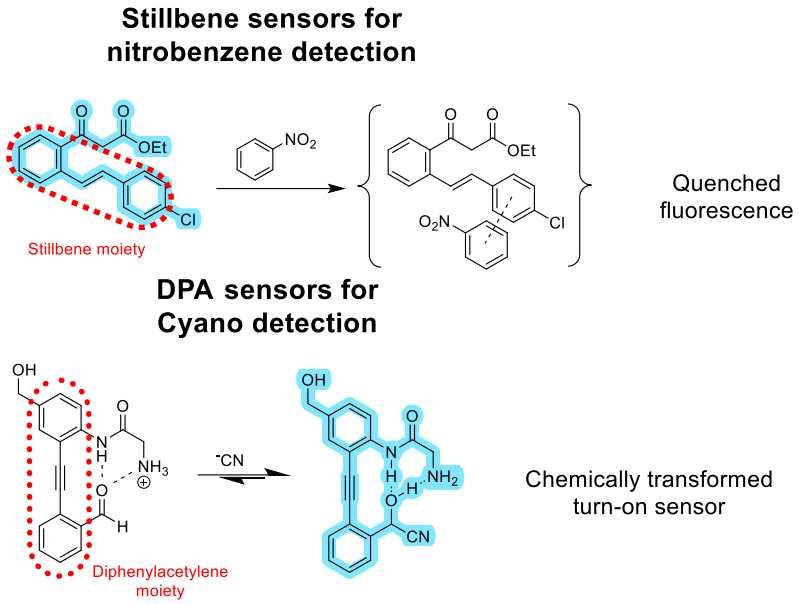

Figure 1.10: Scheme showing applications of stilbene[84] and DPA[87] moieties as sensors.

Another closely related dye system that drew our attention is a diphenylacetylene (DPA) group, where the bridging double bond is replaced with an alkyne. DPAs are interesting alternatives to explore as their photo-physics are well-studied,[88–90] and the rigidity of the triple bond would most likely affect dimerization dynamics. Their fluorescence can also be affected by factors like temperature and substituents,[91] which shows promise in obtaining new unique fluorescent behaviours. DPA-based sensors have been developed, and they mainly have been used for the fluorescent and colorimetric sensing of cyanide,[92] showing very distinctive changes in its fluorescence and absorbance properties. In Figure 1.10 we can see an application as a sensor with a turn-on fluorescence, where we have an initial quenched dimer due to the substituent groups. The dye can react with cyanide in aqueous solutions removing the quenched group and giving a fluorescent response. Similarly to stilbenes, there is a report by Vikalog where they used a DPA as a fluorophore in a calixarene sensor used

for nitric oxide (NO) detection.[93] But once again, this is used as bi-functional units but the proof-of-concept demonstrates a potential in using these types of fluorophores with a calixarene scaffold.

This shows some of the background for the current state of supramolecular drug sensing. There are exciting possibilities to be explored from combining fluorophores of interest (like Stilbenes or DPAs) with the versatility of calix[4]arenes. However, it can be seen the examples in the literature are limited and there is there is not yet as much focus on getting information-rich systems from drug samples, as there usually is in biochemical systems. In this project we wish to expand upon the previously developed DimerDye family of molecules, having an integrated fluorophore, but trying to get a more information-rich output by having selective responses that depend on the identity of the analyte. This will not only give a similarly effective sensing system but will allow for better differentiation between closely related molecules, something which has already started to be explored with adaptive networks of hosts.

1.5 Summary and goals of this thesis

In summary, we have shown that there is a need for novel sensing systems that can be rapidly obtained for use in aqueous media and salty solutions which can tolerate biological and real-world conditions. Calix[4]arenes offer a variety of scaffolds upon which we can construct these new sensing systems because their simple synthesis and modification can allow us to insert these desired traits, including the coupling of a fluorescent conjugated moiety into the

binding pocket. This project will demonstrate the synthesis, characterization, spectrophotometric properties, as well as binding mechanics of a series of new stilbene-calix[4]arene (StiCx) analogues with some of the following overall objectives:

- To obtain a series of new StiCx derivatives using a rapid two-step synthesis and high-throughput screening methodologies. Once obtained, characterize target compounds using NMR and HPLC-MS techniques.
- To do a spectral analysis and perform a binding study of the top-performing candidates using fluorescence spectroscopy with an array of drug molecules of interest.
- To get information on the mechanisms behind observed fluorescence behaviour and possible configuration and interactions using solution-phase structure determination studies.

Chapter 2 will show our results with the synthesis of a small initial library of new dye-integrated calixarene sensors, and preliminary screening assays that helped us to identify a new set of competent hosts. We will also report their unique sensing properties, showing a selective turn-on and turn-off fluorescence response to different guests, which is a feature never before seen in these systems. And lastly, we will look into the potential of our hosts for discriminating between closely related drug molecules. Chapter 3 will focus on investigating the mechanisms behind the observed binding behaviours. We will use NOESY and DOSY to get information on binding relationships and supramolecular mechanisms that are active for the new sensors and their guests. We will also report the chemical properties of the stilbene moiety via some control experiments.

Chapter 2: Synthesis and binding assays of upper-ring functionalized *p*-sulfonatocalix[4]arenes. A new synthesis pathway and new fluorescent properties.

2.1 Introduction

In this Chapter, we will discuss the synthesis and characterization of a library of novel hosts, including a newly proposed synthetic approach for rapid access to a family of analogues. For this, we will look into how we wished to approach this challenge and the first things that needed to be defined. First is the type of group we wished to use as a fluorophore group, and we initially wished to use a diphenylacetylene (DPA) pendant arm in our studies. We will report our efforts on a new synthetic approach to obtain these analogues. While there is considerable literature on the synthesis of DPAs using cross-coupling reactions,[94,95] we needed to adapt these procedures to work with water-soluble calixarenes. The Sonogashira reaction has been by far, the most routine way to do chemistry with terminal alkynes. This approach has also been adopted in the world of calixarenes, to introduce functionalization to the cavity. [96] There has even been a report by Vigalok,[97] showing polymeric sulfonatocalixarene scaffolds with a DPA functionalization as sensors for nitrous oxide (NO) in protic media. The effectiveness of this reaction and the background demonstration of DPA calixarenes as sensors were two of the main reasons behind our choice to target DPAs as we built our library of new sensors.

However, in all cases, synthetic approaches to insert the necessary reactive handles onto calixarenes using regioselective modifications require multiple steps and are time-

consuming. To save time and effort, we wanted to optimize the synthetic route to get quick access to our library of compounds. It is now common practice in screening assays to use a combinatorial and/or parallel approach, becoming an important toolbox for many synthetic chemists and receiving more and more attention.[98] High throughput screening consists of a methodology where many small-scale experiments are run in parallel to optimize assay parameters or look for "hits" in a large number of compounds. Such an example is a library of fluorescent styryl scaffolds where a combinatorial approach allowed for the screening of hundreds of analogues and their potency as staining agents.[99] To build a library of compounds to screen for an optimal sensor, a more efficient approach to the building block needed for parallel synthesis of calixarene-based sensor candidates was necessary. We wanted to use a similar approach in our screening and test a small library of analogues of cross-coupled calixarenes as fluorescent hosts against a small group of relevant drug analytes.

As we aimed to make a small library of DPA-functionalized calixarenes, unexpected side reactions led us to obtain a stilbene product instead. This was still an acceptable outcome as stilbenes are also reported fluorophores of interest.[100] Subsequent optimizations allowed us to make several examples of a new family of stilbene calixarene (StiCx) sensor candidates, prepared via a new two-step synthetic route for easy access to a small library of different host-type sensors. We were able to also test the top candidates of our library as potentially novel sensors with information-rich outputs and we were able to use this system to differentiate between a small group of target drug molecules in solution.

2.2 Results and Discussion

2.2.1 Synthesis of a brominated calixarene – 'sCx4-Br'

As we discussed, previous work has developed functionalized calix[4]arenes through different electrophilic aromatic substitutions, some of which have been used in Suzuki cross-coupling reactions.[101] In Chapter One we discussed introducing fluorophores of interest into the calixarene cavity. The initial goal of this project was to use a Sonogashira reaction to introduce a diphenylacetylene pendant arm on one of the aromatic rings. We designed a library of diphenylacetylene derivatives to analyze different absorbance and fluorescence properties.

Functionalized calixarenes can be synthesized from "sCx4-Br".[101–104] Its previously reported synthetic route (Scheme 2.1) starts with the synthesis of the calixarene backbone from tert-butylphenol, which is then de-tertbutylated to obtain Calix[4]arene. Benzoylation occurs on three of the four rings due to steric hindrance yielding OBz-Cx_4, leaving only one activated ring upon which we can do bromination, this is the key step that provides regioselectivity. After insertion of the bromide through bromination to obtain OBz-Cx_4-Br there is a deprotection step to remove the benzoyls obtaining sCx_4-Br. The final product is then obtained by sulfonation with sulfuric acid, inserting the sulfonate groups and yielding sCx_4-Br. The total synthesis involves 6 steps to obtain the final scaffold giving a total yield of 6% (with yields ranging from 49%-85% across reaction steps).

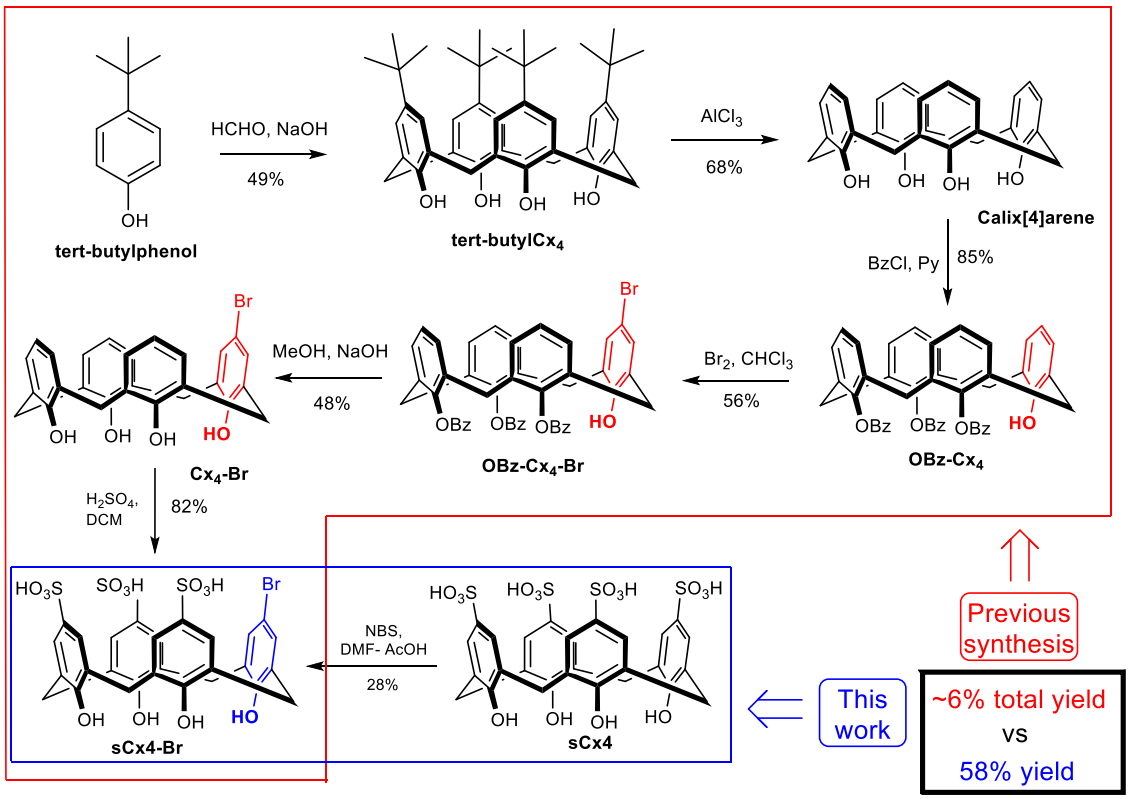

Scheme 2.1: Synthesis pathway previously used (red) and used in this work (blue) for obtaining starting material sCx4-Br.

To improve the synthetic route, we developed a more efficient and regioselective single halogenation using previously reported reaction conditions.[105] This *ipso*-substitution was initially done on a study of the effects of succinimides on quinolinol sulfonic acids. The fact that the halogens managed to displace the sulfonate groups served as the inspiration to adapt this procedure for our calixarenes. The easy commercial availability of *p*-sulfonatocalix[4]arene (sCx4) offered the possibility of a one-step approach to sCx4-Br.

It was found that the reaction of sCx4 with NBS in a DMF-Acetic acid mixture provides access to sCx4-Br in only one step. NBS is a convenient reagent, as it is inexpensive but

needs to be purified by recrystallization before use. The reaction can be done at room temperature, under an hour and purified by preparative HPLC. In the absence of any regiocontrol, multiple substitutions of the calixarene sulfonates can occur, and indeed we see two additional di-brominated products on HPLC purification. One of these is more predominant than the other, which we assume is the 1,3-dibrominated product as it would be favored due to steric hindrance. However, these byproducts can be minimized by tuning reaction time and reagent concentration. Our protocol was then optimized to give the maximum yield of the product while minimizing excess bromination. While the isolated yield is only 58%, an additional advantage of the reaction is that the starting material sCx4 can be recovered on HPLC purification with approximately 36% yield and can be reused to get further conversion. Overall, this reaction proves to be a great improvement on previous work as we have cut down a 6-step synthesis, of which three steps require inert conditions and one requires column chromatography. Not only do we skip long and laborious reaction set-ups, but we also obtain an overall better yield of 58% compared to the overall 6% previously reported. In summary, we can obtain our starting material for cross-coupling reaction in a single reaction from a commercial product, providing rapid access to a reactive handle from which we can introduce our fluorophore unit.

2.2.2 Synthesis of library

Having quick access to sCx4-Br allowed a synthetic handle that we could further functionalize *via* cross-coupling chemistry to introduce our fluorophores of interest. Initially, we wanted to obtain a library of diphenylacetylene analogues, so we used a Sonogashira

cross-coupling reaction with different substituted ethynylbenzene compounds (Scheme 2.2). The reaction was carried out by adapting literature procedures.[106] While our calixarenes are compatible with water, Palladium catalysts are usually not, so DMF was used as the solvent for our cross-coupling reactions. The reaction was done under inert nitrogen and using oven-dried glassware as this cross-coupling reaction is also air-sensitive. Solids were pre-weighed before being sealed in a microwave vial and dissolved in DMF, using TEA as the base and XPhos Pd G3, a third-generation Palladium pre-catalyst commonly used in cross-coupling reactions[107] as the catalyst. The product was precipitated by the addition of toluene and then directly purified by preparative HPLC.

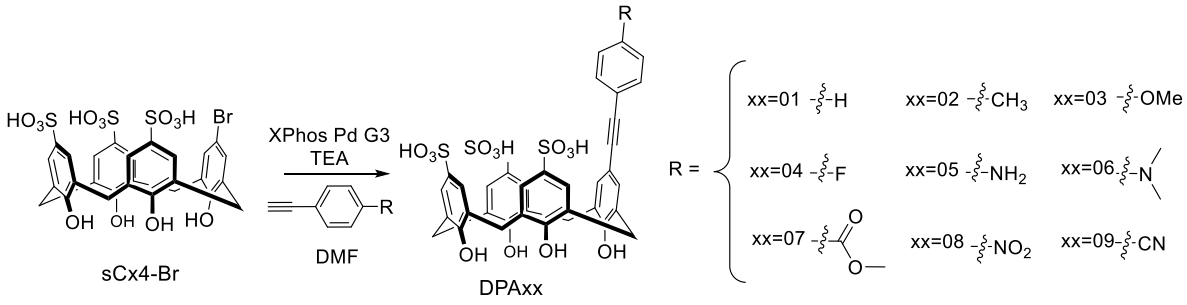

Scheme 2.2: Sonogashira cross-coupling reaction with different substituents used in attempts to build the initial library of DPA calixarene sensors.

Initial results showed that the reaction was carried out successfully, and it tolerates diversely functionalized DPA analogues. Functionalization of the aromatic rings included a variety of groups with different electron-donating and -withdrawing properties, to change the overall electronics of the ring and hopefully their spectral and sensing properties. Evidence of the desired DPA-containing products was obtained by NMR and MS. An interesting observation is that the compound is obtained mixed with TEA, possibly as a counterion, as observed in

the characterization spectra (Section 2.5.2). This residual base could not be removed but it wasn't found to interfere with sensing properties or purity. However, more detailed analysis through High-Resolution Mass Spectrometry (HRMS) showed the persistent presence of additional compounds with molecular masses 2 and 18 units higher than expected. When characterized by NMR, we confirmed that the pendant arm had been inserted into the calixarene, as shown by the additional aromatic signals, as well as some characteristic signals from the substituents. These additional masses indicated side reactions were occurring. One obvious candidate is a hydration reaction on the triple bond, which would explain the +18 mass byproducts as one equivalent of water is added. The acid-catalyzed hydration of triple bonds to produce ketone byproducts (via an enol-type intermediate) is a known reaction.[108] On the other hand, the +2 mass byproducts could only be attributed to an equivalent of two hydrogen atoms being added, therefore indicating a semi-reduction of the triple bond to an alkene. This reaction has much less precedent and is explored in more detail later in this Chapter.

We ultimately confirmed that the DPA pendant arm was susceptible to both hydration and semi-reduction. Further, we found that both occurred during product purification *via* preparative reverse-phase HPLC, which uses water as the solvent and trifluoroacetic acid (TFA) additive which is generally thought to improve peak shape and separation due to protonation and ion pairing.[109,110] Some simple experiments that varied HPLC elution conditions showed that treatment with TFA and high aqueous content mobile phases led to the conversion of the DPA pendant arm to the respective ketone (Figure 2.1). This problem

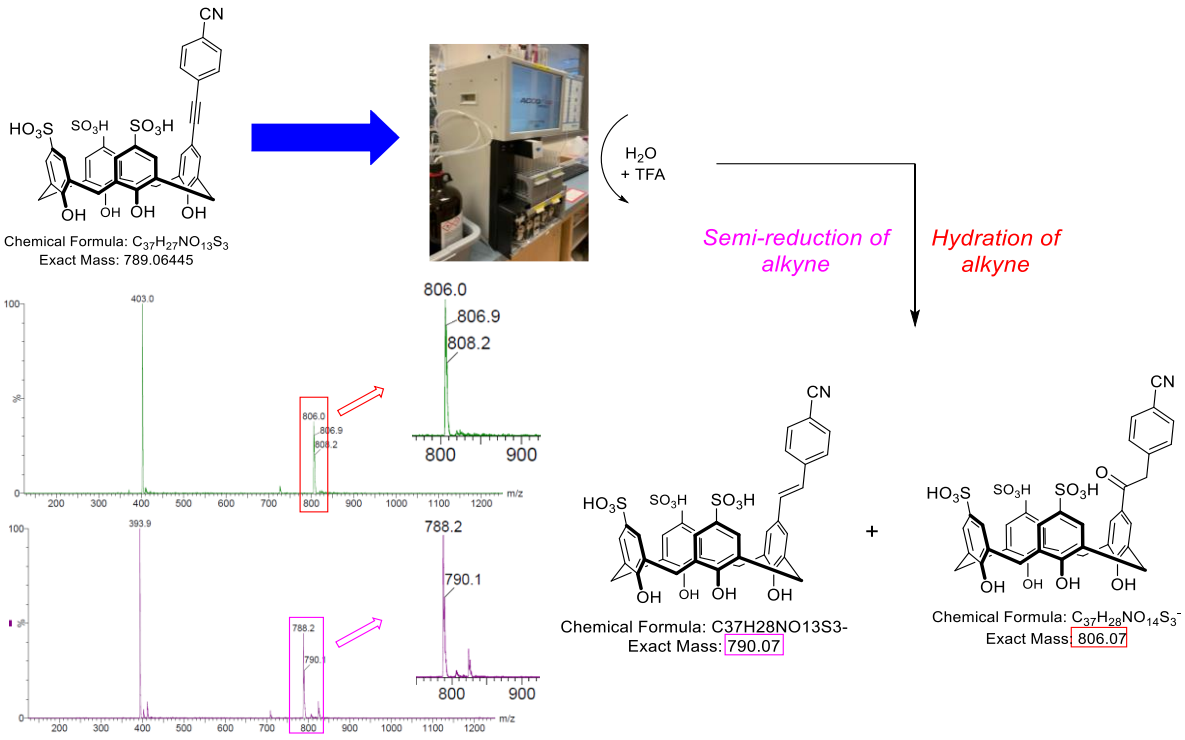

Figure 2.1: Reaction scheme showing degradation of product upon purification with HPLC. Both degradation products are depicted with UPLC ESI- scan showing respective masses.

even more prominent during the concentration step required after fractions are collected from the HPLC. Since TFA serves as a counterion in solution it is not so easily removed by evaporation. This means that as the solvent is removed the TFA concentration, and therefore acidity, increases and pushes hydration and reduction reactions forward.

Our attempts to remove TFA from the HPLC mobile phase proved unsuccessful. Reducing the concentration of the TFA additive resulted in a broadening of the peak and loss of peak separation, and replacement with a milder acid such as formic acid (FA) yielded similar results. Even when adapting the TFA-containing HPLC protocols by using milder methods

to concentrate the sample, the extent of hydration was reduced while the semi-reduction reaction still occurred to a large degree. This second unwanted reaction was a surprise and sparked a great deal of interest, as alkynes do not normally undergo side reactions so easily in such mild conditions. Some literature procedures were found concerning the semi-reduction of diphenylacetylenes using palladium catalysts, base and either DMF or formic acid (which were both present in our reactions) as the reducing agent.[111–113] These reports suggest that the TFA and trace remnants of palladium were the reasons that we consistently observed significant amounts of semi-reduction during purification even when hydration was minimized. However, it was impossible to remove these reagents from our procedure.

Despite our best efforts the alkene product was still obtained in our reaction product, an unusual result for a Sonogashira cross-coupling. Alkynes do not react so readily, and special conditions are usually required to activate the triple bond. Typical alkyne reductions require strong reducing agents like H_2 and specific catalysts to work, and hydrations need to be facilitated with the addition of Mercury (Hg^{2+}) or other catalysts. It was unexpected to see reactions proceed so readily, and it was still unknown to us what was the role of the calixarene on the reaction. Characterization by NMR confirmed the stilbene product was obtained after purification. This was confirmed by the additional peaks in the ^{1}H-NMR at ~7.0 ppm and the absence of signals in the 90-110 ppm region in the ^{13}C-NMR where we would expect to find alkyne carbons. Fortunately, stilbenes still give us a conjugated system that could be used as a fluorescent sensor. Furthermore, when testing the absorption properties of these compounds, they were found to maintain their fluorescence behaviour regardless of the semi-

reduction happening. As a result, we switched our approach to using a family of stilbene calix[4]arenes as the studied sensing system.

To synthesize the calixarene derivatives, we took advantage of the high reactivity of the calixarene triple bond to drive the *in situ* semi-reduction forward. We adapted a semi-reduction procedure from literature in which formic acid was used as a reducing agent, as shown in Scheme 2.3A.[111] When we added 0.1 mmol (1.25 equivalents) of formic acid to the reaction mixture *in situ*, the two-step reaction proceeded successfully and we obtained the stilbene product exclusively. We found that the stilbene product was stable during purification and was able to be isolated by preparative HPLC with no evidence of hydration or any other side reactions. It came to our attention that the net conversion from a halide group to a stilbene through a cross-coupling could be obtained through Heck coupling reactions. However, when we attempted to directly do a Heck reaction on sCx4-Br to yield the same stilbene products, the reaction didn't take place, as represented by Figure 2.3B. This presents an interesting alternative to using this indirect route using a Sonogashira followed by *in situ* semi-reduction of the product in situations where Heck couplings are not viable. We generally refer to calixarene hosts as "Cx" compounds, and so we call the "stilbene calixarene" hosts StiCx-##, where the numbers correspond to different substituents on the pendant aromatic ring as indicated in Scheme 2.3C.

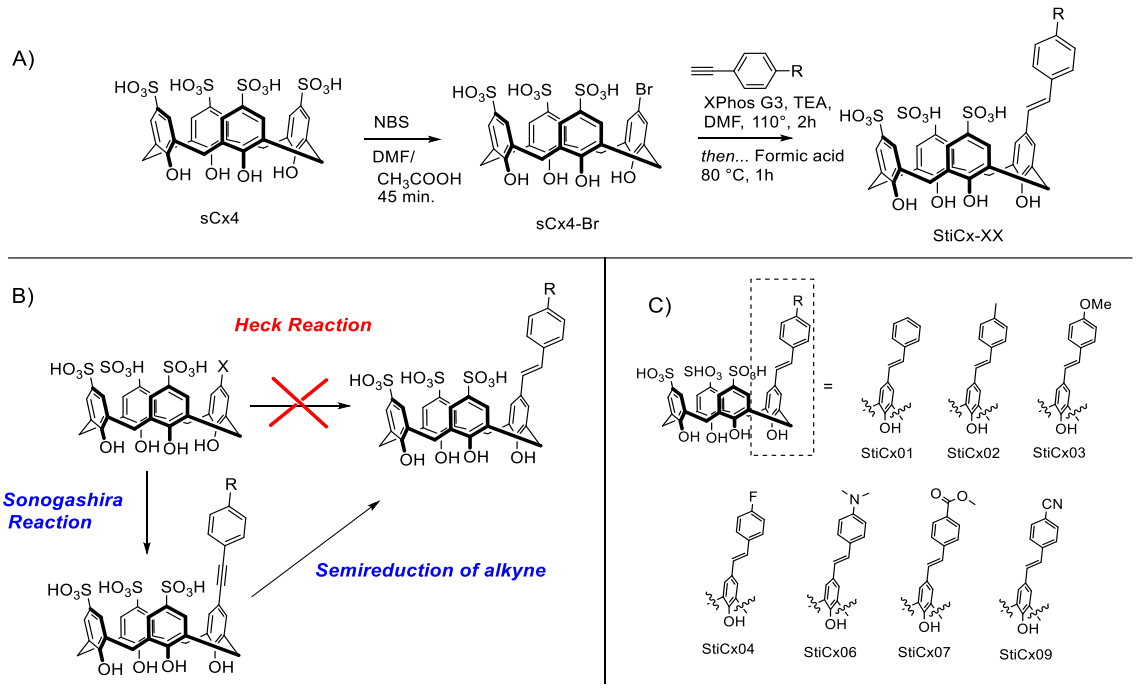

Scheme 2.3: A) Schematic used for the Sonoghasira cross-coupling of sCx4-Br, followed by a semi-reduction to obtain the StiCx analogues. B) Schematic showing an indirect route to obtain a styrene analogue where Heck reactions did not proceed. C) Synthesized library of StiCx.

Using this procedure, we were able to successfully synthesize a library of 7 out of the 9 planned StiCx analogues with different electronic properties. StiCx05 (R = $-NH_2$) and StiCx08 (R = $-NO_2$) showed rapid decomposition even with the newly adapted procedure so they were discarded. Three products ended up being the focus of our sensing studies (StiCx03, StiCx07, StiCx09; (Section 2.2.4) and were subjected to full characterization by NMR, IR, and HRMS to confirm structure (Supporting information, Section 2.5.2). ^{1}H-NMR showed coupling constants for the alkene protons of 16 Hz for all analogues, indicating that we obtained exclusively the trans isomer from this synthetic protocol. The isolated yields for these three products after HPLC purification were as follows: StiCx03 = 34%, StiCx07 = 26%, and StiCx09 = 27%).

2.2.3 Stilbene dye control synthesis

As previously mentioned, the peculiar chemistry of the semi-reduction of our DPA moiety was of interest. We decided to synthesize and test a series of controls to understand the reaction chemistry and ultimately, to provide controls for fluorescence properties. We adapted literature procedures[94] to our reaction to prepare the diphenylacetylene moieties (procedure in section 2.4.1.3). The transformation allowed the comparison of the semi-reduction chemistry on the individual stilbenes from our calixarene StiCx hosts. Since we mainly wanted to compare data with the hosts used in our binding studies (see below), we prepared the analogues for three candidates, with R = -OMe, -COOMe, and -CN. The reaction is shown in Scheme 2.4, in which we employed a Sonogashira reaction of phenylacetylene analogues with bromophenol followed by formic acid addition, analogous to the synthetic procedure we used to make the StiCx compounds. To our surprise, we saw that no semi-reduction occurred. When followed through UPLC-MS, only small traces of stilbene could be observed even after increasing reaction time (as high as 6 hours) and temperature (as high as 145°C). This was our first indication that the introduction to the calixarene host was activating the triple bond, as the semi-reduction was carried out completely when using the StiCx hosts. This presents a very interesting and unique chemical feature in the hosts, the mechanism behind why this happens is not clear and not the main objective of this thesis. The direct through-bond electronic influences on the diphenylacetylene moiety are essentially identical for the control DPAs and the calixarene-based DPAs. One theory to explain the unique reactivity of the calixarene DPAs is that the large buildup of sulfonate negative charges near the conjugated system influences the approach of catalyst or other reagents, or it increases the reactivity of the triple bond by

through-space electrostatic effects. Another possible theory is that host dimerization could be a factor in said activation. Each of these ideas would need to be explored with detailed mechanistic studies that are not the focus of this thesis.

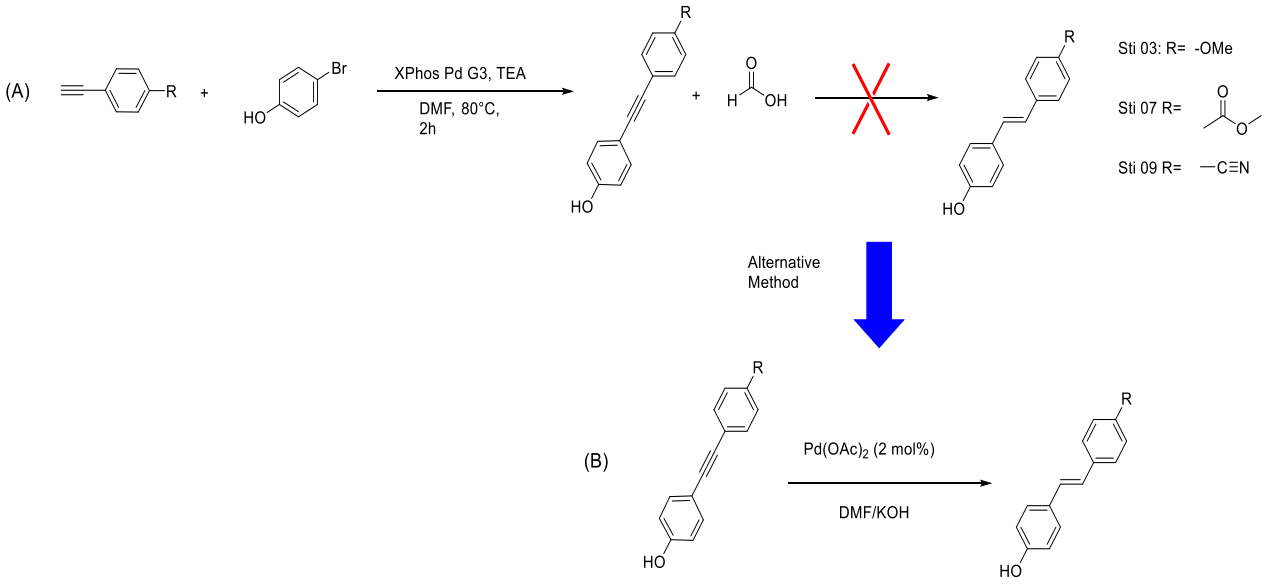

Scheme 2.4:(A) Reaction pathway for Styrene derivatives controls synthesis. Though a similar reaction procedure was used, no semi-reduction after formic acid addition was seen. (B) Scheme with conditions that led to obtaining a successful semi-reduction.

We still wanted to obtain the control stilbene fluorophores for mechanistic studies, so we once again took to the literature to find a different route to the stilbene dyes. We already knew semi-reduction was possible, so we decided to use a reported and optimized procedure[112] to reduce our DPA analogues to the stilbene products. We decided to focus exclusively on the cyano analogue (Sti09) as the host StiCx09 had unique binding behaviours that warranted additional study (see Section 2.2.4). We followed the procedure depicted in Scheme 2.4 where we used a mixture of KOH/DMF as the reducing agent and $Pd(OAc)_2$ as the catalyst. The procedure also required 6 hours of reaction time at 145°C, another indication of the difference in reactivity for these controls with our hosts. The reaction was carried out

successfully and provided the control dye Sti09, as confirmed by UPLC-MS and NMR. These control dyes will be useful as control conditions in the investigation of the fluorescence properties of the pendant arm. Spectroscopic studies on this compound will be discussed in Chapter 3 (Section 3.2.4).

2.2.4 Absorbance and fluorescence studies

We subjected the seven successfully prepared StiCx analogues to preliminary studies to see if the integrated stilbene dye yielded useful levels of fluorescence. As the goal is to create water-compatible systems for sensing biologically active analytes, all tests were done in a 100 mM sodium phosphate buffer (pH = 7.4). Absorbance spectra were taken, and fluorescence emission spectra were taken with the absorbance maxima used as the excitation wavelength. StiCx03, StiCx07 and StiCx09 showed the most promising results, and their fluorescence can be observed even under a handheld UV light (Figure 2.2). Something we can observe is how StiCx07 and StiCx09 have an absorbance maximum at 340 nm while StiCx03 shows its maximum at 290 nm (Spectral data in Table 2.1). This difference shows how the difference in the electronic properties of the upper ring can have drastic effects on the absorbance behaviour. This difference could be attributed to the methoxy being an electron-donating group, while the methyl ester and nitrile groups are electron withdrawing. Similarly, we hope to see how this difference could also affect binding affinities and sensing responses.

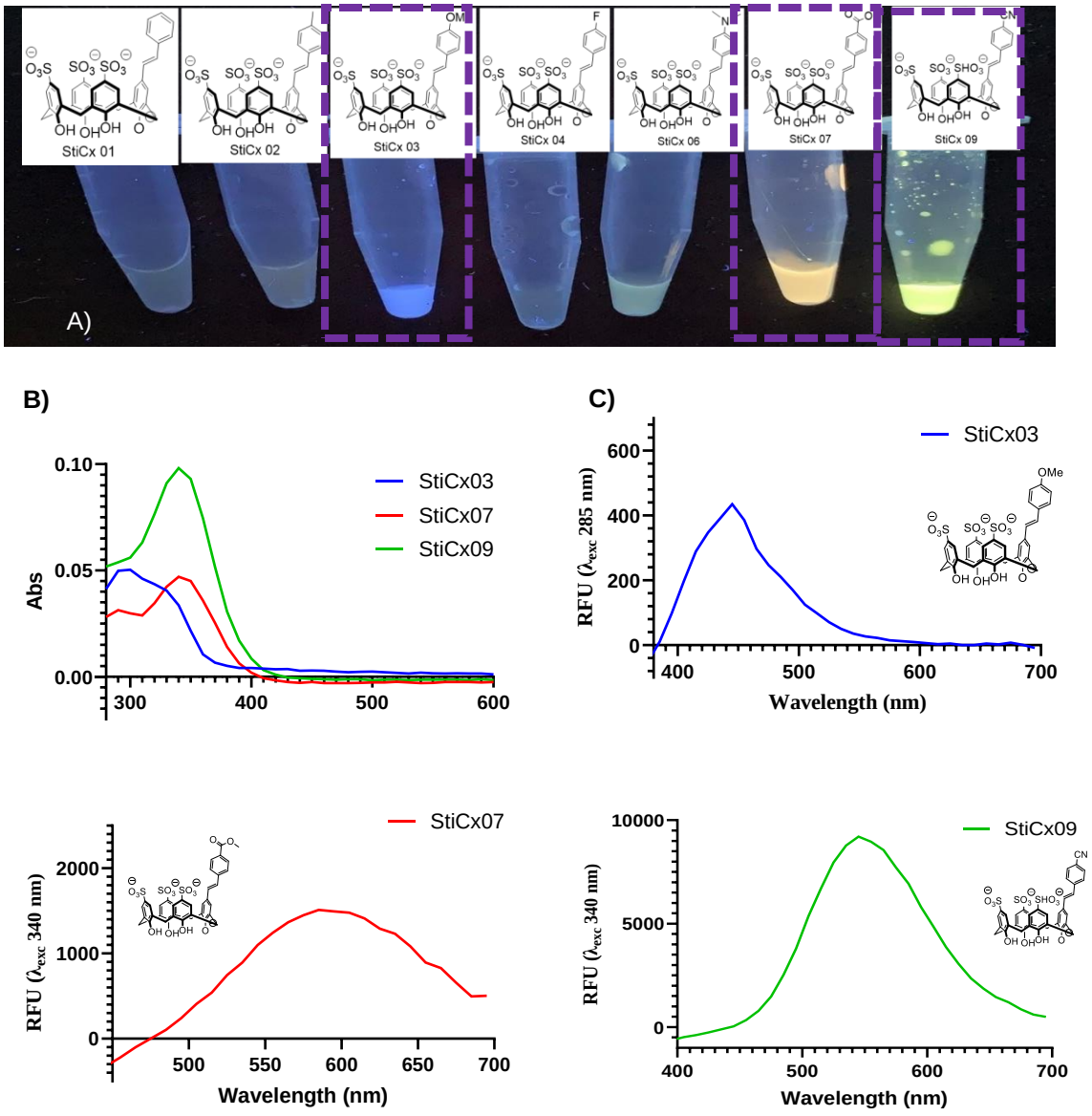

Figure 2.2: A) Picture of analogues under a UV-vis lamp with their respective structures. B) Absorbance spectra of the top three promising candidates from the library. C) Fluorescence emission spectra of each host. All trials were done in 8 µM concentration of StiCx in a phosphate buffer (10 mM, pH 7.4) solution.

Table 2.1: Spectral characterization data with absorbance maxima (λ_{max}), and molar absorptivity (ε). Fluorescence emission maxima (λ_{em}) and stokes shift for top three StiCx and DimerDye DD1.[53]

	λ_{max} (nm)	ε (M^{-1} cm^{-1})	λ_{em} (nm)	Stokes shift (nm)
StiCx03	290	$19.9 \times 10^3 \pm 0.01$	445	190
StiCx07	340	$18.8 \times 10^3 \pm 0.01$	585	240
StiCx09	340	$39.3 \times 10^3 \pm 0.01$	545	240
DD1	385	-	590	205

Once the three candidates were identified, we proceeded to run binding assays using a selection of drug analytes that were of interest to us (Figure 2.2B). To run these binding assays, titrations were done where each of the three StiCx hosts was treated with an increasing concentration of each of the analyte guests (0-400 µM). The full spectra show changes in emission intensity as guest concentration increases. However, to get a better representation of the changes in response, the RFU at the emission maximum was plotted against guest concentration, as shown in Figure 2.3.

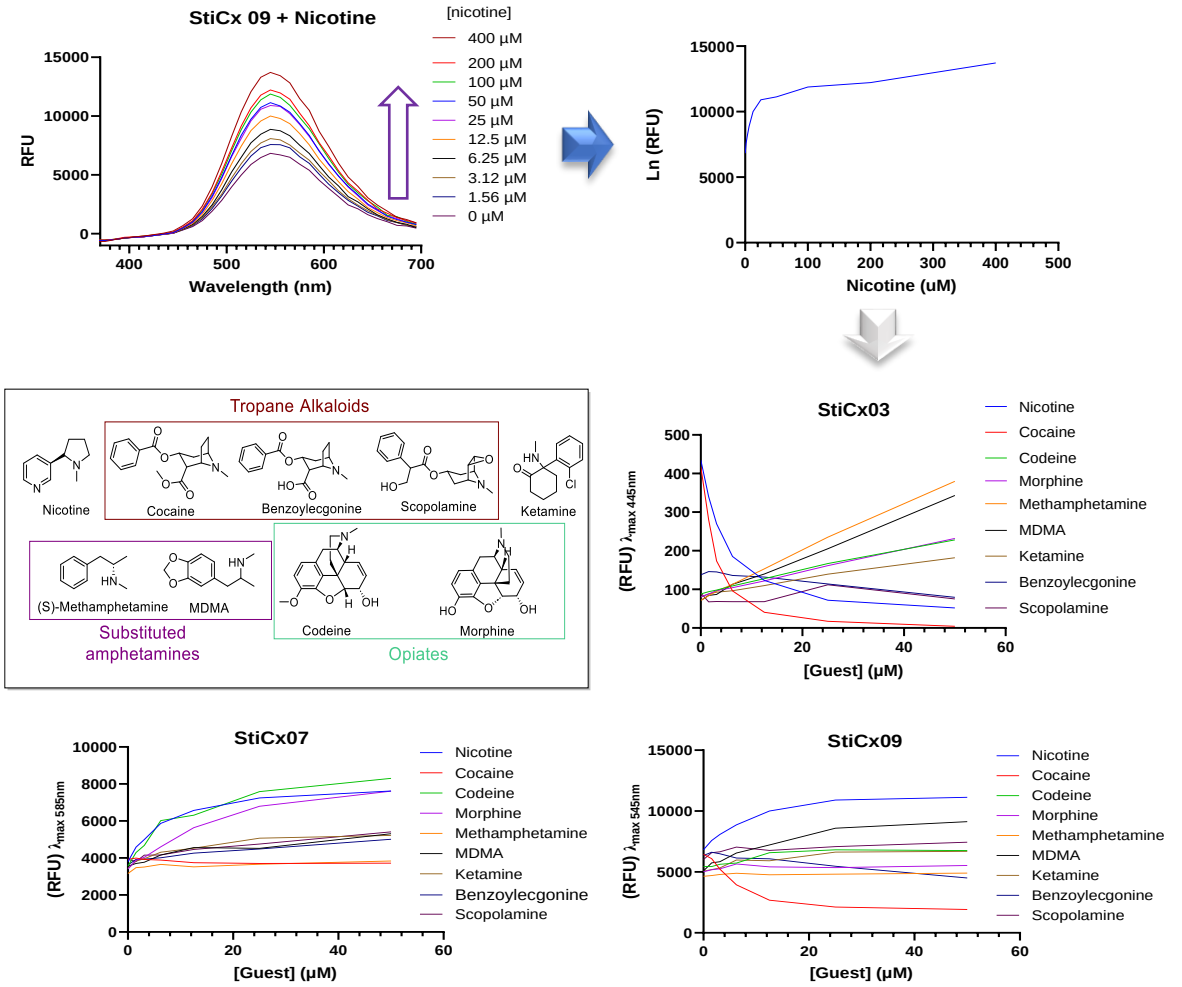

Figure 2.3: Fluorescence curves showing an increase in intensity correlated to nicotine concentration. Binding curves showing "Guest concentration vs (RFU)" are then graphed from this. All trials were done with host concentration fixed (8 µm). All trials were done in 8 µM concentration of StiCx in a phosphate buffer (10 mM, pH 7.4) solution.

Just as is the case with DimerDyes, we expected to see some kind of fluorescence change in intensity or emission wavelength with the increasing concentration of guests. However, we came across some very interesting results when we observed that different guests induced different responses in some of the hosts. For example, we can see that in the case of StiCx09, there is an increasing fluorescence intensity with increasing nicotine concentration, but a decrease in fluorescence intensity with increasing cocaine concentration. Differently, StiCx03 showed only a turn-off response to both nicotine and cocaine and StiCx07 has a turn-on fluorescence for all guests except cocaine, where there is barely any change. This unique and distinctive behaviour with turn-on and turn-off responses was a novel set of phenomena that hadn't been seen before using DimerDye systems, which always showed a turn-on fluorescence response independent of the identity of the guest.[53,114] In Figure 2.4 we can see this idea represented, in which we have a selective fluorescence response based on the identity of the analyte.

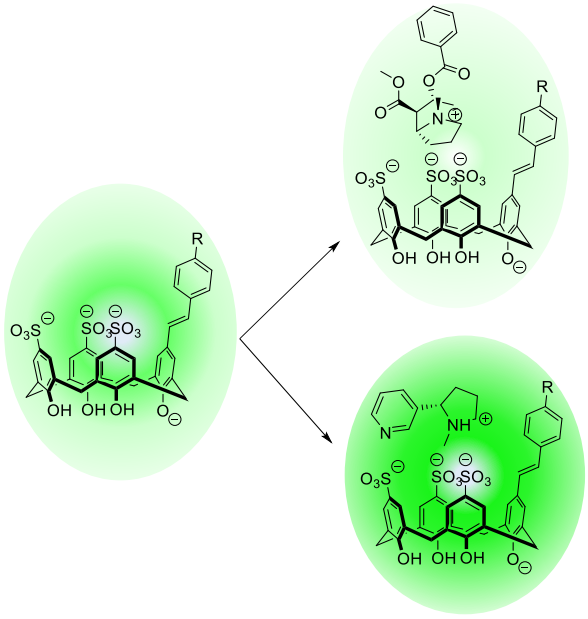

Figure 2.4: Cartoon representation of selective fluorescence responses.

This diversity of photophysical responses presents an opportunity to get more diverse and information-rich data from an individual sensor or a small set of sensors. For example, using only the information from StiCx09 we could now sense the presence of cocaine in a given sample, and with this selective behaviour we could differentiate it from other guests because of this unique (or rare) turn-off response. It is worth noting that the turn-off response is very unique to cocaine, and its closely related metabolite benzoylecgonine.[115] Even other compounds from the tropane alkaloid family, like scopolamine, don't show this turn-off response for StiCx09, which shows the potential of this host as a selective sensor for cocaine and its analogues. If we can get this much information from a single sensor, we hypothesized that we could get a very powerful system for drug discrimination when we use all three. Because of this, we wanted to explore how powerful this recognition and differentiation tool could be, so we next attempted to use the three hosts as a sensor array for drug identification.

2.2.5 Sensor Array Results

Following earlier results from the literature,[53] we used a sensor array approach to see if the combined data outputs from a small number of StiCx sensors could be enough to differentiate between different, closely related drugs. It is now becoming more common to use sensor arrays to analyze complex mixtures of closely related analytes.[56,116,117] The approaches almost always rely on a multivariate statistical analysis of data, and those data sets tend to consist of different degrees of turn-on signal that arise from different analytes engaging different sensors within a sensor array.[53] It was of general interest to us to explore

the use of our new hosts in this approach. Moreover, the selective turn-on/off responses in response to different analytes from among the test sets could potentially allow for a greater degree of discrimination between analytes.

To set up these experiments, we first determined a range of analyte concentrations that would be practical for these sensors. For this, we used the binding curves we obtained in Figure 2.3 and we analyzed only the initial linear ranges of these curves. It is important to use the linear range, because as we can see the fluorescence plateaus after a certain concentration is reached. Limits of detection (LODs) were determined for each host with a selection of 4 drugs and reported in Table 2.2. The LODs were calculated using standard literature[118] procedures using the slope of the initial linear portion of the response curve (b) and the standard deviation (S) using equation 1:

$$LOD = \frac{3*S}{b} \qquad \text{Eq. 1}$$

We chose to determine LODs for nicotine and cocaine because they show the most intense responses and for codeine and morphine as representatives of a different family of compounds that showed the best R^2 values. Our LOD values are in the range of 1-8 μM (Table 2.1). These are comparable to some DimerDye LODs, which have a minimum value of approximately 1 μM. StiCx03 shows some of the biggest slope values across the board, meaning it has very sensitive responses to analyte presence, while other slopes ranged around 0.03. LODs were very dependent on the host and guest used, as sensors presented a unique response to each drug. This shows different levels of response to the presence of each analyte which is good for us as we want variable responses which would allow us to differentiate

them from each other. The highest LOD we see is 7.8 µM so we would want our assays to be above this concentration. It can be seen from the graphs in Figure 2.3 that different hosts reach their plateau of intensity in different concentrations, ranging between 20-60 µM.

Principal component analysis (PCA) is a multivariate statistical method for analyzing large sets of data that is particularly useful in the field of sensor array-based chemometrics. Thoroughly explaining the principles behind this technique is beyond the scope of this thesis, but ample literature on the topic exists.[119] It is enough to know that it allows for a better visual representation of large sets of data by reducing the dimensionality while preserving `variability´. It does so by creating a new set of variables, called "principal components," which are linear functions of the original dataset. These variables are calculated in such a way so that they are unrelated while still maximizing variance and in this way, we will reduce statistical information loss. By using different sets of data, such as absorbance and fluorescence, we can increase the possible difference in response. Having a turn-on/off response would likely further increase the variability in response, leading to better differentiation and a more information-rich system.

To carry out the sensor array experiment we took StiCx03, StiCx07 and StiCx09 and our set of 9 guests from the titration assays. We separately took absorbance and fluorescence measurements of a mix of the individual host (8 µM) and guest (40 µM). We used these concentrations as they provided the best results after some optimization, and they are swell above our LODs. The experiment consisted of 12 replicates of a host-guest mixture, of which

the most representative 10 were selected to rule out outliers. PCAs are then plotted, and specific wavelengths of absorbance and fluorescence were selected to optimize separation. Specifics on sample preparation and measurements can be seen in the experimental description (Section 2.4.3). In a PCA plot, we would expect to see the replicates for each guest clustered separately in our assays. The more statistically different our measurements the separation we would observe, and the better our sensing system would be in differentiating the different guests.

Table 2.2: Reported values for slope, standard deviation (S) and Limits of Detection (LOD) for the top three hosts with 4 drug analytes taken from linear regression of the curve.

	Nicotine			**Cocaine**		
	Slope	**S**	**|LOD| (μM)**	**Slope**	**S**	**|LOD| (μM)**
StiCx09	0.03	0.04	4.3	-0.07	0.04	1.7
StiCx07	0.04	0.09	6.5	-0.005	0.01	6.7
StiCx03	-0.1	0.1	3.5	-0.2	0.2	2.8
	Codeine			**Methamphetamine**		
	Slope	**S**	**|LOD| (μM)**	**Slope**	**S**	**|LOD| (μM)**
StiCx09	0.02	0.02	4.1	0.03	0.04	5.0
StiCx07	0.04	0.1	7.8	0.02	0.02	2.5
StiCx03	0.03	0.01	1.3	0.05	0.06	3.7

The PCA plot is shown in Figure 2.5, which shows the PCA scores and the plots with 95% confidence ellipsis shown around each data set. In this analysis, we focused on the separation of our analytes, how the selective turn-on/off responses influenced the separation, and whether we could differentiate between guests and their respective families. The PCA plot shows an overall great separation from our compounds with the ellipses for each of them being spread out and with minimal overlap. The plot does show some overlap exists between some of our guests like codeine with morphine, but this latter overlap can be explained due

to the structure similarity of the two. Other structural similar molecules like cocaine and benzoylecgonine don't show any overlap and are well separated. It should also be noted that this data only used fluorescence data from StiCx 09 and StiC07, with StiCx09 contributing very little to the variance. So, using only two sensors we are getting surprisingly good discrimination power, nearly as good as DimerDye systems that usually employ five sensors.

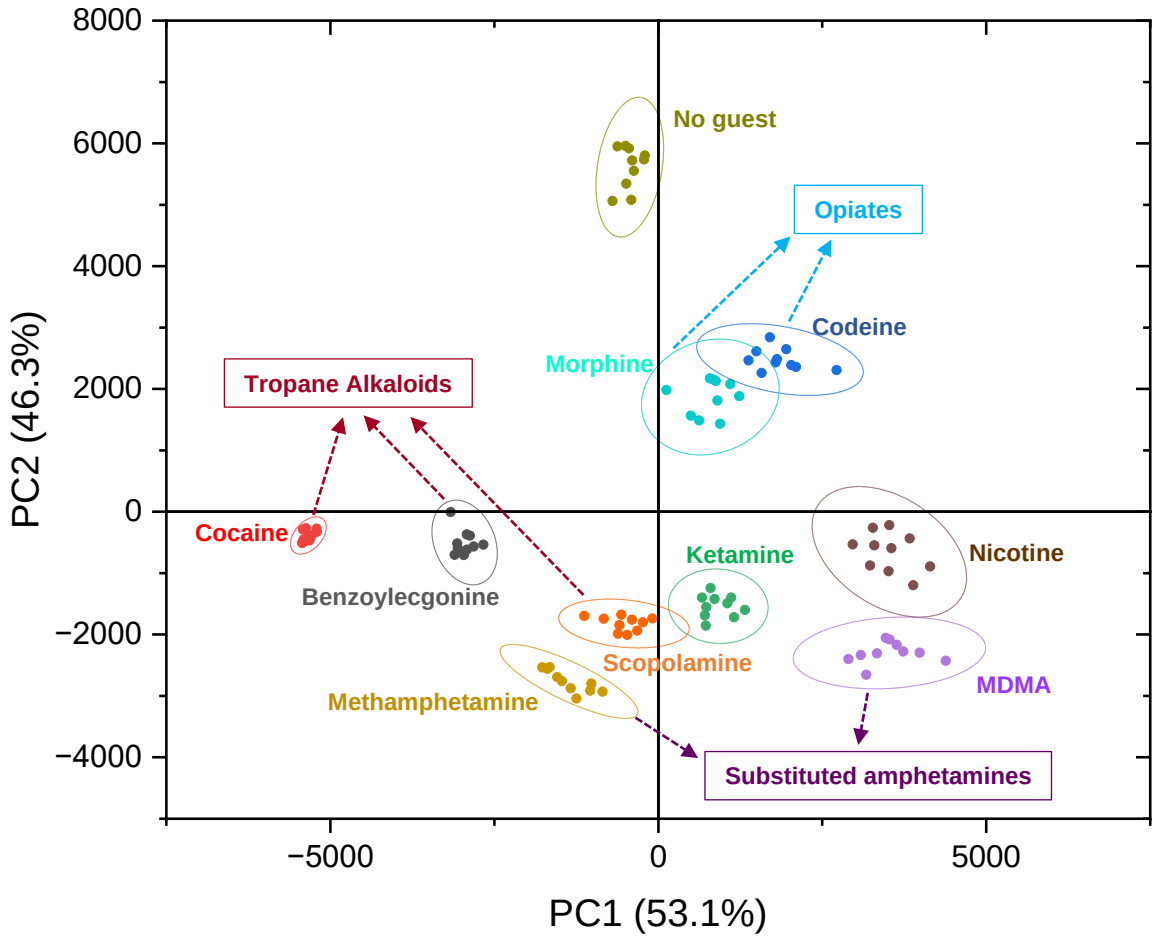

Figure 2.5: PCA plots of StiCx sensor array with 95% confidence ellipses. Separation among drug families can also be seen (dotted arrows). Datasets and parameters for building the plot can be seen in Section 2.4.3. Solutions were prepared at 8 µM host and 40 µM guest in a Sodium Phosphate buffer (75 mM, pH 7.4).

Now looking into the differentiation patterns, the most obvious one we could expect to see is a clear distinction between nicotine and cocaine, as they showed the opposite responses in

initial trials. We can see they are effectively well separated, being at nearly opposite ends of the graph. We can also see how differentiation is seen across the different families of compounds. Opiates are widely separated from all other families. Substituted amphetamines which consisted in this case of MDMA and methamphetamine also have good separation, with minimal overlap of MDMA with nicotine. Scopolamine is the only member of the tropane alkaloid family that intersects with another drug, in this case, ketamine. However, the other two, cocaine and benzoylecgonine, are also pretty well separated. These results are promising for a system that would want to differentiate between specific drugs in a mixture. For example, a common drug mixture is cocaine and opioids (commonly called "speedball") which can cause heightened symptoms than either drug by itself.[120] These systems could identify cross-contamination for a laced sample, ensuring purity and avoiding possible side effects or overdoses from unknowing users.

Overall, we have a system with good differentiation properties and specific behaviours from each sensor that we can take advantage of to give additional information. DimerDyes have already shown how we can exploit this system, and we only scratched the surface by exploring three potential candidates among the large set of possible stilbenes that we could introduce. Since the methyl ester (StiCx07) and cyano-substituted analogue (StiCx09) showed the strongest fluorescence emission and gave all the datasets necessary for discrimination, we can conclude that having electron-withdrawing groups on the top ring is beneficial to this system. It could be further improved by making and testing more candidates that fit within this category. Of course, to better understand the most appropriate paths to

pursue it is necessary to have a better understanding of the mechanism of fluorescence and how binding changes that fluorescence. Since StiCx09 has the highest emission intensity in the absence of guests, and the most distinctive turn-on and turn-off responses in the presence of different guests, we chose it as the best candidate on which to carry out these mechanistic studies and will report on this in Chapter 3.

2.3 Conclusions

We initially set out to obtain a small library of new sensors, and we did achieve the synthesis of such even though the exact identity of the target compounds changed due to an unexpected synthetic result. The stilbene calixarene (StiCx) compounds can be made using a novel two-step synthesis, which makes the synthesis and screening of a small library of compounds very efficient compared to earlier efforts. The new sensors generated new kinds of fluorescence responses depending on the host and/or guest used in the assay, and we showed that we could differentiate different drugs using a two-sensor array. Here are some of the main findings from this Chapter:

- Using a Sonogashira cross-coupling reaction on sCx4-Br yielded a stilbene derivative after an in situ semi-reduction of the intermediate alkyne product. Control experiments show calixarene plays a role in making the triple bond susceptible to this semi-reduction reactivity.
- A small library of stilbene calixarene (StiCx) derivatives was prepared using a two-step synthetic method. Preliminary assays allowed us to select three candidates with the most promising fluorescence properties.

- The tested candidates showed unique binding with a selective turn-on and turn-off response that is dependent on analyte identity. Cocaine showed a peculiar behaviour in its turn-off response, which it shares with its metabolite benzoylecgonine.
- PCA showed that a sensor array built from only two StiCx sensors gave enough information to differentiate between a variety of drug molecules.

There is room for improvement in the differentiation, and we anticipate that gaining insight into the mechanism of StiCx-based drug sensing could provide a basis for future improvements.

2.4 Experimental Procedure

2.4.1 Synthesis Procedures

2.4.1.1 Scaffold A synthesis

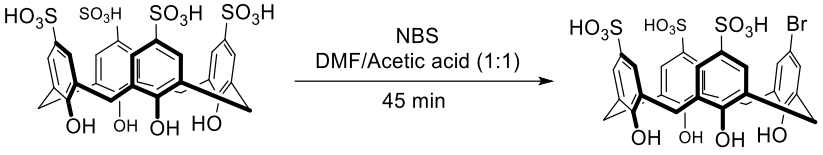

sCx4 (1.00 g, 1.34 mmol, 1 eq.) was added to a 250 mL round bottom flask and dissolved in approximately 100 mL of a 1:1 mixture of DMF and Acetic Acid. The system was sealed and purged three times with Nitrogen in a Schlenk line. Separately, freshly recrystallized NBS (107.5 mg, 0.6 mmol, 0.45 eq.) was dissolved in 5 mL of DMF/Ac. Acid mixture (1:1). This solution was immediately added to the round bottom drop by drop with a syringe. The mixture was allowed to stir at room temperature for 45 minutes. The reaction flask was then removed and the solvent evaporated under reduced pressure (to about < 5 mL volume). The crude was dissolved in a 90:10 H_2O/ACN (+0.1% TFA) mixture and purified in a preparative HPLC system and ran over a 10 min gradient (method parameters in Section 2.5.1). Product fractions were collected, ACN was removed by rotary evaporation and water by lyophilization to obtain Scaffold A as a solid white powder. Isolated yield: 260 mg (58%) calculated from NBS as limiting reagent. Starting sCx4 was recovered: 320 mg (32% yield). NMR and UPLC-MS data agree with previously synthesized samples (Figures S2.1-S2.2).

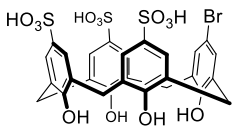

sCx4-Br. **^{1}H NMR (300 MHz, Deuterium Oxide)** δ 8.06 (s, 2H), 7.61 (d, *J* = 2.1 Hz, 2H), 7.54 (s, 2H), 6.16 (s, 2H), 4.23 (s, 2H), 3.88 (s, 2H), 3.68 (s, 4H). **UPLC-MS:** Found 743.1 (calculated for **$C_{28}H_{22}O_{13}S_3^{-1}$ [M-H]$^{-1}$** = 742.56).

2.4.1.2 General procedure for Sonogashira cross-coupling with semi-reduction

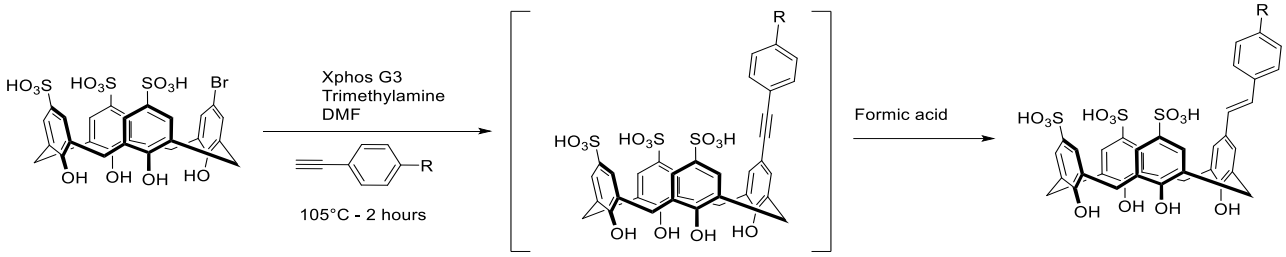

sCx4-Br (100 mg, 0.13 mmol, 1 eq) was weighed and transferred to an oven-dried microwave vial, to the vial the corresponding alkyne analogue (0.54 mmol, 4 eq) and XPhos Pd G3 (0.03 g, 0.04 mmol, 0.3 eq) were added. Vials were filled with nitrogen and clamped to seal. Triethylamine (682 µL, 6.72 mmol, 50 eq) was dissolved in 1 mL of DMF and added to the reaction vial with a syringe. A nitrogen balloon was attached to the vial and the reaction was stirred at 105°C for two hours. A solution of formic acid (6.3 µL, 0.17 mmol, 1.25 eq) was prepared by dissolving in 0.5 mL of DMF and then added to the reaction vial. The mixture was stirred for an additional hour at 85°C. After this time, the vial was allowed to cool to room temperature, and then the crude was transferred into a Falcon tube where the calixarene was precipitated by the addition of approximately 30 mL of cold toluene and then centrifuged for 10 minutes at 3000 RPM. The supernatant was discarded, and the crude was then purified by reverse HPLC where the pellet was dissolved in a water-acetonitrile mixture (90:10 + 0.1%TFA) run over a 10 min gradient (Full method is available in Section 2.5.1). HPLC fractions were collected and then the sample was concentrated using a centrifugal evaporator (Genevac) to obtain a solid product.

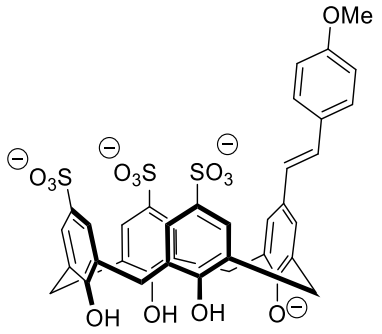

CCS03. Obtained as a dark grey/black solid powder. Isolated yield: 34%. Mp: >201C° (decomposed). **IR (ATR, cm^{-1}):** 3191.9 w br, 2925 w, 1594 w, 1510 w, 1492.1 m, 1209.6 m, 1109.4 s, 1033.7 s, 885.1 m, 810.8 m, 784.3 m, 653.3 s, 623.9 s, 544.6 s. **^{1}H NMR (500 MHz, Methanol-*d*$_4$):** δ 7.68 (d, *J* = 2.2 Hz, 2H), 7.65 (s, 2H), 7.61 (d, *J* = 2.2 Hz, 2H), 7.44 (d, *J* = 8.6 Hz, 2H), 7.35 (s, 2H), 6.99 (d, *J* = 16.3 Hz, 1H), 6.90 (d, *J* = 8.6 Hz, 2H), 6.86 (d, *J* = 16.4 Hz, 1H), 4.03 (s, 8H), 3.80 (s, 3H), 2.18 (q, *J* = 7.3 Hz, TEA), 0.22 (t, *J* = 7.3 Hz, TEA). **^{13}C NMR (126 MHz, MeOD)** δ 159.3, 151.9, 151.4, 148.8, 131.7, 130.3, 128.5, 128.0, 127.7, 127.6, 127.1, 126.8, 126.7, 126.6, 126.4, 125.2, 113.7, 54.3, 46.0 30.6, 30.6, 6.8. **HRMS:** Found 797.10274 (calculated for **$C_{37}H_{33}O_{14}S_3^{+1}$ [M+H]$^{+1}$** = 797.10270).

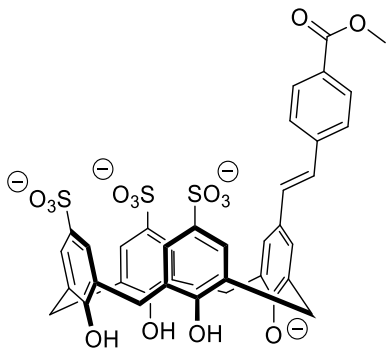

CCS07. Obtained as a light brown/beige solid powder. Isolated yield: 26%. Mp: >242C° (decomposed). **IR (ATR, cm^{-1}):** 3158, w br, 2946.1 w, 2853 w, 1704, w, 1597, w, 1452 w, 1275 m, 1212 m, 1154 m, 1109 s, 1035 s, 961.8 m, 886.9 m, 623 s, 546 s. **^{1}H NMR (500 MHz, Methanol-*d*$_4$):** δ 7.98 (d, *J* = 8.1 Hz, 2H), 7.67 (d, *J* = 6.9 Hz, 4H), 7.64 – 7.58 (m, 4H), 7.45 (s, 2H), 7.15 (q, *J* = 16.4 Hz, 2H), 3.97 (m (br), 11H), 2.19 (q, *J* = 7.1 Hz, TEA), 0.23 (t, *J* = 7.3 Hz, TEA). **13C NMR (126 MHz, MeOD):** δ 167.0, 151.9, 151.2, 149.9, 142.5, 130.6, 130.4, 129.6, 128.4, 128.2, 128.2, 127.7, 127.6, 127.6, 127.5, 126.8, 126.8, 126.6, 125.8, 125.4, 113.5, 51.2, 46.0, 30.7, 30.6, 6.8. **HRMS:** Found 825.09754 (calculated for **$C_{38}H_{33}O_{15}S_3$ [M+H]$^{+1}$** = 825.09761).

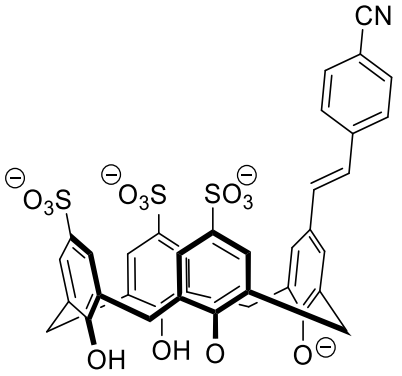

CCS09. Obtained as a pale-yellow solid powder. Isolated yield: 25%. Mp: >237C° (decomposed). **IR (ATR, cm^{-1}):** 3185 w br, 3172 w, 2229 w, 1670 w br, 1597 w, 1453 w, 1264 m, 1132 s, 1111 s, 1038 s, 785 m, 654 s, 626 s, 552 s. **^{1}H NMR (500 MHz, Methanol-*d*$_4$)**: δ 7.71 – 7.62 (m, 8H), 7.60 (d, 2H), 7.45 (s, 2H), 7.21 (d, *J* = 16.4 Hz, 1H), 7.10 (d, *J* = 16.4 Hz, 1H), 4.19 – 3.84 (s (br), 8H), 2.21 (q, *J* = 7.3 Hz, TEA), 0.23 (t, *J* = 7.3 Hz, TEA). **^{13}C NMR (126 MHz, MeOD):** δ 152.2, 151.4, 150.2, 142.6, 132.2, 132.2, 131.5, 130.3, 128.3, 128.2, 127.7, 127.7, 127.6, 127.6, 126.8, 126.8, 126.6, 126.5, 124.7, 118.6, 109.5, 46.0, 30.6, 30.6, 6.8. **HRMS:** Found 792.08724 (calculated for **$C_{37}H_{30}NO_{13}S_3$ [M+H]$^{+1}$** = 792.08738).

2.4.1.3 General procedure for Stilbene control dyes

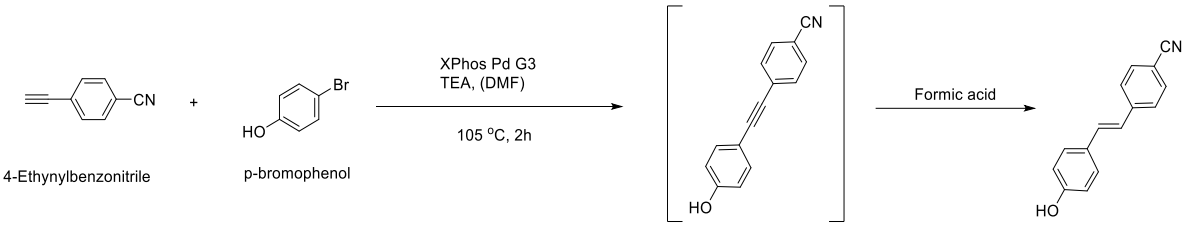

Bromophenol (175 mg, 1 mmol, 1 eq.) and phenylacetylene (1.2 mmol, 1.2 eq.) were weighed and added to an oven-dried reaction vial. Under an inert atmosphere (flow of nitrogen or inside a glovebox) XPhos Pd G3 (4.2 mg, 0.005 mmol, 0.005 eq.) was added. A solution of TEA (210 µL, 1.5 mmol, 1.5 eq.) on DMF (1 mL) was prepared. The solution was slowly added to the reaction vial and stirred in an oil bath at 105°C for two hours. To carry out the semi-reduction a mixture of formic acid (48 µL, 1.25 mmol, 1.25 eq.) in 0.5 mL

of DMF was prepared and added to the reaction vial. The reaction was then left stirring for an additional hour at 80°C.

The reaction was then removed from heat and allowed to cool down to room temperature. 3 mL of water was then added to quench the mixture. The solution was extracted 3 times with diethyl ether. The organic layer was dried over Magnesium Sulfate and the solvent was removed under reduced pressure. The crude was purified using a BIOTAGE with a 25g Silica column and run over a 10-minute gradient in a hexane/ethyl acetate mixture (See method details in Section 2.5.1). Separation was assessed by TLC and product identity was checked with ^{1}H NMR. Respective fractions were collected and the solvent was removed to obtain the corresponding solid.

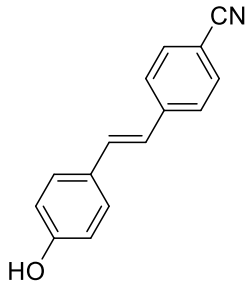

Sti09: Obtained as a brown solid poder. Isolated yield: 8%. **^{1}H NMR (500 MHz, Methanol-*d*$_4$):** δ 7.66 (s, 4H), 7.46 (d, *J* = 8.6 Hz, 2H), 7.28 (d, *J* = 16.4 Hz, 1H), 7.03 (d, *J* = 16.3 Hz, 1H), 6.81 (d, *J* = 8.7 Hz, 2H). **^{13}C NMR (500 MHz, MeOD):** δ 158.0, 142.9, 132.2, 132.1, 130.5, 128.1, 126.3, 123.3, 118.7, 115.2, 115.0, 109.2, 48.1, 47.9, 47.8, 47.6, 47.4, 47.3, 47.1. **HRMS:** Found 220.07691 (calculated for **$C_{15}H_{10}NO$ [M-H]$^{-1}$** = 220.07679).

2.4.2 Fluorescence titrations of StiCx 03, 07 and 09.

Direct titrations of drug guests into StiCx sensors were done in triplicate in black 384-well plates with clear bottoms. Stock solutions of StiCx analogues and drug guests were prepared in milli-Q water, and stocks of Sti analogues were prepared in methanol. All final solutions were tested in NaH_2PO_4/Na_2HPO_4 buffer water system (10 mM, pH 7.4). Concentrated stock solutions were prepared separately and then mixed appropriately to obtain desired final concentrations, which were then transferred into the 384-well plates to a final volume of 50 μL. UV-Vis spectra were taken of hosts and the absorbance maxima was used as the wavelength of excitation for all trials. Host concentration was kept constant at 8 μM and titrations were then run using a guest concentration range of 0-50 equivalents of guest. All spectra shown are blank subtracted spectra where the blank is the buffered water solution with no host or guest added. To plot binding curves, the maximum emission intensity of each trial was taken and plotted against guest concentration.

2.4.3 Principal Component Analysis (PCA) plots

PCA plots were built from fluorescence spectra taken in solution with a fixed concentration of 8 μM host and 20 μM guest. For this one host and one guest were mixed in 384 well plates to a max volume of 50 μL and twelve replicates were run of these solutions under the same buffer water system of NaH_2PO_4/Na_2HPO_4 (10 mM, pH 7.4). Absorbance and fluorescence spectra are taken and of the twelve replicates ten are selected by removing the highest and lowest intensities. The spectra taken for each compound are the following:

- StiCx03: UV-Vis spectra and Fluorescence spectra with λ_{ex} 290 nm and λ_{ex} 340 nm
- StiCx07: UV-Vis spectra and Fluorescence spectra with λ_{ex} 340 nm.
- StiCx09: UV-Vis spectra and Fluorescence spectra with λ_{ex} 340 nm

Data is processed with GraphPad Prism to generate the principal components via PCA, and then graphs are generated in Origin to make plots of replicates with 95% confidence ellipses for the identification of each analyte. The data points selected to use in the PCA where the wavelength maxima showed the most significant differences, both in absorbance and fluorescence. These points were selected based on resulting PCA plots and optimized to obtain the best degree of separation; using PCA loading graphs (Figure S2.16) redundant datasets were also eliminated. The points in the spectra taken for analysis on the PCA were as follows for each compound:

- StiCx07: RFU at 535 nm (λ_{ex} 340 nm), RFU at 555 nm (λ_{ex} 340 nm), RFU at 565 nm (λ_{ex} 340 nm) and RFU at 575 (λ_{ex} 340 nm)
- StiCx09: RFU at 545 nm (λ_{ex} 340 nm), RFU at 575 nm (λ_{ex} 340 nm) and RFU at 585 nm (λ_{ex} 340 nm).
- StiCx03: This compound didn't provide much contribution to the separation so no detailed datasets were taken for this one.

2.5 Supporting information

2.5.1 General considerations

Proton ^{1}H and Carbon ^{13}C NMR were recorded in a Bruker Avance Neo 500 MHz spectrometer or Bruker AV300 MHz spectrometer and processed with MestReNova or TopSpin 3.6. Infrared (IR) spectra were obtained in a Perkin Elmer Spectrum-2 (ATR-FTIR). Melting points were taken on a Gellenkamp Melting Point Apparatus. High-resolution mass spectra were taken in a Thermo Scientific Ultimate 3000 ESI-Orbitrap Exactive. Reagents for synthesis were purchased from either Sigma-Aldrich or TCI chemicals and used as received.

HPLC purification of library of host analogues was carried out in Teledyne ACCQPrep HP125 HPLC system on a Phenomenex Luna C18(2) column (21.2 mm x 250 mm) with 5 μm particle and 100 Å pore size. The gradient consisted of water and acetonitrile, both spiked with 0.1% of TFA, and a DAD detector set to 280 nm was used. Samples were dissolved in a 90:10 mixture of H_2O/ACN (0.1% TFA), centrifuged and pre-filtered using Captiva Premium Syringe filters with a 0.45 μm PES membrane. Gradients started with a 90:10 H_2O/ACN hold for a minute, and then it switched to a 10:90 H_2O/ACN over the course of usually 10 minutes (gradient time was adjusted depending on peak retention time).

Stock solutions of hosts were prepared by dissolving them in Milli-Q water. Guest solutions of nicotine and benzoylecgonine were prepared in the same way, using purchased reagents and dissolveing appropriate amounts in water for a stock solution. All other guests were purchased from Sigma-Aldrich as ampules of a 1 mg/mL solution in methanols which was evaporated under a gentle flow of Nitrogen, after which the solid compound was redissolved in Milli-Q water to make stock solutions. UV-Vis and fluorescence spectra were collected in ThermoFisher 384 Well Black Plate with optically clear polymer bottom and read in a BioTek Cytation 5 Multimode Plate Reader.

2.5.2 Characterization data

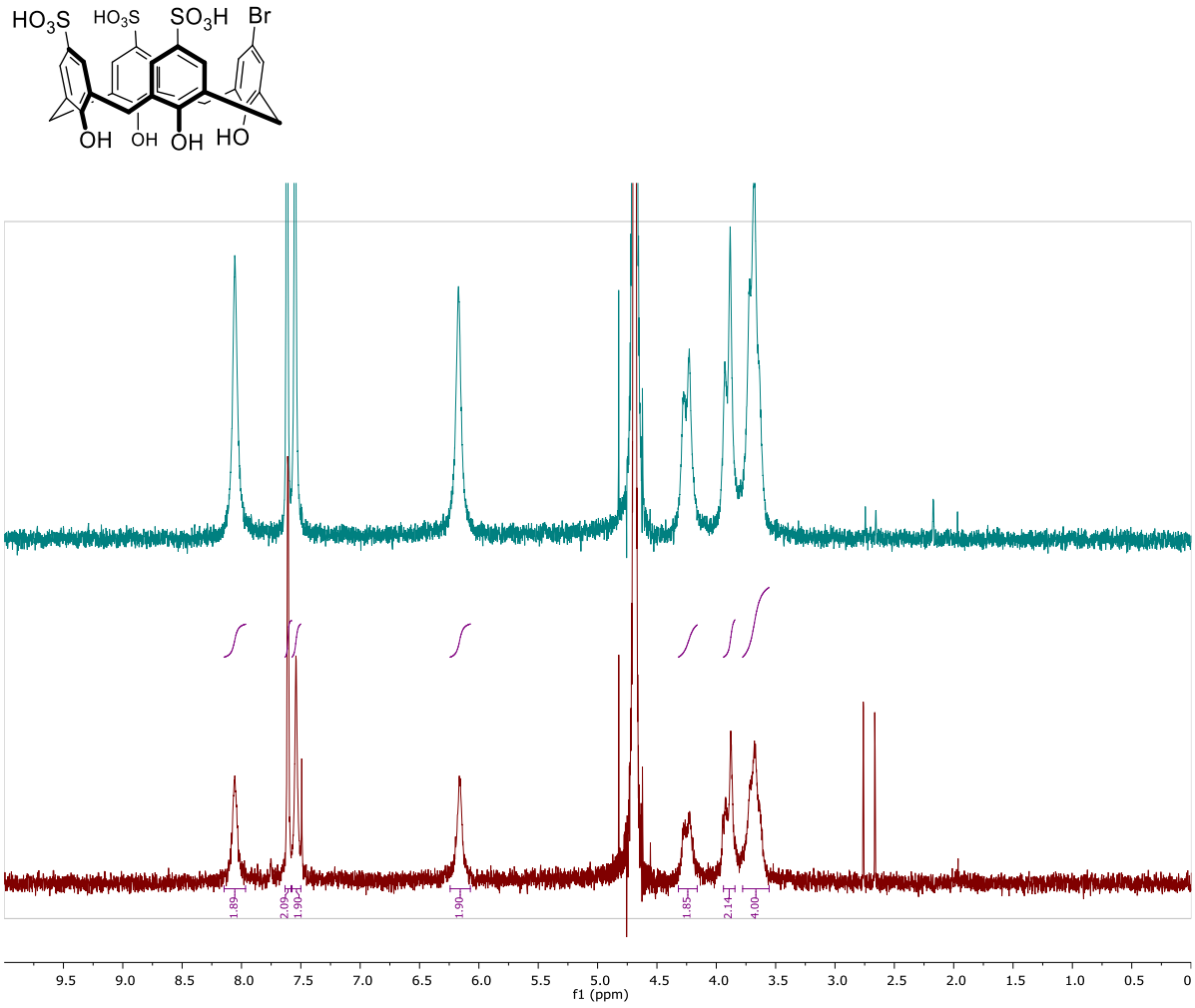

Figure S2.1: ^{1}H-NMR spectra of sCx4-Br in D_2O (Bottom-Red). Stacked spectra with previously stored sample (Top-Blue).

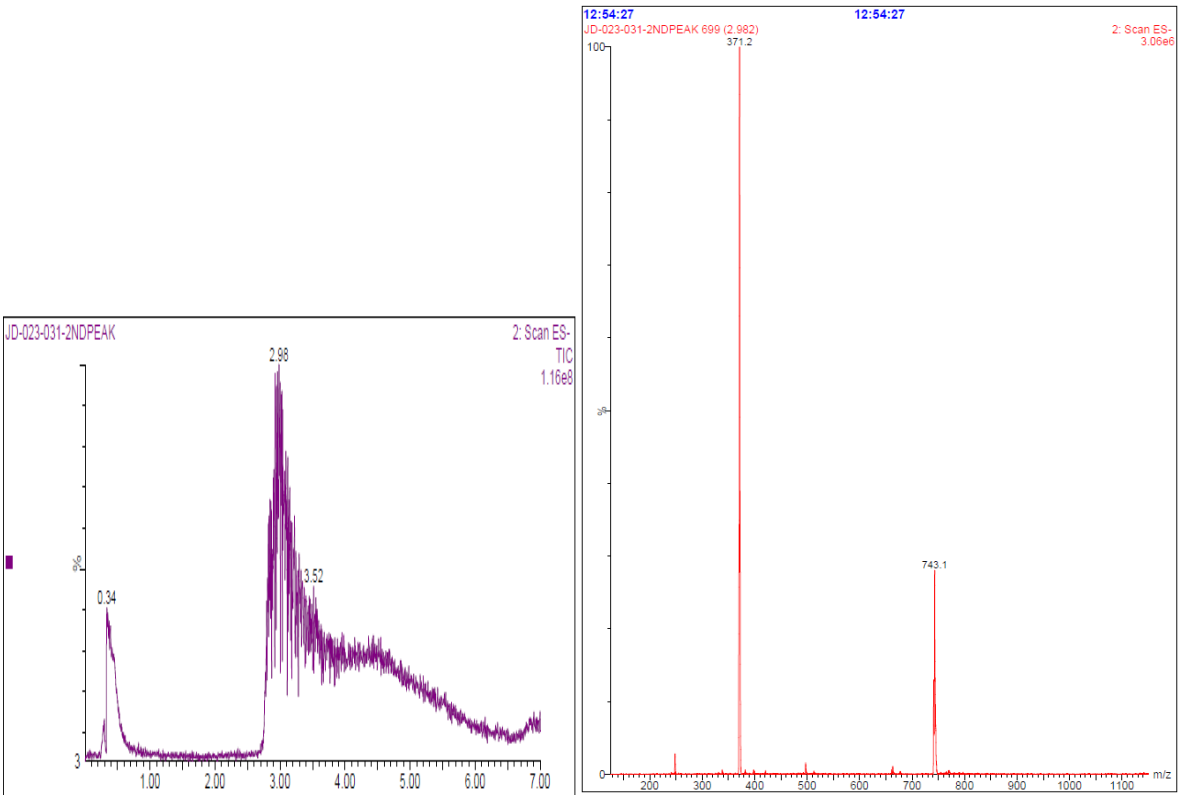

Figure S2.2: UPLC-MS traces confirming synthesis of sCx4-Br.

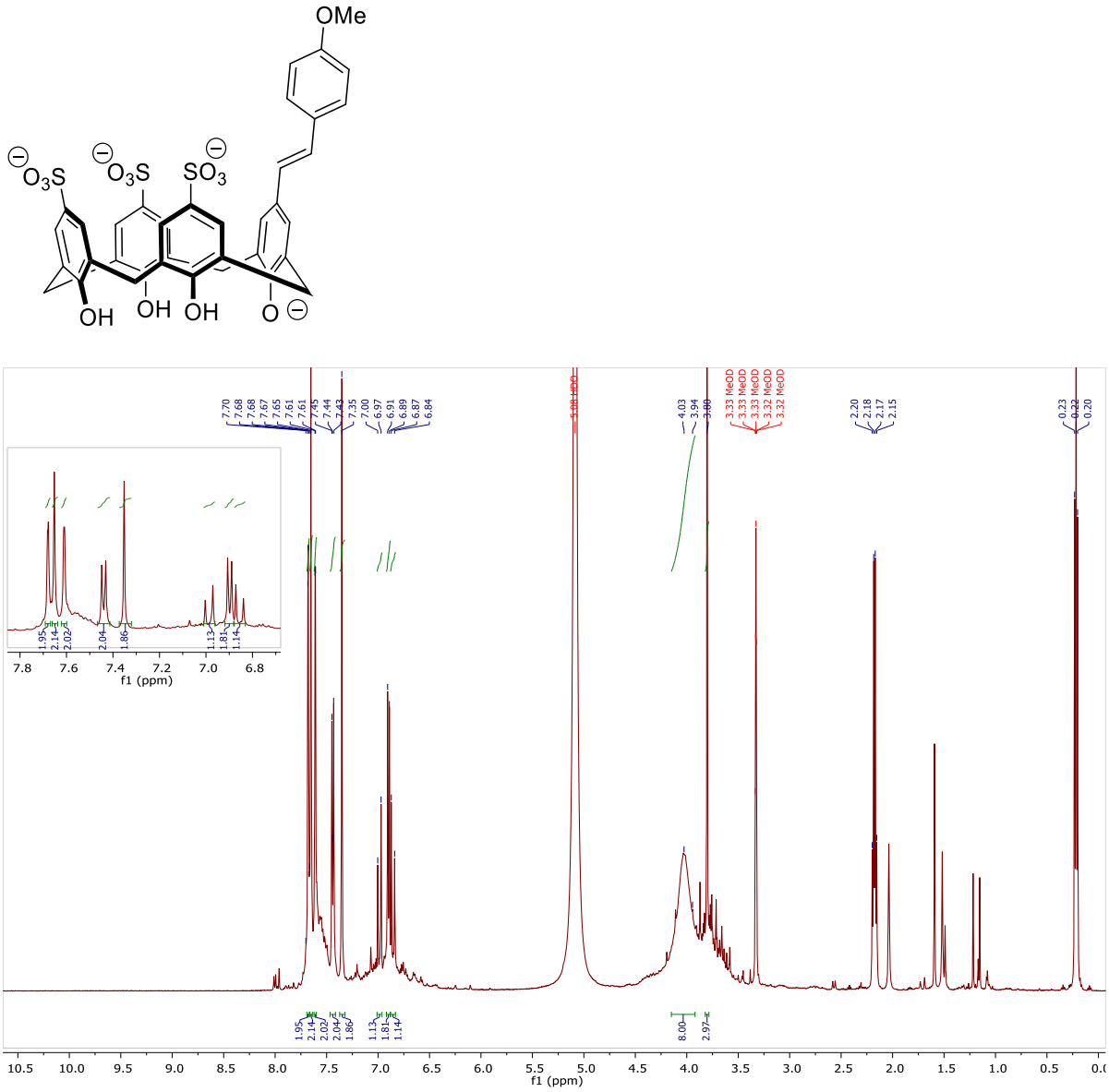

Figure S2.3: [1]H-NMR of StiCx03 in MeOD. Large solvent signals are attributed to TEA. HPLC trace shows 91% purity.

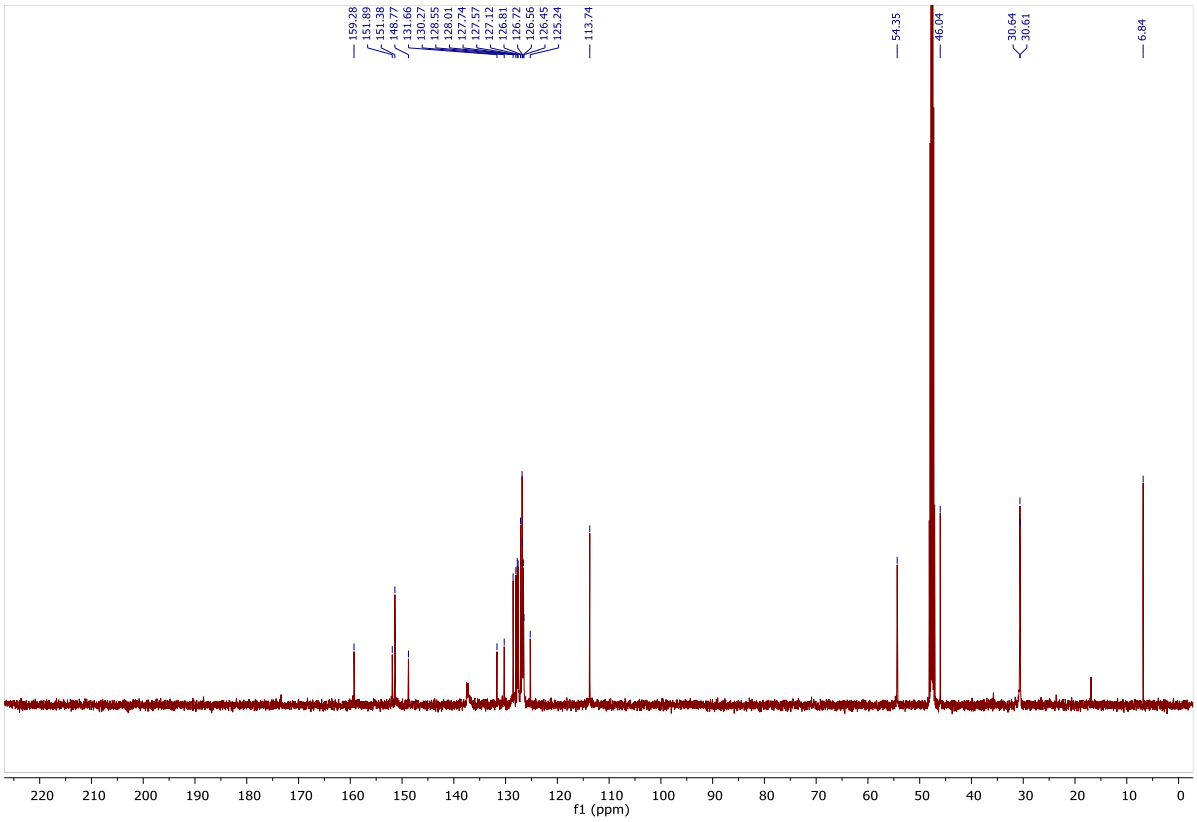

Figure S2.4: ^{13}C-NMR spectra of StiCx03 in MeOD.

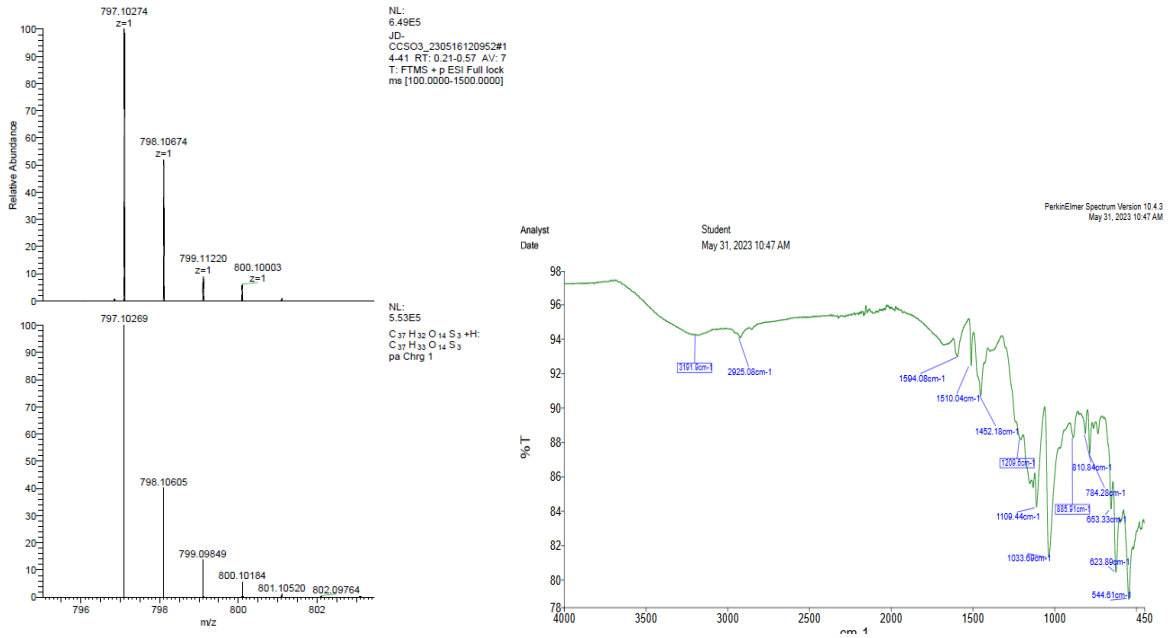

Figure S2.5: HRMS Spectra (left) and IR spectra (right) of StiCx03.

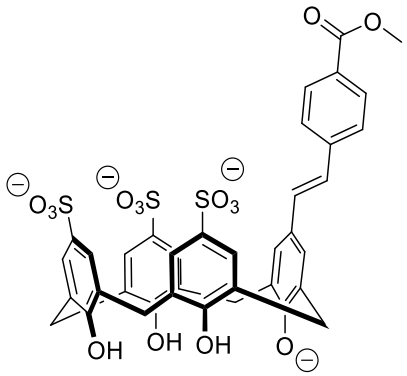

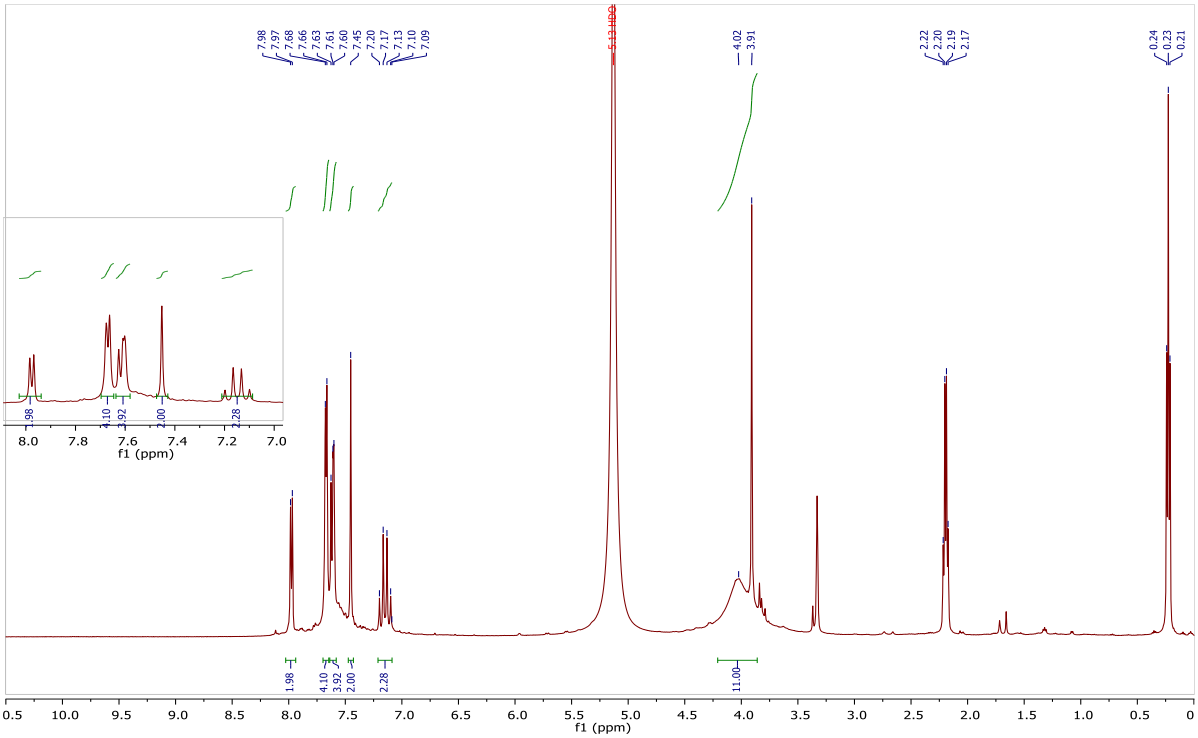

Figure S2.6: [1]H-NMR of StiCx07 in MeOD. Large solvent signals are attributed to TEA. HPLC trace shows 97% purity.

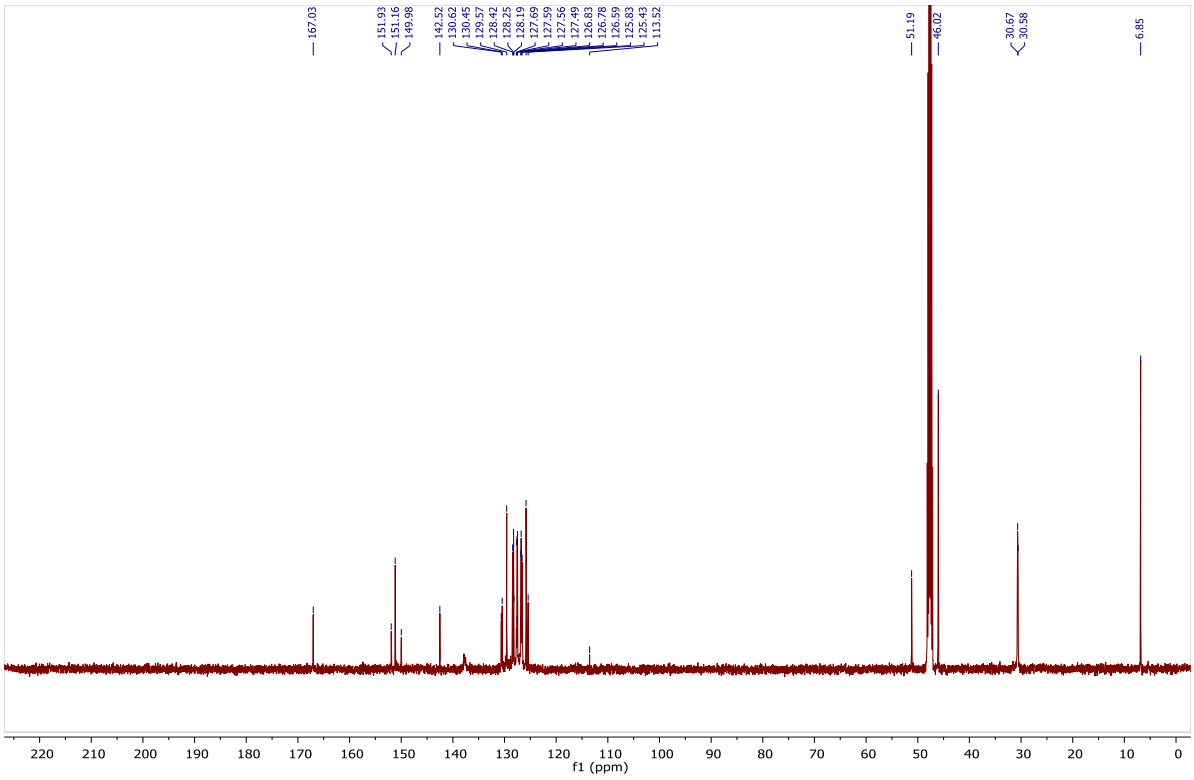

Figure S2.7: ^{13}C-NMR spectra of StiCx07 in D_2O.

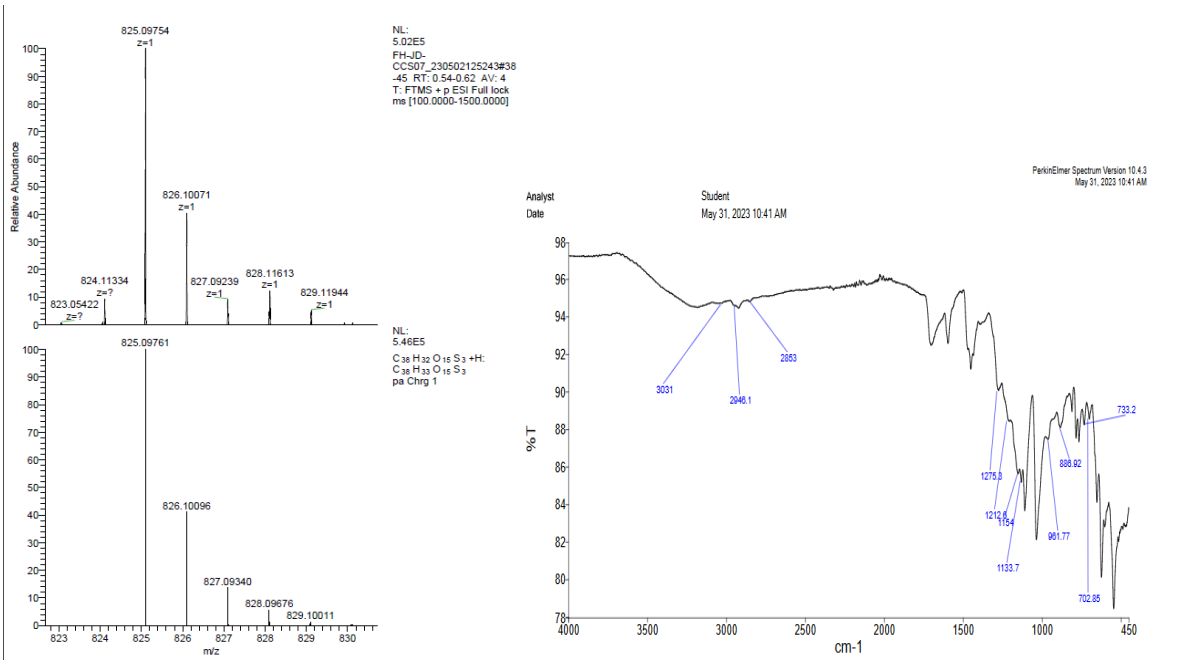

Figure S2.8: HRMS Spectra (left) and IR spectra (right) of StiCx07.

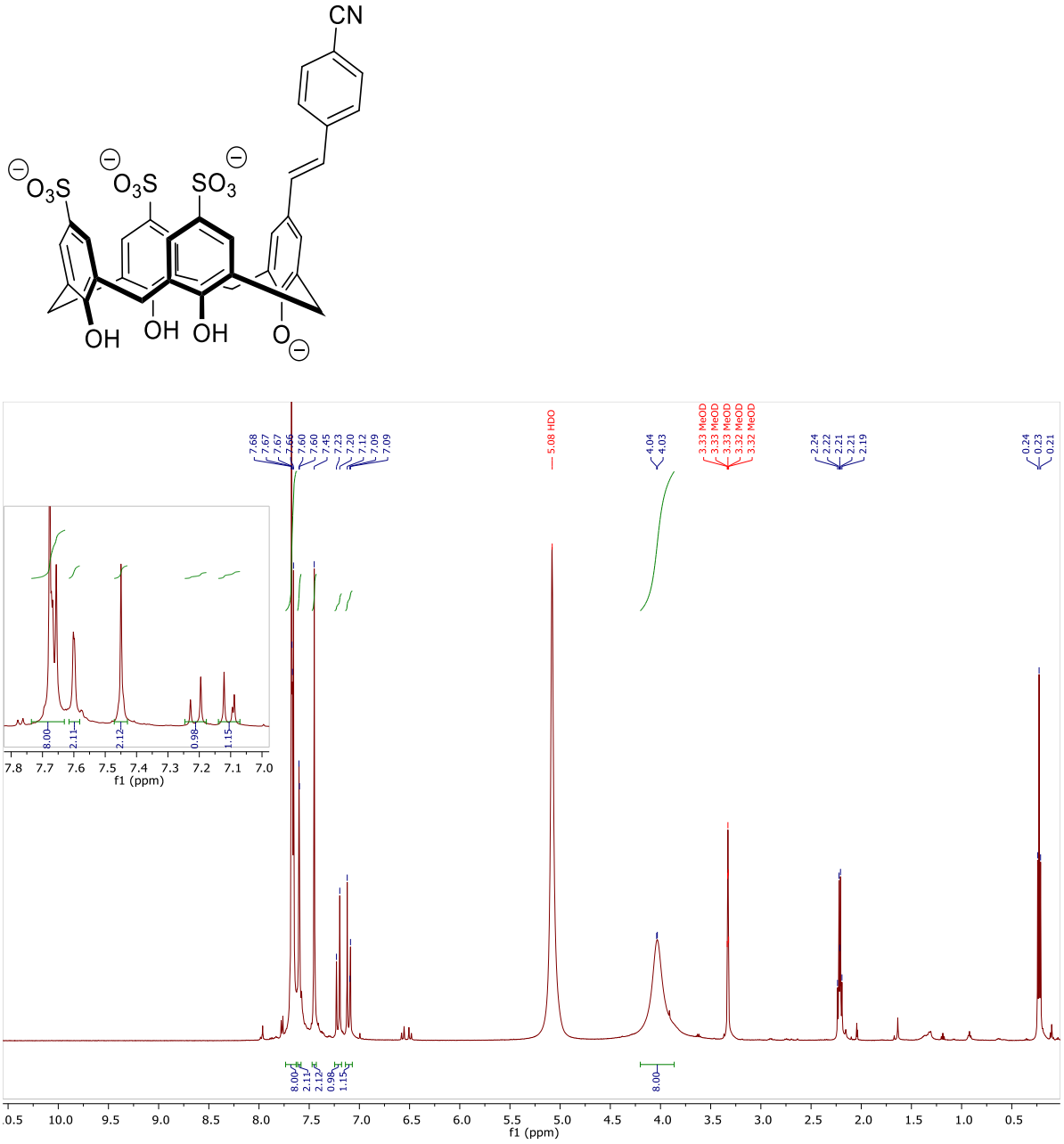

Figure S2.9: ^{1}H-NMR of StiCx09 in D_2O. Large solvent signals are attributed to TEA. HPLC trace shows 92% purity.

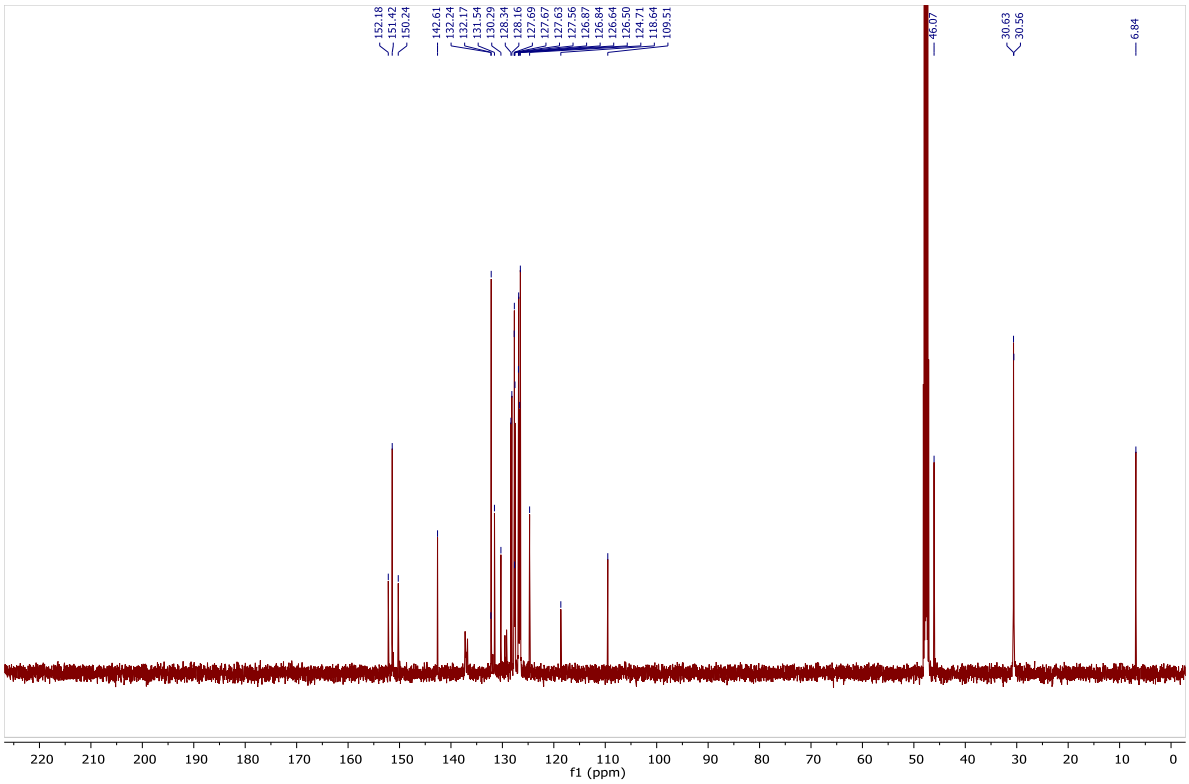

Figure S2.10: ^{13}C-NMR spectra of StiCx09 in D_2O.

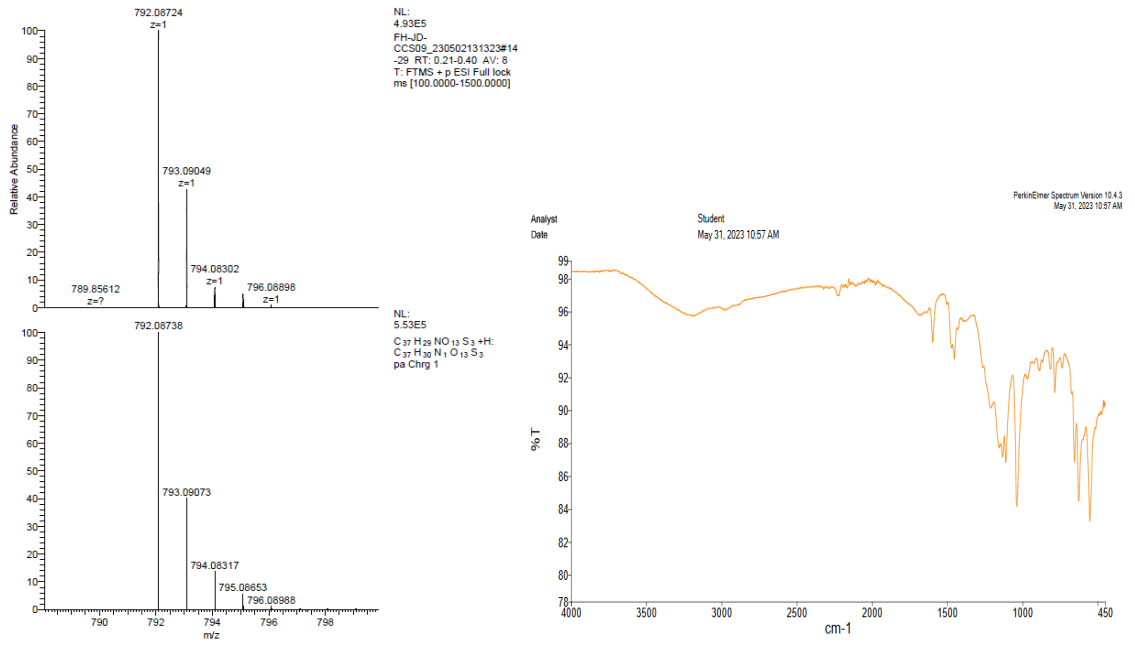

Figure S2.11: HRMS Spectra (left) and IR spectra (right) of StiCx09.

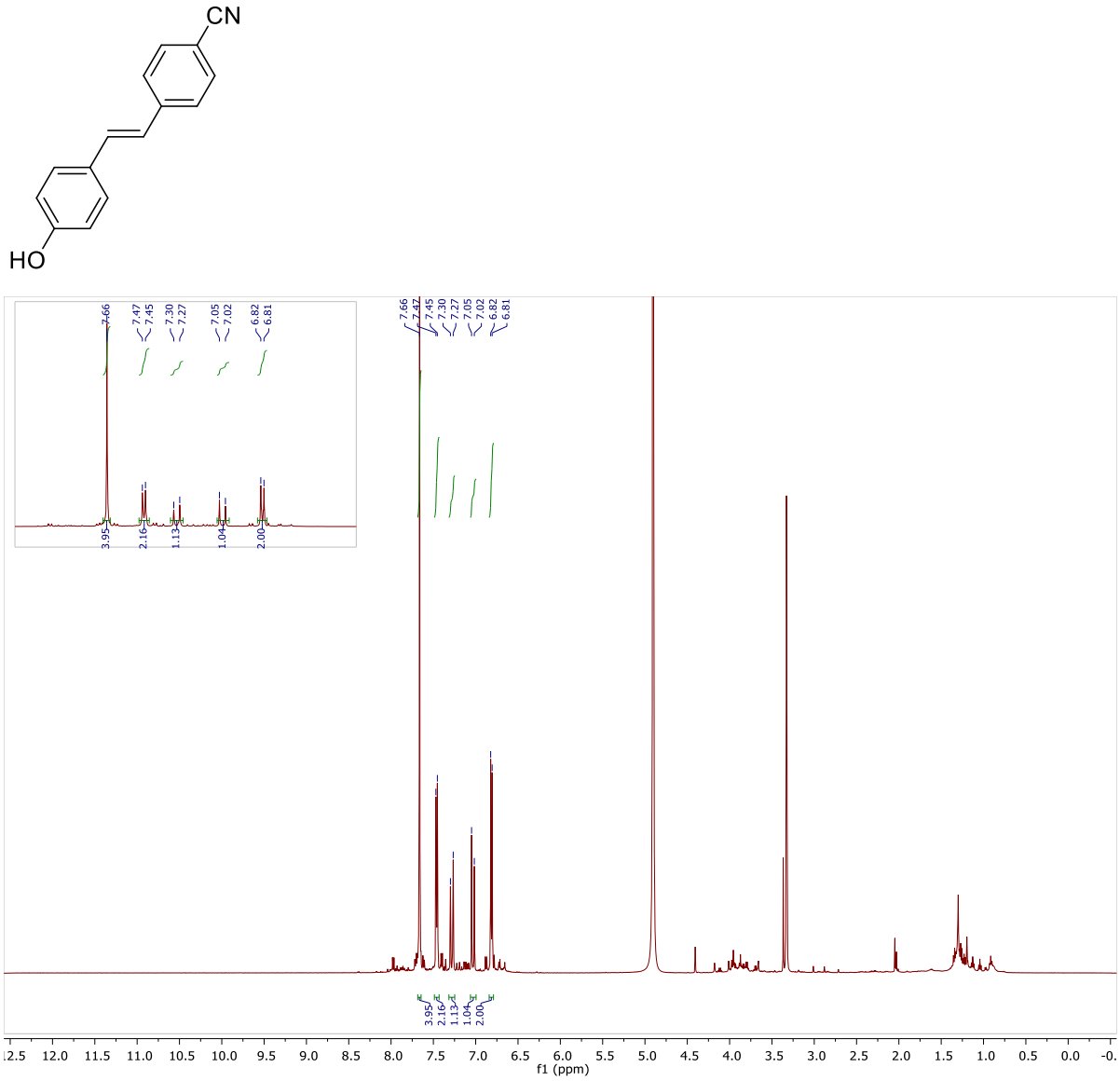

Figure S2.12: [1]H-NMR of Sti09 in MeOD. Solvent signal in 4.91 ppm is due to a sequence error in the NMR instrument, DMSO setting had to be used. Trace solvents from biotage are seen. NMR integration shows 97% purity.

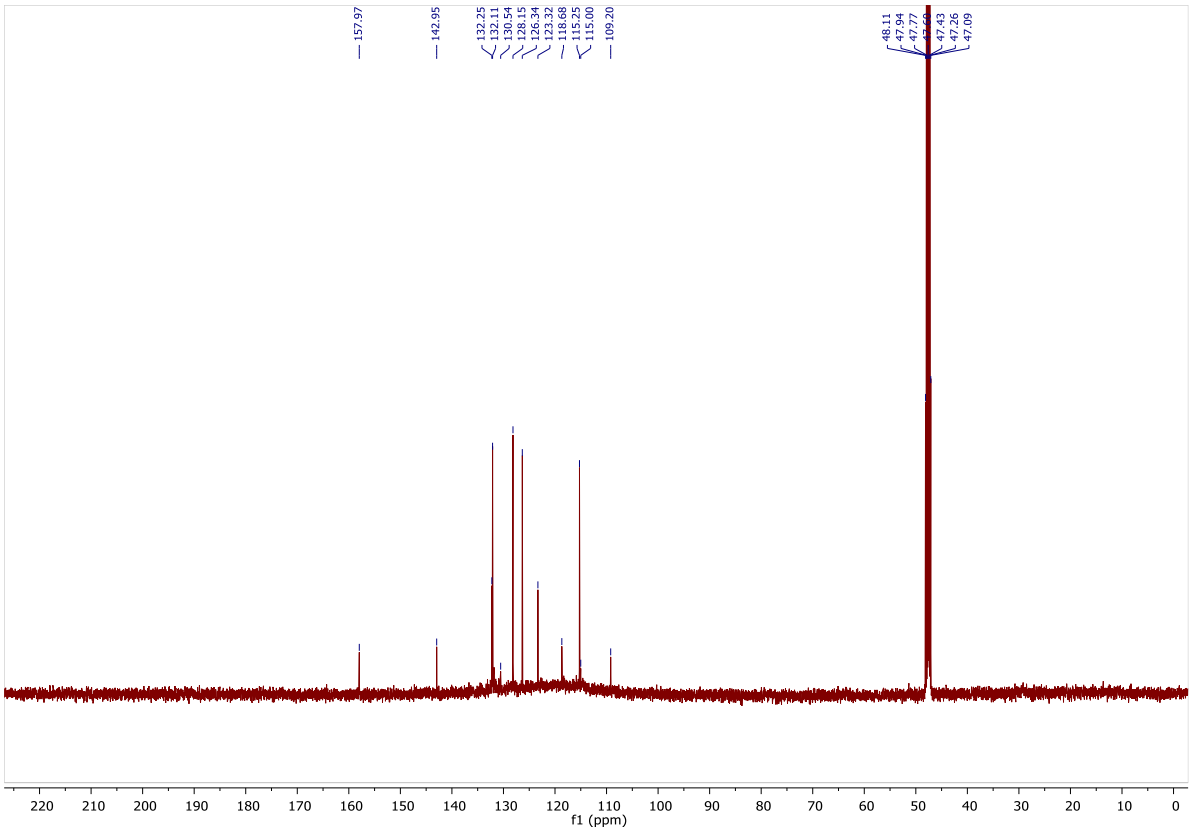

Figure S 2.13: ^{13}C-NMR spectra of Sti09 in MeOD.

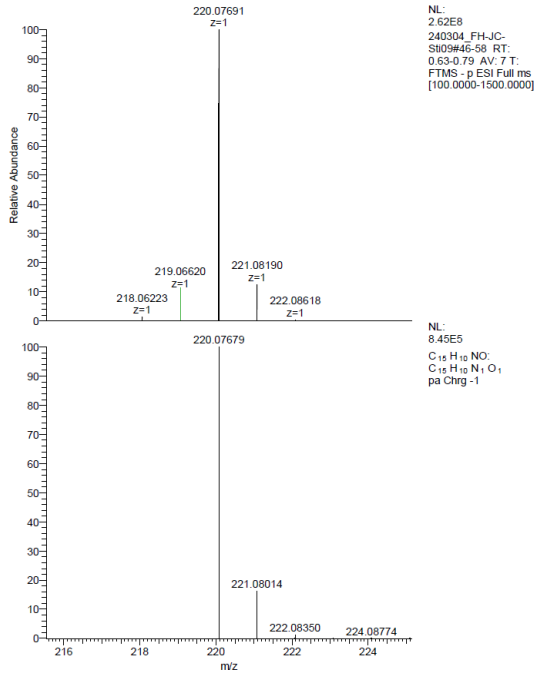

Figure S2.14: HRMS spectra of Sti09.

2.5.3 Absorbance and fluorescence measurements

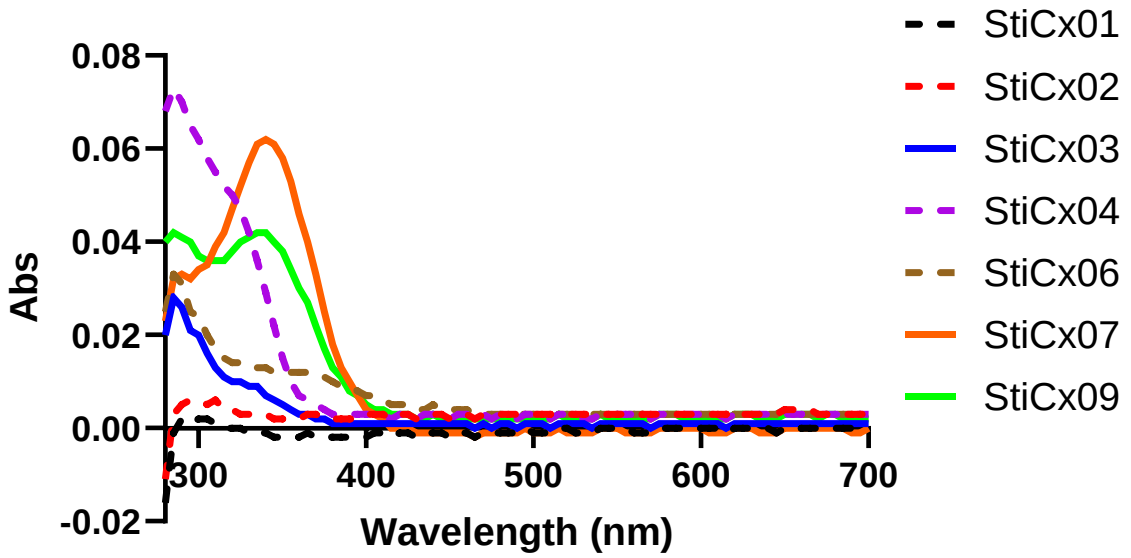

Figure S2.15: UV-Vis spectra of the synthesized library in sodium phosphate buffer (100 mM, pH 7.4). Top three candidates are highlighted to show high absorbance values. All hosts are at 8 µM concentration.

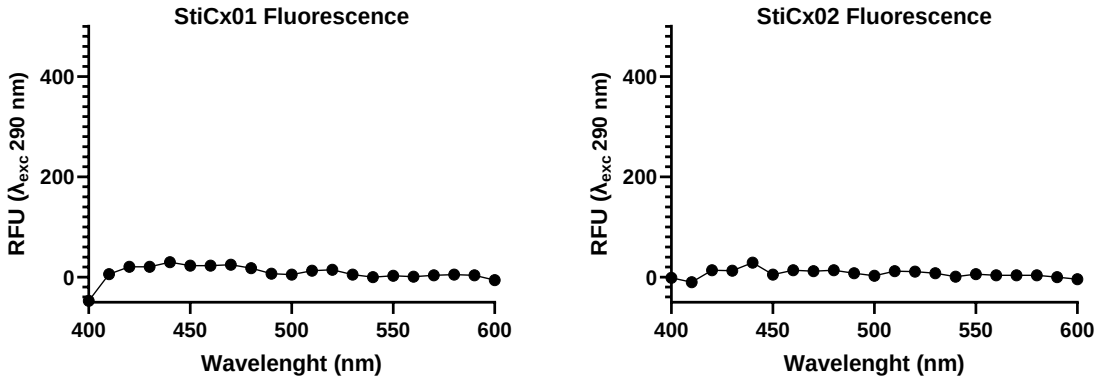

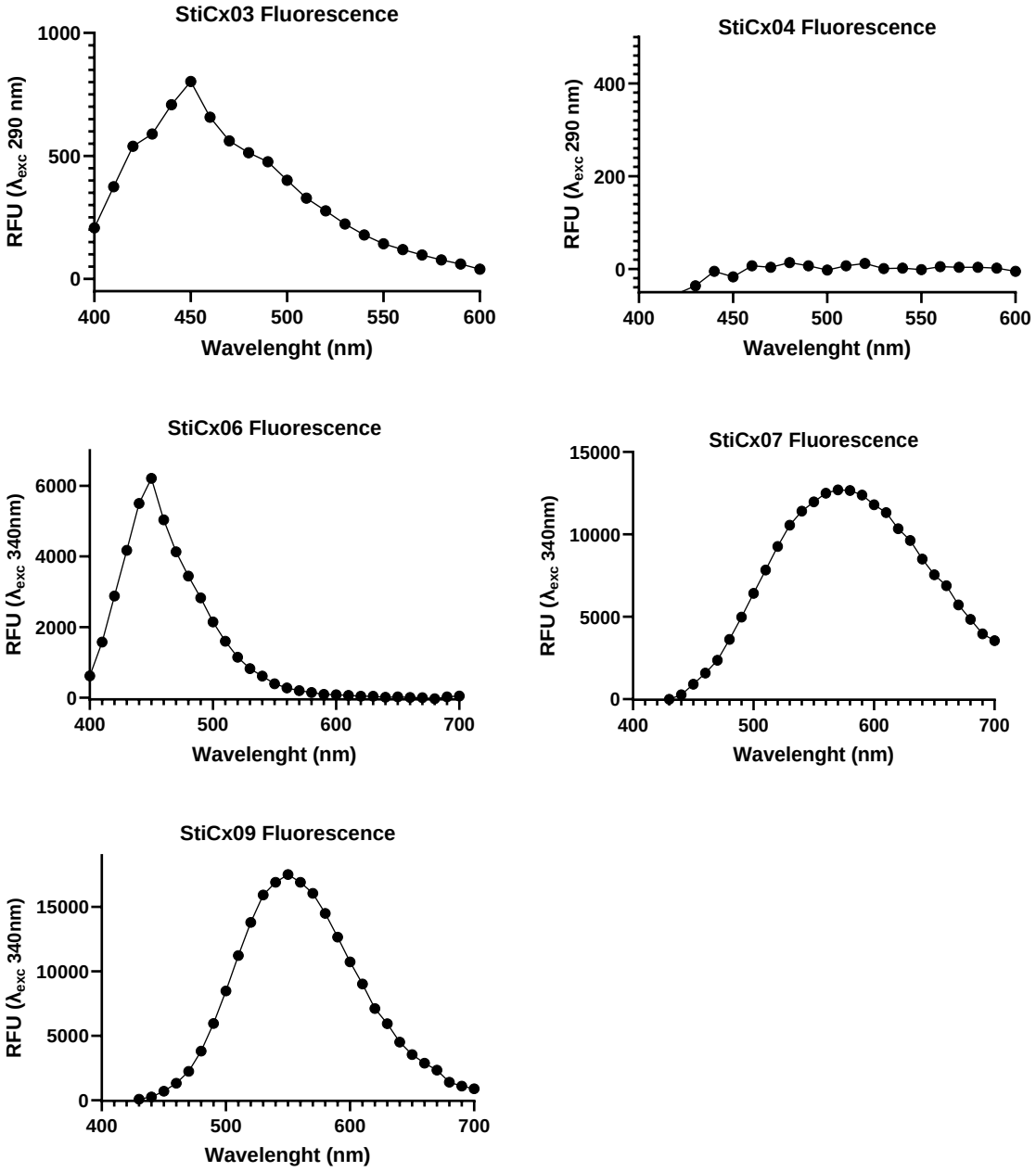

Figure S2.16: Fluorescence spectra of synthesized library compounds at 8 µM in sodium phosphate buffer (100 mM, pH 7.4). The Y-axis shows wavelengths of excitation for each compound.

2.5.4 PCA Experiments

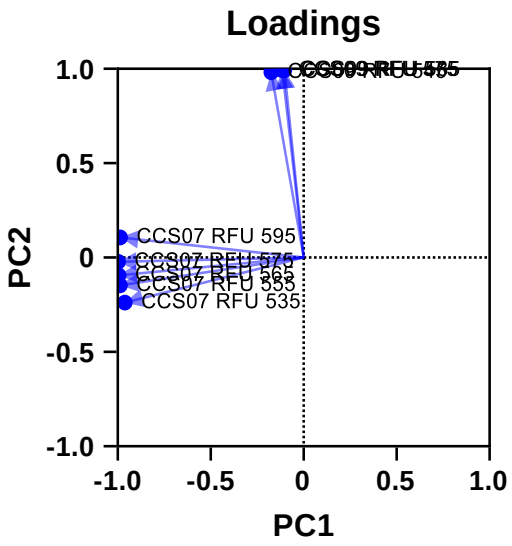

Figure S 2.17: Loading plots for the PCA graphs.

Table S2.1: Fluorescence data points used to construct PCA.

Guest	CCS09 (λ_{ex} 340nm) RFU (545 nm)	CCS09 (λ_{ex} 340nm) RFU (575 nm)	CCS07 (λ_{ex} 340nm) RFU (565 nm)	CCS07 (λ_{ex} 340nm) RFU (575 nm)	CCS07 (λ_{ex} 340nm) RFU (595 nm)	CCS03 (λ_{ex} 340nm) RFU (425 nm)	CCS07 (λ_{ex} 340nm) RFU (535 nm)	CCS07 (λ_{ex} 340nm) RFU (555 nm)	CCS09 (λ_{ex} 340nm) RFU (585 nm)
Nicotine	7139	5991	2755	3018	3221	119	1788	2496	5369
Nicotine	6811	5708	3044	3298	3383	152	1833	2693	5028
Nicotine	7134	6194	3018	3228	3290	146	1816	2753	5403
Nicotine	6625	5539	3027	3227	3409	76	1844	2640	4944
Nicotine	6931	5823	3181	3426	3489	81	1911	2800	5142
Nicotine	6845	5850	2895	3105	3179	127	1758	2494	5040
Nicotine	6404	5450	2966	3150	3297	124	1821	2661	4723
Nicotine	6719	5494	2856	3082	3182	30	1771	2501	5012
Nicotine	6592	5613	3221	3410	3571	166	2003	2815	5083
Nicotine	6530	5438	3117	3408	3441	122	1944	2803	4937
Cocaine	1374	1130	1588	1677	1658	43	1133	1493	946
Cocaine	1318	1021	1540	1543	1487	24	1035	1366	873
Cocaine	1350	1017	1576	1582	1619	3	1104	1436	936
Cocaine	1329	995	1521	1572	1514	25	1117	1396	894
Cocaine	1399	1051	1634	1657	1638	30	1211	1508	972
Cocaine	1282	1000	1595	1660	1601	29	1137	1532	872
Cocaine	1307	1048	1494	1617	1457	-16	1066	1408	909
Cocaine	1364	1077	1600	1637	1553	-2	1113	1448	930

Cocaine	1346	1058	1537	1601	1499	5	1077	1442	979
Cocaine	1253	947	1582	1653	1560	41	1139	1514	909
Codeine	5113	3844	4166	4344	4108	875	3187	3997	3444
Codeine	5933	4522	4178	4214	4055	1082	3157	3915	3902
Codeine	5559	4095	4054	4153	3909	951	3045	3933	3693
Codeine	5403	4196	4131	4161	3864	946	3066	3882	3629
Codeine	5061	3746	4031	4110	3838	736	2985	3770	3302
Codeine	5320	4009	4129	4110	3996	1188	3044	3859	3452
Codeine	5267	3951	4054	4117	3955	763	3094	3798	3596
Codeine	5058	3810	4128	4147	3980	784	3078	3823	3337
Codeine	5398	3997	4315	4203	3952	851	3064	4022	3522
Codeine	5138	3967	3905	4096	3788	963	2960	3735	3475
MDMA	6723	5750	2096	2272	2437	705	1304	1843	5288
MDMA	7008	5996	2327	2561	2677	705	1479	2088	5428
MDMA	7401	6331	2312	2552	2640	659	1440	2107	5685
MDMA	6944	6035	2201	2435	2561	728	1385	1922	5410
MDMA	7561	6648	2353	2553	2737	608	1437	2051	5938
MDMA	6788	5928	2163	2368	2477	614	1347	1889	5300
MDMA	7141	6121	2308	2568	2668	650	1454	2044	5507
MDMA	6988	6029	2048	2272	2230	542	1292	1775	5347
MDMA	7220	6178	2253	2521	2678	679	1407	2046	5602
MDMA	6933	6038	2352	2496	2760	597	1476	2072	5596
Morphine	4275	3253	3606	3622	3490	817	2658	3344	2917
Morphine	4675	3541	3757	3891	3753	778	2759	3510	3137
Morphine	4899	3620	3658	3641	3587	637	2687	3425	3261
Morphine	5039	3617	3835	3832	3602	805	2789	3622	3256
Morphine	4808	3590	3438	3457	3259	841	2669	3254	3176
Morphine	5100	3824	3786	3741	3596	803	2788	3495	3349
Morphine	4705	3613	3792	3807	3633	687	2829	3592	3167
Morphine	4707	3521	3421	3471	3366	695	2614	3278	3073
Morphine	4738	3648	3833	3854	3615	807	2799	3531	3159
Morphine	5025	3720	3497	3515	3386	791	2598	3243	3350
Methamphetamine	4472	3891	1194	1269	1318	602	783	1037	3472
Methamphetamine	4327	3694	1073	1163	1279	580	672	985	3582
Methamphetamine	4562	3989	1218	1257	1329	537	808	1110	3609
Methamphetamine	4214	3616	1180	1271	1317	468	758	1040	3198
Methamphetamine	4300	3723	1143	1207	1321	502	743	1028	3298
Methamphetamine	4137	3541	1214	1247	1361	544	777	1052	3199
Methamphetamine	3912	3342	1199	1303	1357	482	801	1132	3177
Methamphetamine	4074	3442	1203	1349	1344	340	812	1092	3016
Methamphetamine	4059	3420	1258	1297	1425	452	823	1092	3094
Methamphetamine	4470	3810	1248	1293	1378	534	813	1122	3515

Ketamine	5655	4660	2082	2231	2351	130	1343	1896	4179
Ketamine	5448	4448	1963	2077	2151	178	1301	1764	4011
Ketamine	5380	4456	2192	2333	2349	119	1421	1974	4010
Ketamine	5312	4463	2003	2153	2291	166	1316	1848	4009
Ketamine	5488	4603	2234	2339	2424	171	1478	2058	4156
Ketamine	5663	4743	2197	2318	2378	149	1429	1967	4302
Ketamine	5513	4592	2205	2291	2344	113	1444	1997	4103
Ketamine	5363	4440	2082	2296	2277	141	1352	1884	3904
Ketamine	5322	4397	2280	2370	2456	160	1432	2050	3891
Ketamine	5281	4353	2155	2305	2329	121	1441	1931	3878
Benzoylecgonine	2820	2363	1876	1983	1966	297	1272	1739	2125
Benzoylecgonine	2836	2391	1986	2014	1984	287	1293	1751	2222
Benzoylecgonine	2715	2291	1810	1945	1836	285	1230	1675	2067
Benzoylecgonine	2710	2272	1874	1971	1919	340	1281	1726	2098
Benzoylecgonine	2892	2546	1969	2029	2042	317	1354	1828	2230
Benzoylecgonine	2788	2403	1842	1938	1930	328	1264	1646	2100
Benzoylecgonine	2753	2279	2034	2098	2032	298	1387	1796	2115
Benzoylecgonine	2724	2248	1886	2003	1965	212	1305	1767	2031
Benzoylecgonine	2481	2126	2130	2188	2187	301	1460	1947	1904
Benzoylecgonine	2786	2320	2042	2121	2026	313	1345	1810	2121
Scopolamine	4342	3716	1715	1869	1836	704	1190	1594	3330
Scopolamine	4166	3493	1744	1810	1830	580	1138	1536	3220
Scopolamine	4760	3933	1747	1840	1868	733	1174	1589	3628
Scopolamine	4523	3852	1639	1777	1789	763	1115	1565	3530
Scopolamine	4868	4062	1910	1960	1980	747	1285	1684	3625
Scopolamine	4533	3820	1727	1878	1837	737	1170	1572	3481
Scopolamine	4744	3997	1806	1922	1947	500	1237	1669	3640
Scopolamine	4580	3916	1822	1881	1938	515	1254	1646	3608
Scopolamine	4687	3970	1694	1734	1840	634	1146	1539	3458
Scopolamine	4487	3903	1781	1913	1956	636	1251	1674	3378
No Guest	2856	2490	4973	4603	4129	276	4509	4933	2197
No Guest	2764	2417	4823	4479	3946	277	4365	4777	2224
No Guest	2939	2599	4846	4629	3992	324	4378	4814	2294
No Guest	2868	2418	5019	4904	4220	237	4534	5007	2299
No Guest	2857	2380	5109	4929	4280	222	4595	5098	2187
No Guest	2886	2518	5198	4954	4340	287	4656	5188	2296
No Guest	2766	2331	5237	4946	4338	347	4657	5194	2122
No Guest	2718	2309	5275	4938	4335	267	4657	5200	2090
No Guest	2626	2258	5207	5003	4293	228	4616	5176	2037
No Guest	2915	2506	5139	5068	4250	207	4574	5152	2290

Chapter 3: Mechanistical studies of binding and fluorescence properties of StiCx hosts

3.1 Motivation

In Chapter 2 we have shown that these new StiCx analogues have good differentiation properties for a variety of analytes. However, there are a lot of lingering questions as to their actual binding properties. As we said before, DimerDyes are very thoroughly studied and it is understood their turn-on fluorescence comes mainly from a change in supramolecular organization that consists of the preformed sensor dimers undergoing dissociation (and turn-on fluorescence) upon binding a competing guest.[75] The positively charged pyridinium ring facilitates dimerization in solution due to ion-ion interactions with the negatively charged sulfonates of the partner molecule. With that being the case, the question stands of whether our StiCx compounds possess any dimerization capabilities, and what drives the selective responses we've observed. This Chapter will focus on exploring the structures and mechanisms behind the behaviours of the StiCx sensors. We will first attempt to explore structural aspects or 'supramolecular mechanisms,' which include exploring the possibility of host dimerization and understanding the nature of host-guest binding. For this, we will use a variety of NMR spectroscopy methods. We will also explore the possibility that different photophysical mechanisms are responsible for the turn-on and turn-off fluorescence responses that are observed.

3.2 Introduction

To explore the structural aspects of our host molecules' behaviours, we will briefly look over the techniques that have thus far been used to conduct similar studies. Studying the structures of binding complexes is no new topic, and interest in this general area comes from such diverse areas as biomolecular complexes, protein-drug complexes, and supramolecular host-guest chemistry.

An argument can be made that X-ray diffraction yields the highest resolution structural data, however, it has a major obstacle of requiring high-quality single crystals of a sample to study. When such crystals are obtainable, as in many protein-ligand complexes, this technique has proven invaluable.[121,122] Supramolecular chemistry doesn´t fall behind and has also taken advantage of this technique for the understanding of binding structural conformations. An example of this is its use for analyzing triflate-functionalized Pillar[5]arene inclusion complexes.[123] Using this technique not only were they able to get structural information, but also study the non-bonding interactions with guests such as 1,2-dibromobutane and n-hexane. While X-ray is a powerful technique, the combination of charges and hydrophobic elements in StiCx and related charged host structures means that they are poorly suited to the growth of single crystals. Only one analogous molecule has been characterized by X-ray crystallography in the 8 years since their first invention,[124] and it was an analogue that did not include a dye element.

NMR spectroscopy is a very powerful tool that can help us understand many aspects of binding interactions through solution-phase studies. Its popularity comes from the fact it can give us information on the structures of organic molecules and their complexes in the solution phase. Calix[4]arene-based host-guest complexation has been elucidated many times using NMR spectroscopy. Some of the first studies that demonstrated host-guest complexation were done using NMR studies.[125] Some of the earliest studies showed one of the particular behaviours of calix[4]arenes in solution, which is how their conformation changes under different conditions. Since the cavity can switch between the different conformations seen in Figure 1.4, the methylene bridges can experience changes in their chemical environments and even these subtle changes are detectable by changes in NMR chemical shift values. This process can be hindered by substituents that impede this process, or also by the addition of a guest in the cavity. What this means is methylene signals will be different depending on how the complexation and hindrance of the cavity affect this conformation change. It is important to keep this in mind, as some of our results reflect this phenomenon.

NMR spectroscopy offers multiple different approaches that can elucidate binding geometries and aggregation states.[126] The technique of using simple 1D ^{1}H NMR to follow changes in chemical shifts during host-guest titrations is one of the main methods used, where the magnitude of change can provide evidence of binding orientation and strength. Because the chemical environment inside the cavity of a calix[4]arene is aromatic and highly shielding, it causes diagnostic upfield shifts in the resonances of protons that are bound inside the pocket. In addition to structural insight, binding constants can also be obtained where the

degree of chemical shift change during titrations can be used to determine association constants quantitatively.[127] Understanding the binding geometry and the molecular interactions behind a binding event is useful in subsequent efforts at structure optimization as we can further optimize and improve our hosts to increase their binding affinity.

Aside from this, another powerful tool for studying host-guest complexation is a 2D NMR method that relies on through-space coupling interactions. Nuclear Overhauser effect spectroscopy (NOESY) takes advantage of the Nuclear Overhauser Effect (NOE), which is a through-space transfer of nuclear spin polarization from one nucleus to another. This phenomenon allows us to see correlations between two nuclei that are close in space to each other. Because this transfer happens through space, it is not necessarily intramolecular, allowing host-guest proximities to be seen.

Diffusion Ordered Spectroscopy (DOSY), on the other hand, is an NMR technique that measures diffusion coefficients, and it is quite useful when analyzing polymers and assembling or aggregating molecules.[128] While the theory is complex, we can lay out some fundamentals sufficient for understanding the data in this thesis. DOSY uses pulse gradients with varying magnetic fields across the length of an NMR tube to measure the rate of diffusion of a molecule through different vertical slices in the NMR tube. The smaller the species, the faster it diffuses in solution and the faster it moves within the NMR tube. By fitting DOSY data, we can obtain the diffusion coefficients of any molecule that has a clear NMR resonance. The power of this technique in supramolecular chemistry is that the

diffusion properties relate directly to the size of the molecule or molecular assembly (e.g. monomer, dimer, or higher aggregate) in solution. The relationship is given by the Stokes-Einstein equation below (Equation 3.1) where D is the Diffusion coefficient, T is the temperature, η is the viscosity of the solution, *k* is the Boltzmann constant and r_h is the hydrodynamic radius. This last term is the parameter from which we can estimate molecule size. It is defined as the radius of a molecule moving through a solution under the assumption that the molecule is shaped like a sphere.[129] While other factors such as solvent viscosity, ionic strength and interactions with the solvent can also affect this parameter, it works as a pretty good estimation for getting the size of molecular assemblies.

$$D = \frac{kT}{6\pi\eta r_h} \qquad \text{Eq. 3.1}$$

A lot of information can be obtained when combining these techniques to get a full picture. Of primary concern here is to understand the structural factors behind the fluorescence sensing properties we observed before. Knowing more about the geometry of binding, the groups involved, and the observed shifts can also tell us about the phenomena that cause either turn-on or turn-off responses. Since the focus is on addressing the sensing mechanism, this Chapter will also include control studies of the influence of the tested drugs on control dyes. This is included to rule out potential interference from guest absorbance or emission. We will also show NMR results for StiCx09 with nicotine and cocaine; this combination was chosen for detailed analysis as it showed good binding, good fluorescence signal intensity,

and selective turn-on or turn-off responses to each guest. We also address the size of the sensors and assemblies formed to aid in elucidating the sensing mechanism.

3.3 Results and Discussion

3.3.1 NMR Titrations of StiCx09

The first step to test host-guest binding complexation and geometry was to do NMR titrations of our host and see the shifts in peaks with increasing guest concentration. Taking Nicotine as an example, we can see from Figure 3.1 that it has different orientations upon which it could interact with the cavity. Because we are working in a buffered system, we need to take into account the protonation state of the molecules in our system to account for their interactions. Sulfanatocalix[4]arenes sulfonates are highly acidic groups, and while phenols normally have a high pK_a, the value for the first deprotonation of a calix[4]arene phenol is around 3.8.[130] This is attributed to the fact that proximity between the other three neighbouring phenol groups creates favourable hydrogen bonding interactions that stabilize the first deprotonated phenoxide anion, rendering it ~6 orders of magnitude more acidic than a typical phenol. Though we don't have direct evidence for this, it could be assumed that the stilbene phenol ring is the major contributor that is deprotonated in the equilibrium among the four calixarene phenols. This idea comes from the fact that electron-withdrawing groups on the top stilbene ring could contribute to further stabilizing the phenoxide if it is formed at this position. It could also explain why electron-withdrawing stilbene groups showed the best results in initial sensor screening, as it could lower energy barriers in the conjugated system.

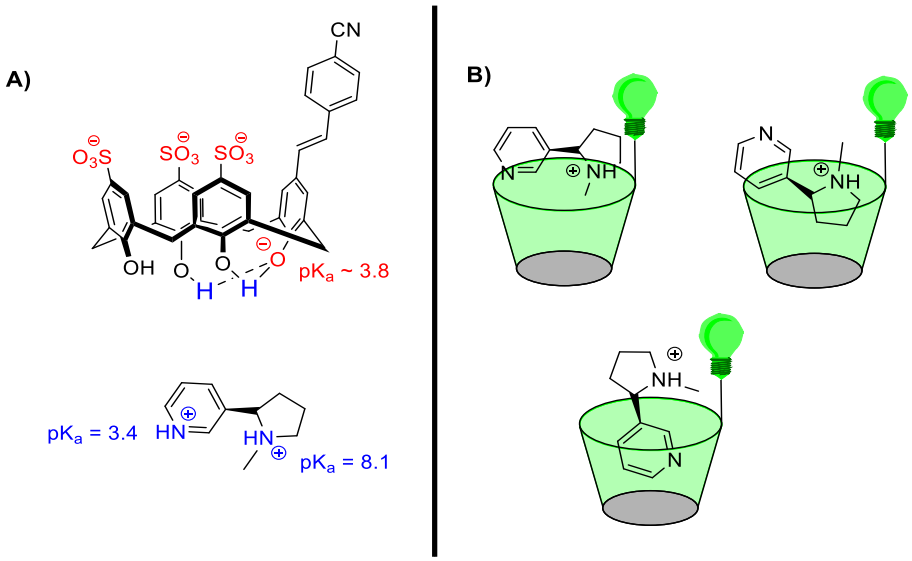

Figure 3.1: (A) Protonation states of host t at pH 7.4 in experimental conditions and deprotonated structure of nicotine, depicting pK_a values. (B) Representation of possible binding orientations of nicotine inside the pocket (Nicotine is shown in its protonated state at experimental pH.

Nicotine on the other hand has two amine groups which can be protonated; however, the pyrrolidine ring is more basic with a pK_a of 8.1. This means only this ring will be protonated at the buffered conditions (pH = 7.4) at which we will be working. It is safe to assume that when nicotine binds a sulfonatocalixarene the protonated pyrrolidine will interact with the negatively charged sulfonates, however, the orientation that the molecule will take in the cavity is unknown. What we hope to understand with NMR titration is to see the shifts in peaks for host and guest, if the pyrrolidine ring is more deeply buried inside the cavity, then we might expect to see greater shifts for those protons as compared to the pyridine ring. The protonation states for cocaine are easier to describe, as there is only one amine which can be protonated.

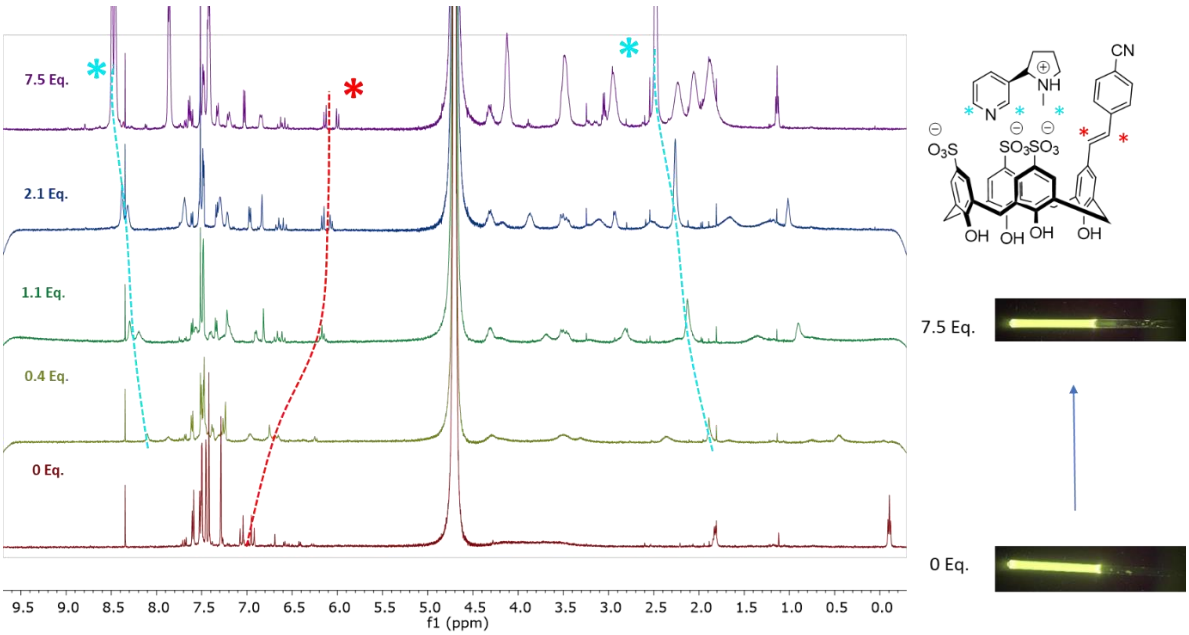

Figure 3.2: NMR spectra arising from the titration of StiCx09 with nicotine. NMR titrations were done at a fixed concentration of host (0.5 mM) in phosphate buffer D_2O (pD 7.4). Pictures of the samples at 0 and 7.5 equivalents of added guests included under UV light.

Experiments consisted of adding increasing concentrations of guest into an NMR tube containing a fixed concentration of our StiCx09 host, taking spectra at each concentration point. Full spectra of the titrations can be found in supporting information, and Figure 3.2 shows the spectra of some of the points of relevance for the titration with nicotine. We saw that not only were shifts in the peaks of host and guest occurring but also that some peaks broadened out significantly, as can be most notably seen at the 0.4 equivalents mark. This can be explained because we will have an equilibrium of complexed guest with free guest, and when the rate of exchange happens on a frequency similar to the NMR time scale we have peak broadening.[131] It is interesting to see that this also happens to the peaks corresponding to leftover TEA, confirming that this base was most likely a counterion bound in the calixarene that guest displaced on guest addition.

The titrations were analyzed based on the shift and shape of the peaks of the guest as its concentration in solution increases. On 1.1 equivalents signals become resolved well enough to be distinguished and we can make out some distinct signals like the methyl from the pyrrolidine ring and stilbene alkene peaks. As we increase guest concentration the signals shift and become more resolved. For the methyl (marked with blue lines in Figure 3.2) there is a shift from 2.13 to 2.49 ppm, a difference of about 0.36 ppm from the 1.1 eq. to the 7.5 eq. spectra. The protons adjacent to the nitrogen in the pyridine ring show shifts from 8.20 to 8.45 ($\Delta\delta$ = 0.39 ppm) and from 8.3 to 8.49 ($\Delta\delta$ = 0.25 ppm), a significant downfield shift. We also see something interesting in the methylene peaks of the calixarene in that while they are broadened out at the start, not surprising because as we said there is an interconversion of the different cone conformations. But we saw that they split into sharp signals as guest concentration increased. As we discussed, the binding of a guest can hinder the conformational changes allowing us to see resolved sharpened methylene signals, this is an additional indication that host-guest binding is occurring.

Both nicotine and cocaine show downfield shifts as concentration increases, no significant difference can be seen that would help explain selective differences in fluorescence. They can however give us hints on their structural orientation. The same experiment was repeated with cocaine, which had more of an issue with overlapping and broadening peaks (Figure 3.3). However, we can see that the methyl from the methylammonium group has some of the highest changes in shift, going from 2.30 ppm at 1 equivalent to 2.69 ppm at 7.5 equivalents ($\Delta\delta$ = 0.39 ppm). This agrees with what was expected as the positive charges in the charged

amine group would interact with the negative sulfonates. The pendant benzoyl ester group in cocaine is in an orientation outside of the cavity because the resonances have the smallest changes (Δδ = 0.05–0.12 ppm).

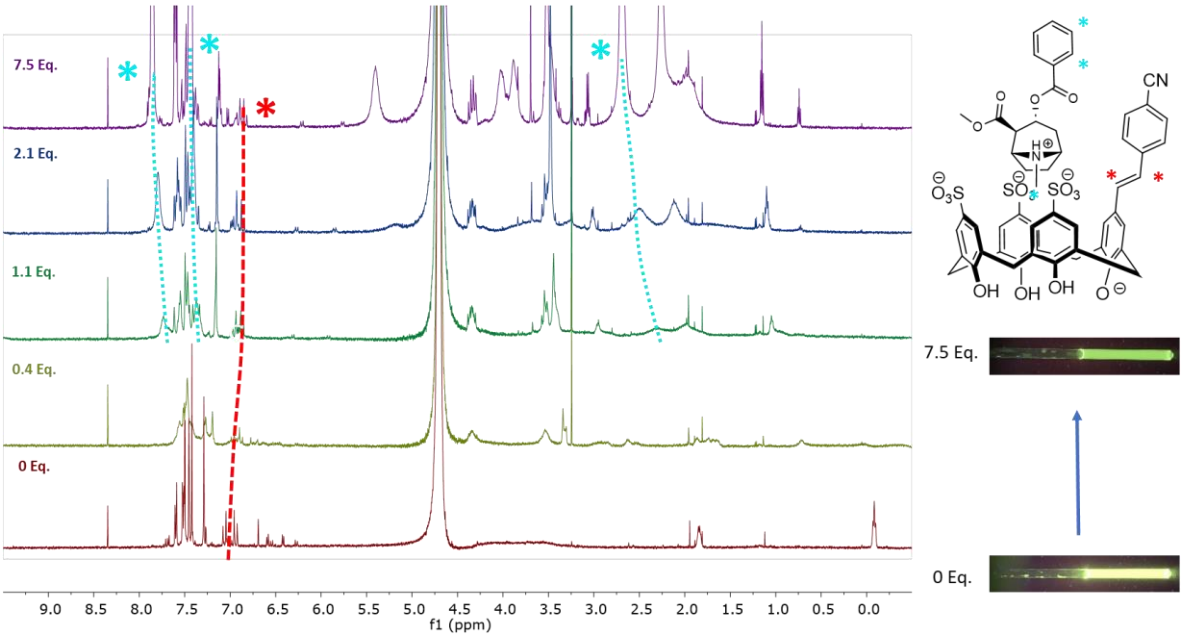

Figure 3.3: NMR spectra arising from the titration of StiCx09 with cocaine. NMR titrations were done at a fixed concentration of host (0,5 mM) in phosphate buffer D_2O (pD = 7,4). Pictures of the samples at 0 and 7,5 equivalents of added guest included under UV light.

The observed shifts, along with the broadening of certain host peaks and changes in multiplicity show evidence of binding, and the observed pattern has given us information on the geometries. The deeper a proton is embedded in the pocket, the more upfield change in chemical shifts we can expect, so the identity of protons that are most upfield-shifted gives us an idea of what orientation the guest has inside. Figure 3.4 shows us the proposed orientations for nicotine and cocaine, with the change in chemical shift (Δδ) calculated from the difference between the spectrum with 1 equivalent of guest and the spectrum with a large

excess of guest (7.5 equivalents). Because of peak broadening and blending into the baseline, only the shifts indicated in the Figure could be accurately calculated. We can also see a visual representation of the fluorescence of the solution in the NMR tubes, although the turn-on activity wasn't so obvious initially it can be more appreciated when compared side to side with the host solution. Additionally, the turn-off fluorescence for cocaine is much more drastic and appreciated visually, with a much dimmer sample and even a slight apparent change in the green tone. However, we wished to explore these proposed models further by using NOESY NMR to show evidence of through-space coupling between the host and guest. The next Section will cover experiments done with the same combination of host and guest for NMR studies.

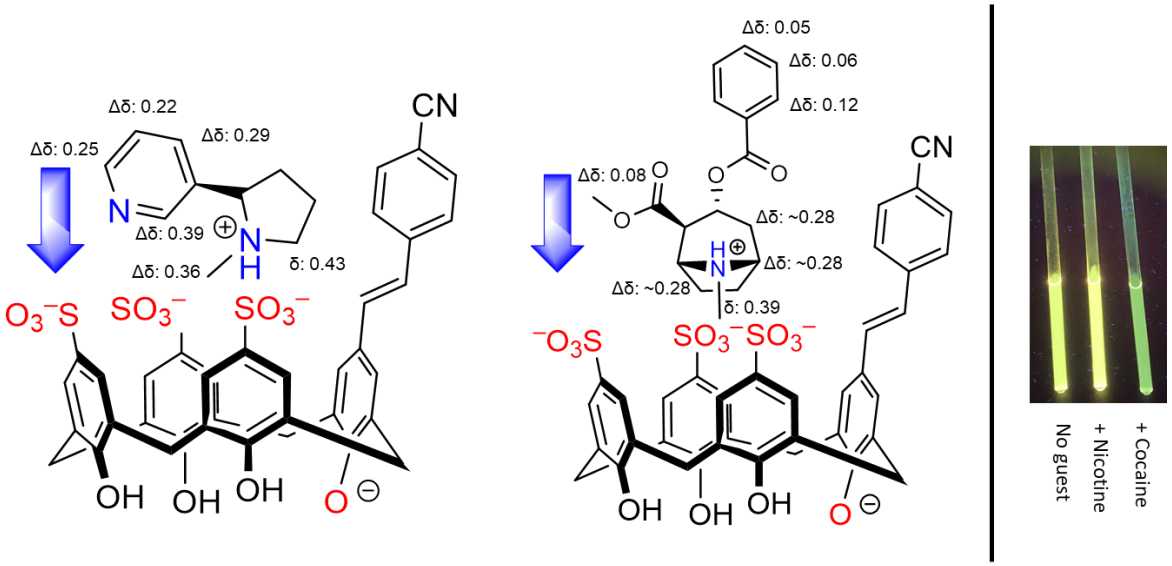

Figure 3.4: Proposed binding geometries based on the binding-induced proton shifts shown over each structure (left). Chemical shift values reported are the changes in chemical shift between samples with 1 equivalent of guest (high proportion bound) and a large excess of guest (7.5 equivalents, high proportion free). Picture of NMR tubes under UV light showing their change in fluorescence (right). All samples are at a concentration of host of 0.5 mM prepared in phosphate buffer in D_2O (pD 7.4).

3.3.2 NOESY studies – Looking for through-space correlations.

Following through on exploring the supramolecular chemistry of the host-guest complexes we next took to NOESY to get additional information on the binding of our hosts. NMR titrations allowed us to get proposed binding orientations based on shifts. However, through-space correlations would allow us to confirm these proposed geometries and serve as decisive evidence for the formation of a host-guest complex. Additionally, we might get more information about our system, such as if our hosts dimerize in solution similar to the DimerDye system. For this, we conducted experiments with a solution containing a 1:1 ratio of host and guest in 7.5 mM concentrations. These concentrations are used as it is the maximum concentration we can go without saturating the buffer, which should always be at ≥10 times the analyte concentration. In the 2D spectra we would expect to see cross peaks of host and guest protons that are close in space and, therefore in the same complex. From our proposed structures and the favourable interaction of the amine with the sulfonate groups, we would probably expect to see the methyl ammonium peaks to be closest to the pocket. Figure 3.5 shows the results of the NOESY spectra of StiCx09 + Nicotine, with a zoom-in of the methyl ammonium peak interactions and a proposed structure and likely interactions of the observed signals.

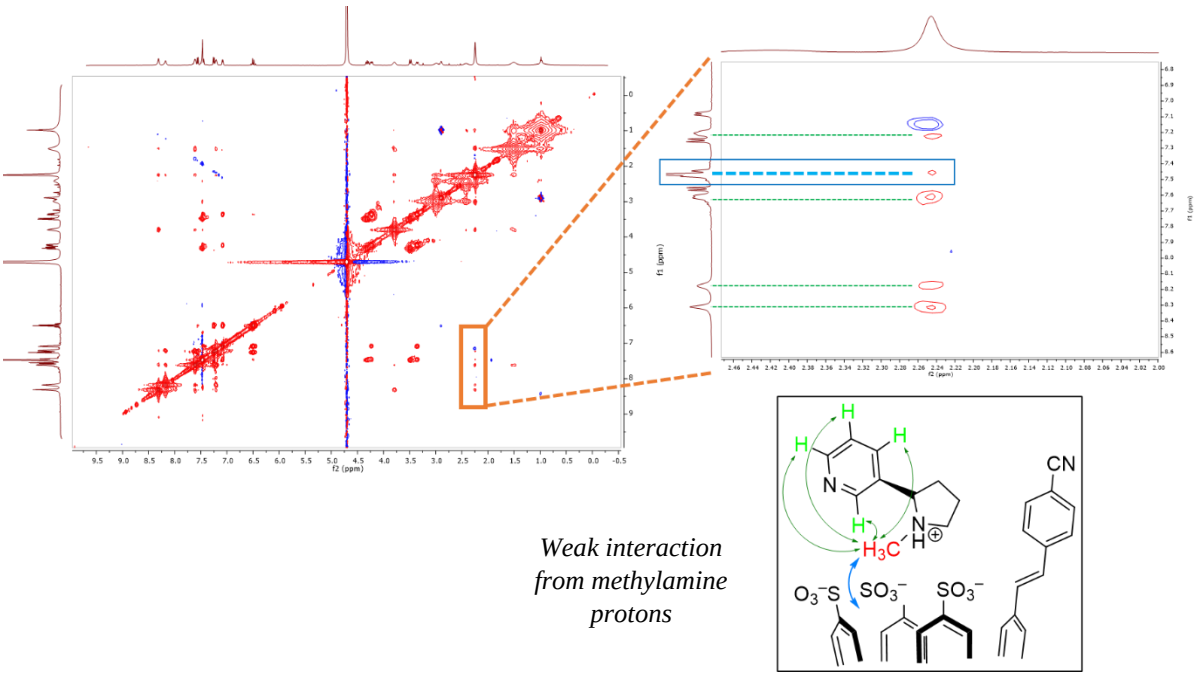

Figure 3.5: NOESY spectra of StiCx09 with Nicotine. Samples were taken in a 1:1 ratio at 7.5 mM concentration in deuterated sodium phosphate buffer (pD 7.4, 75 mM).

From the NOESY results, we can see the intramolecular interaction of the methylamine peaks with the aromatic protons of Nicotine, which is to be expected as the groups are in the same molecule and close in space to each other. We used COSY NMR to help assign and differentiate peaks from host and guest and in doing so, to rule out intramolecular interactions intrinsic to both molecules (see Section 3.5.2). We were interested in looking at intermolecular signals correlating peaks from the calixarene unit to the guest nicotine, showing evidence of the proximity of the compounds. The only such signal that could be found is a weak cross peak (highlighted in blue) with protons from the aromatic rings of the cavity. The peaks themselves overlap and broaden too much to get an idea of which protons are interacting. However, we can conclude they are aromatic protons from inside the calixarene cavity, as the pendant arm protons are on lower chemical shifts (7.30-7.00 ppm) from the results of basic characterization data studies. All other observed signals in the

NOESY were attributed to intramolecular interactions, and no other host-guest signal cross-peaks were observed.

These results suggest a conformation where the guest's methylamine protons are the closest in proximity to the binding cavity, therefore having this group directly facing into the pocket. This correlates with the previous results of the 1D-NMR titrations in which the methyl group had the largest change in chemical shift. However, from the proposed orientations we would also expect cross-peaks from an adjacent aromatic proton in the pyridinium unit and the adjacent methylene protons from the pyrrolidine ring. NOESY results from the binding with cocaine were not much better, and we couldn't see any cross-peaks from the methyl ammonium peak, even for intramolecular interactions. Aside from that, there is much more overlap with the aromatic signals of the host and guest, as well as a broadening of signals when compared to guest spectra in solution. Once again, we can attribute this to the equilibrium of the host-guest complex, but it makes assignment and differentiation difficult. Therefore, it can be hard to conclude from the NOESY results if there is indeed any proximity between the host and guest in solution.

We also wanted to see if self-dimerization occurred at any level for our StiCx hosts. Recall that self-dimerization is a central mechanism by which DimerDyes function as sensors.[114] From NOESY NMR, evidence of dimerization would appear as cross-peaks between protons from the pendant arm of one unit with the calixarene protons from the cavity of its partner. A NOESY spectrum was taken of just the host in solution and no such cross-peaks were

observed (Spectra in Supporting Information 3.5.2). This can be a preliminary result to indicate that our hosts exist as monomers in solution, so the fluorescence doesn't follow the quenched mechanism of DimerDyes.

We can attribute these poor results to the nature of the NOE effect itself which is not always very sensitive. It should be noted that in NOESY spectra, NOE is usually a signal that can arise from both dipolar relaxation and exchange contributions in addition to through-space spin interactions.[132] These last are not only the weakest so high concentrations of sample are needed, but it also means the sample is susceptible to interference from other factors such as fast exchange.[133] While our protons of interest aren't exchangeable with solvent, we do have an equilibrium of the guest entering and exiting the cavity so a similar principle can apply. If the dynamics of the equilibrium happen faster than the NMR timescale, then we would have a loss of information from those signals. Conformer changes can also cause problems in the cross-peaks, and the change in calixarene cone conformations could also contribute to the overall broadness of the spectra.

There are ways in which the experiment could be optimized to correct some of these errors. As the NOE intensity is dependent on the experiment parameters such as mixing time, optimizing for this value could give us better sensitivity for NOE peaks. This has the disadvantage however that increasing mixing time also means measuring at longer relaxation times, so we lose overall sensitivity in the experiment. Rotating-frame Overhauser effect spectroscopy (ROESY) is a good alternative as ROE can give better signals on molecules

with high molecular weights.[132] However, we didn't see any better results with this technique in the initial trials (ROESY spectra in Section 3.6.2). Doing experiments at lower temperatures could also be another alternative, as we would slow down exchange and equilibrium processes allowing us to better measure through-space coupling. However, the need to do the studies in water limits the ability to reduce temperature. Because of this, we switched our approach to DOSY as an alternative way to get evidence on the complex formation of our hosts.

3.3.3 Using DOSY to compare complex sizes

DOSY is a technique used to study the size of assemblies and it is commonly used to check the oligomeric state of biomolecules, polymers, micelles and other macromolecular structures.[134] It has been previously used to characterize the dimerization (and guest-induced disassembly) of DimerDye sensors,[53] and it is of additional interest to us to corroborate the state of our compounds in solution by comparing to this data. To do this we tested our top StiCx09 host in solution by itself and with the addition of guest to compare assembly sizes. We also measured DOSY for the guests on their own. Once again nicotine and cocaine are chosen for this due to the unique responses observed, and the calculated hydrodynamic radii are shown in Table 3.1. Values are calculated from peak integration and for each case most well-resolved peaks were used, the results shown are the average of the peak results with their respective uncertainties.

Table 3.1: Diffusion coefficients (D) and hydrodynamic radii (r_h) calculated from the DOSY experiments. [a]

	D [m2/s]	**r_h (Å)**
StiCx09	(2.8 ± 0.1) x10^{-10}	8.7 ± 0.4
StiCx09 + Nicotine	(2.4 ± 0.001) x10^{-10}	10.2 ± 0.01
Nicotine	(5.5 ± 0.01) x10^{-10}	4.4 ± 0.05
StiCx09 + Cocaine	(2.1 ± 0.06) x10^{-10}	11.6 ± 0.3
Cocaine	(4.5 ± 0.06) x10^{-10}	5.4 ± 0.1
DimerDye (DD4) [b]	(1.96 ± 0.05) x10^{-10}	12.4 ± 0.7

a) All experiments were done in a 1:1 ratio of host (and guest, where applicable) at 7.5 mM in a deuterated sodium phosphate buffer (75 mM, pD: 7.4) b) DimerDye(DD4) values were taken from literature;[53] *buffer concentrations are 50 mM at pD 7.4.*

Full DOSY spectra, parameters and concentrations can be found in the experimental section and supporting information (Section 3.5.3). Hydrodynamic radii are calculated from the diffusion coefficients using equation 3.1, and because our solvent and temperature are kept constant any changes we see can only arise from differences in molecular size. From Table 3.1 we can see an r_h of 8.7 Å for StiCx09, and this number increases to either 10.2 Å or 11.7 Å in the presence of either nicotine or cocaine. This increase is indicative that we have a larger assembly in solution, forming a host-guest complex. It also makes sense that the increment is bigger for cocaine than for nicotine as it is the larger of the two guests. Controls taken for each guest by themselves help to corroborate this, we see values of 4.4 Å and 5.4 Å for nicotine and cocaine, respectively. Each guest consists of a small molecule, that is expected to show a smaller size than our much bigger calixarene hosts, so this result also lines up with what we expected. Figure 3.6 shows a representation of what we discussed; a larger molecule will show higher r_h values. Because this comes from the diffusion in solution and part of the guest is embedded inside the host cavity the numbers are not additive, so we do not expect our complex to be an exact sum of the host and guest. But the comparison of

each number serves our purpose of demonstrating we do have complexation happening, confirming the binding properties of our StiCx compounds.

Another result we obtained from this experiment is information on the state that our hosts exist in solution in the absence of guests. We so far have not seen any information suggesting that our hosts form dimers in solution, but DOSY can give us that answer definitively when we compare our data to the literature. We can see that the reported r_h for a DimerDye, which is highly similar in structure and is known to dimerize, is 12.4 Å. This number is much greater than any of our systems, which should be expected as two calixarene units are complexed together creating a larger structure. The fact that our StiCx09 host by itself has a smaller size is indicative that our compound exists as a monomer in solution and that no dimer is formed. For further comparison, the r_h of a DimerDye complexed with nicotine was 8 Å which is closer to our values measured for monomeric host-guest complexes in the StiCx family. The slight discrepancy in the numbers can come from the fact that the DimerDye system was tested in slightly different buffer concentrations. And like we said before these sizes are calculated from diffusion so slight differences in solvent (and ionic strength of the solution) can give rise to differences in the observed numbers.

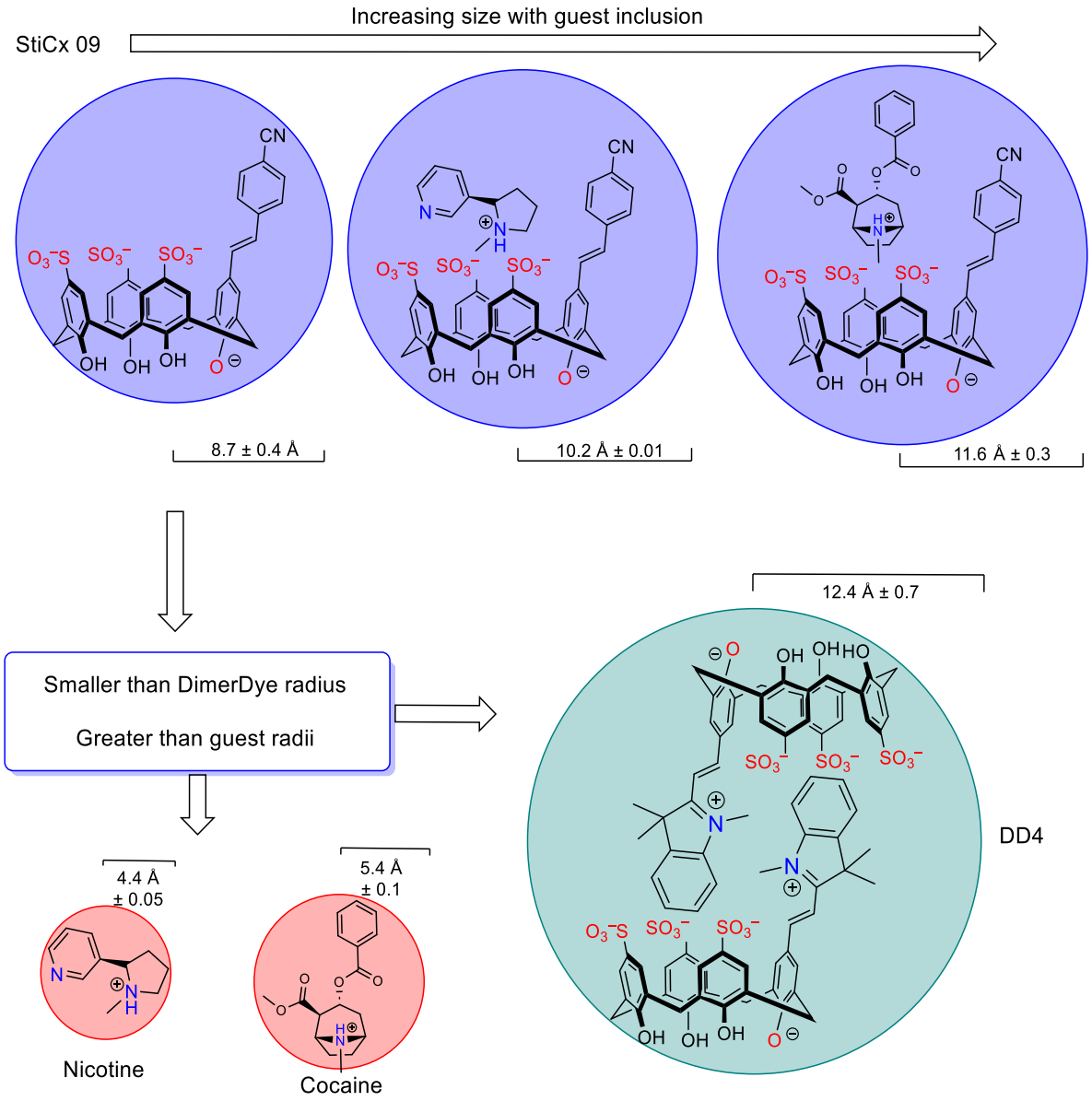

Figure 3.6: Representation of changes of hydrodynamic radius with different size complexes. An increase in StiCx09 size is observed with the addition of nicotine and cocaine. The initial value is smaller than a DimerDye indicating a monomeric state in solution.

Despite the generally similar shapes of the DimerDyes and StiCx sensors, we can rationalize the differences in supramolecular organization based on the functional groups involved. The DimerDye hosts all have cationic heterocycles as their appendages (e.g. a pyridinium unit in DD1 and an indolinium in DD4), which are good guests for anionic calixarene pockets

because of favourable interactions with the sulfonate units. The StiCx hosts all have neutral polar functional groups on their appended rings (PhCN, $PhCO_2Me$, and PhOMe), which are weak guests for sulfonatocalixarenes and are expected to make favourable interactions with hydrating water molecules because of their heteroatoms. This explains why the StiCx hosts studied do not form dimers either in the absence or presence of guests.

This structural knowledge can inform our understanding of the photophysical mechanisms. The fluorescent elements in the DimerDyes undergo a self-quenching when in the dimeric state because the two dyes are stacked on top of each other in an antiparallel arrangement. This is the classic H-aggregate geometry that is known to lead to nonradiative quenching of excited states.[135] The StiCx sensors exist as free monomers in the absence of guest, which is why the stilbene fluorophores display a moderate level of fluorescence emission. We are still unclear as to why the fluorescence intensity increases for some guests and decreases for cocaine but having ruled out guest-induced changes in supramolecular architecture, we can focus on the more typical photophysical mechanisms by which a bound guest can influence the emission of an adjacent fluorophore.

To understand the nature of the fluorescence behaviours of our system, we needed to study the behaviour of the fluorophore we used. As discussed in Chapter 1, stilbenes have their own background as fluorophores and sensors in their own right. So, our next steps would consist of using the control stilbenes prepared in Section 2.2.3 to get some additional information on their spectral properties. These control experiments can also help us see if the

control fluorophore had any sort of response to our guests, helping us to confirm the calixarene's role in binding. Finally, with more information on the fluorophore's emission properties, we could also have enough insight to discuss possible photophysical mechanisms behind our system.

3.3.4 Studies with control dye

To continue our mechanistic studies, control experiments with guest addition to the control dyes will be done to help us understand what fluorescence changes are intrinsic to the stilbene dyes, as opposed to responses caused by calixarene binding. It will also be useful to compare the fluorescence emission and see if it correlates directly to the fluorophore used, or if there is a change of photophysical properties of the dye upon integration into the calixarene. It is important to consider the differences that attachment with the calixarene will bring into the fluorophore stilbene moiety. One of the main ones, calling back to Figure 3.1, is the difference in the pK_a which is around 3.8 in the calixarene and 9.3 in hydroxystilbene.[136] This causes a fundamental difference in the protonation states of the molecule at the experimental pH of 7.4 that we have been working with. This change in acidity can have drastic effects on the excited states of the molecule and can have a direct influence on the fluorescence properties we observe.

We must also note how interaction with the guest might affect the fluorescence emission. Because binding happens in the calixarene pocket there is a forced proximity between the guest and the fluorophore that wouldn't happen in free solution. This proximity

could induce non-bonding interactions which could affect the emission of the fluorophore. Looking into the proposed binding orientations in Figure 3.3, it could be possible there are π-π interactions with the aromatic ring of cocaine and the top ring of the pendant arm. This would not be the case for nicotine in which the aromatic ring is too closely bonded to the methylamine unit, while there is enough of a distance in cocaine for this overlap to happen. This is only speculation though, as scopolamine has a similar structural motif, and no turn-off fluorescence is seen. Similarly, the pendant arm top group seems to affect this behaviour, as it is different for each of the top hosts.

StiCx09 which has a nitrile as the top group was the focus of our NMR characterization studies because of its selective turn-on/off response. Because of that particular behaviour and to remain consistent in our studies, we kept to the structural moiety we used the non-calixarene Sti09 analogue and tested its binding with nicotine, cocaine, benzoylecgonine and MDMA. These guests were chosen because they showed the greatest variance in the PCA, meaning they should have some of the most distinct changes in fluorescence. They have both turn-on and turn-off responses on the calixarene trials, and they represent different drug families. Results are shown in Figure 3.7, with the absorbance and fluorescence spectra of the controls before and after an excess of drug addition. Additionally, we include StiCx spectra to show how the calixarene induces a change in the spectral properties. We can see there is very little change in the spectral properties of the control dyes even with a high amount of guest. Only at the very high concentration of 400 μM do we see

a slight increase in the fluorescence intensity, which at that point could be interference from the guest itself.

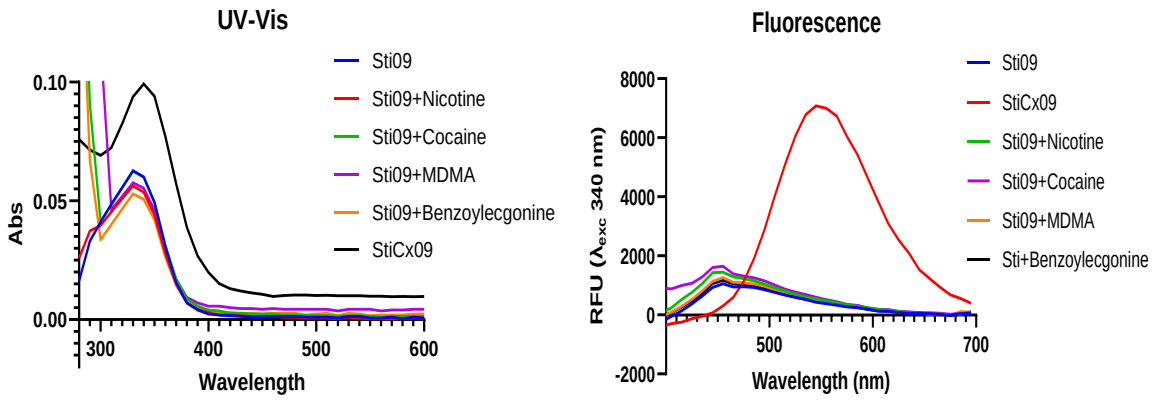

Figure 3.7: Absorbance and fluorescence spectra of stilbene control Sti09 (8 µM) against 4 guests (400 µM) in a sodium phosphate buffer (100 mM, pH 7.4). Full titration spectra can be seen in supporting information (Section 3.5.4). Spectra of StiCx09 is also shown as a comparison.

The spectra of the original StiCx09 are also included and we can see that not only does it have a much higher absorbance at the same concentration, but there is also a big red shift in its fluorescence emission and drastically higher RFU. Even without the addition of any guest, we have a much more potent fluorescence activity when we integrate the fluorophore into the calixarene. Not only that but from the results in Chapter 2 (Table 2.1) we know our StiCx09 has an LOD of 4.3 µM for nicotine and 1.7 µM for cocaine, and in their respective titration curves we saw significant changes in emission at these concentrations. These results suggest that the much lower pKa imparted by the calixarene skeleton means that the fluorophore is deprotonated, giving the fluorophore favourable properties for sensing. However, it should be kept in mind that there are four calixarene phenols and we can't be sure if the fluorophore's phenol is the one that is deprotonated first. To explore this we

decided to test the fluorescence of our control dye in an acidic and basic media and see how the change in the protonation state affected the fluorescence.

For this another experiment was run, this time we measured our controls in aqueous basic (pH: 12.1) and acidic (pH: 2.2) conditions, to work around the pK_a of 8.5 for 4-cyano-4-hydroxystilbene (Sti09).[137] For this solutions at these pH ranges were prepared using NaOH and HCl and compared to the standard buffer system at pH: 7.4 that we had been working on. The results can be seen in Figure 3.8, and we see there is a significant change in both absorbance and fluorescence spectra when the pH is adjusted. First, we have a big red shift in both cases in basic conditions, where the stilbene should be in the deprotonated state. We can see some similarities when we compare to our StiCx09 spectra. In the absorbance spectra, we can see that the StiCx09 maxima sits in between the acidic and basic spectra. But more interestingly, we have the same λ_{max} of fluorescent emission (at ~545 nm) as the deprotonated species, albeit with a bigger RFU. Buffer conditions seem to sit very close to the acidic results, indicating the stilbene is almost fully protonated at this pH range, which would agree with the previous experiments. This leads us to conclude that in buffer solution the StiCx09 chromophore must be in a deprotonated (or partially deprotonated) state which gives the stilbene an emissive fluorescence profile similar to what we observe here.

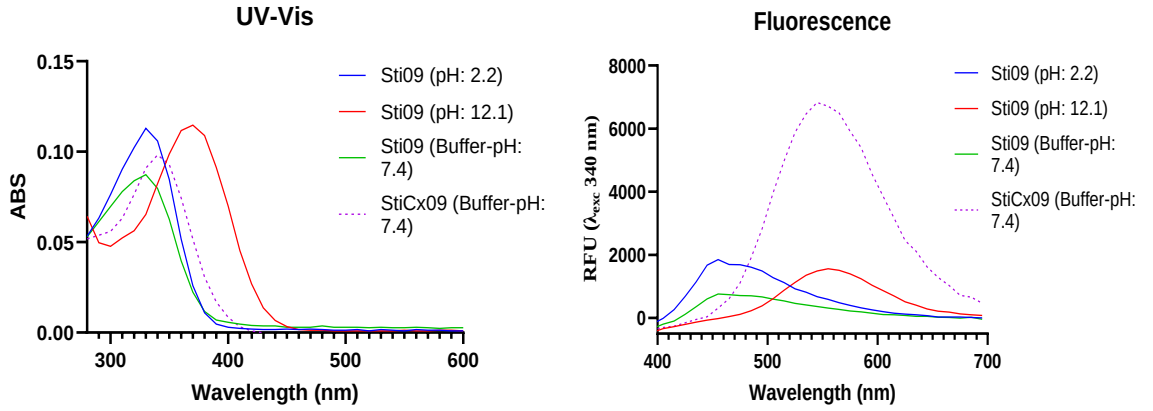

Figure 3.8: UV-Vis (left) and fluorescence (right) spectra of control studies at different pH. Aqueous basic and acid solutions were made in water adjusting the pH using 0.1M NaOH/HCl respectively. Buffer trails were done in a 10 mM phosphate buffer (pH = 7.4) solution.

Now that we understand the protonation state of our fluorophore, and that the deprotonated state is the emissive form, the question stands on what could be the photophysical reasons behind guest-induced changes in intensity. For that, we contrasted our results with some studies that investigated hydroxystilbene photochemistry.[136,138] We found that emission from these molecules can occur via an excited state proton transfer (ESPT), which agrees with what we know as it implies the deprotonated species is the one responsible for the emission. The Jablonski diagram in Figure 3.9 helps elucidate this, when the molecule (ROH) is excited (ROH*), there is a proton transfer generating an excited deprotonated species (RO^{-}*) which relaxes through fluorescence emission. This transition from RO^{-}* to RO^{-} is the emission that we see both in our StiCx09 and our deprotonated experiment results. However, there are competing non-emissive pathways such as internal conversion as well as torsion around the C=C bond. Studies by Crompton have shown that hydroxystilbenes with a cyano substituent at the para positions decrease the barrier for C=C torsion attributing this as the main decay pathway and resulting in low quantum yields for these molecules.[139] The quantum yield for

Sti09 will then be determined by the dissociation rate (k_a) in the excited state, internal conversion (k_{ic}) and C=C torsion (k_t) rates.

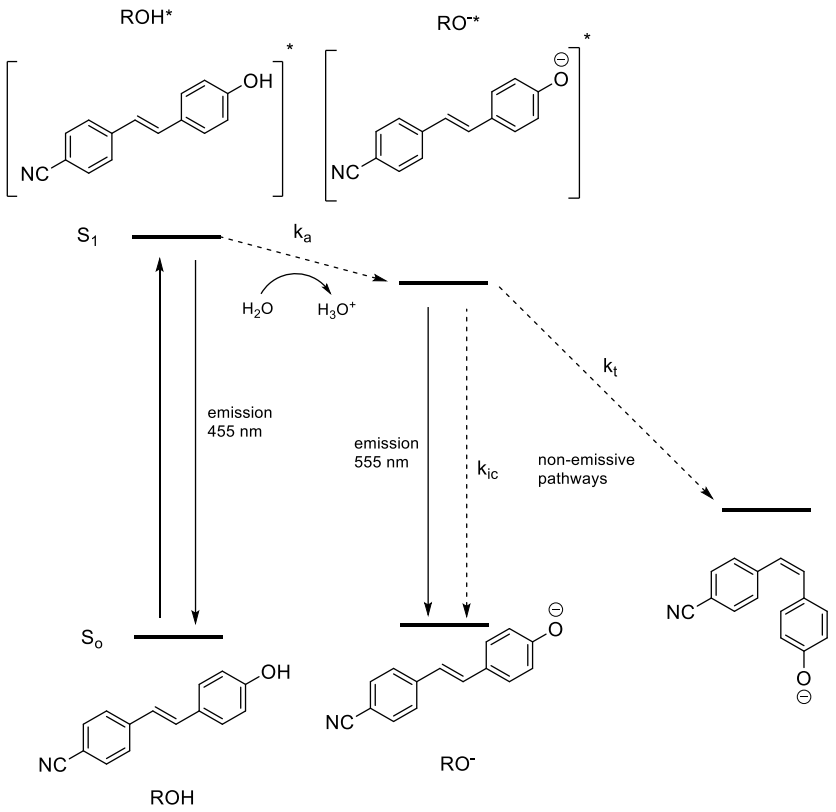

Figure 3.9: Jablonski diagram illustrating excited state proton transfer fluorescence of Sti09. Non-emissive pathways include internal conversion and torsion around the C=C bond which affect quantum yields. Figure adapted from Crompton's work.[139]

We still see a higher intensity for the StiCx09 than Sti09 in a basic medium, so aside from having the deprotonated species inclusion, the calixarene must increase the quantum yield in some other way. It could be hypothesized that the calixarene increases the torsional barrier in the stilbene limiting the non-radiative pathway of relaxation. Steric hindrance might be a possible reason, as the *trans* isomer is exclusively obtained in the initial synthesis hints that this is the thermodynamically favoured state. Since we don't see any shifts in absorbance or

fluorescence from guest inclusion in any of our trials, we can conclude that binding doesn't change the protonation state of the emissive species. Turn-on fluorescence could be attributed to guest inclusion enhancing this behaviour, hindering the energy barrier even more or also limiting the internal conversion pathways as well. Turn-off fluorescence is harder to explain, but it could be possible that cocaine and benzoylecgonine have an inverse effect and lead to lower barriers for the non-emissive relaxation pathways. The tropane alkaloid moiety could be considered responsible, however, scopolamine which also contains this group didn't show the same quenching. This demonstrates that the substituents in the tropane ring have an influence in inducing this response.

3.4 Conclusions

In summary, we were able to use NMR to get more information into the binding properties of our StiCx hosts. NMR titrations allowed us to see a change in the chemical shift of host and guest peaks indicating a change in the chemical environment which can be associated with binding. We used this information to propose a binding geometry where the methylamine group in both nicotine and cocaine is the most deeply embedded part of the molecule in the cavity. NOESY spectra gave us little evidence of proximity between the chemical species with only one considerable cross-peak interaction between the two species. It could be possible to optimize the experiment parameters to get more sensitivity for the NOE effect. DOSY on the other hand gave us very good results towards confirming host-guest complexation and we were able to get information on assembly sizes. First of all, we saw bigger sizes when the hosts were in solution with our guests, demonstrating the formation

of a host-guest complex. We were also able to demonstrate that our hosts exist as a free monomer in solution, ruling out a homo-dimer formation. Control studies with the stilbene moiety demonstrated that the emissive species is the deprotonated phenol and that this deprotonated form is present in our calixarene hosts. We also have found that integration of the fluorophore into the calixarene leads to vast differences in fluorescence intensity. We have proposed that changes in emission come from a change in the internal conversion and torsional barriers that affect the quantum yields of our system. This has brought a better understanding of the properties of our sensors which will help optimize and design new systems in the future.

3.5 Experimental Procedures

3.5.1 NMR titrations

NMR titrations were done in a deuterated sodium phosphate buffer (75 mM) that was prepared by dissolving 303.2 mg of Na_2HPO_4 and 50.9 mg of NaH_2PO_4 in 20 ml of D_2O and checking the pD to make sure it was in the 7.4 range (Range was adjusted with DCl and NaOD as required). A solution of 0.5 mM of host in 0.6 mL is prepared in an NMR tube and a spectra is taken, separately a stock solution of guest is prepared at 20 mM concentration. Increasing concentrations of guest are added to the NMR tube and a spectrum is taken at each concentration interval using a range from 0 to 20 equivalents of guest (0-10 mM). The volumes for the titrations are shown below in Table 3.2.

Table 3.2: Volumes of guest solution used in NMR titrations.

Eq. guest	Guest vol. added (uL)
0.4	6
0.8	6
1.1	5
1.5	6
2.1	10
3.3	20
4.6	23
5.7	20
7.5	34
10	52
20	391

The host and guest peaks were assigned based on shift and compared with the control spectra of each compound by itself in solution (See supporting information 3.5.1). Binding was attributed to a change in the chemical shift of most predominant and defined peaks. Changes in chemical shift ($\Delta\delta$) for guests were assigned as the difference between the respective peak shift at 1.1 equivalents and 10 equivalents. This range is chosen as 1.1 was the minimum concentration in which peaks were defined enough to select a maximum and in less concentrations they were too broad. Pictures were taken under a UV lamp to check for changes in solution brightness.

3.5.2 NOESY procedure

NOESY solutions were prepared in a deuterated sodium phosphate buffer (75 mM, pD 7.4) which was prepared as described in Section 3.4.1. A 1:1 host-guest solution at 7.5 mM is prepared in an NMR tube. Because NOE peaks are very weak, we use this concentration as it is the maximum we can go without saturating the buffer (10 times higher in concentration). The solution is then degassed by bubbling a flow of Argon on the solution for a few minutes, after which the tube is closed and sealed with parafilm. Degassing is done as dissolved Oxygen can promote spin relaxation leading to decreased NOE.[140] The experiments were run with a relaxation time (D_1) = 1 sec and mixing time (D_8) = 0.5 sec. A COSY is taken of the same sample for additional information on the intramolecular and intermolecular cross peaks.

3.5.3 DOSY procedure

For these experiments, solutions were prepared in a deuterated sodium phosphate buffer (75mM, pD 7.4) prepared as described in Section 3.4.1. All solutions used contained a 7.5 mM concentration of either host, guest or a 1:1 mixture of host-guest. Parameters for the DOSY experiments were manually determined in the following way:

- Pulse length (P1) is estimated by measuring the pulse length at 360°. P1 at 90° will equal this result divided by 4.
- Relaxation time (D1) is estimated by an inversion recovery pulse sequence where D1=T1*10. T1 is found manually changing D7 and using the equation T1=D7/ln(2).
- D20 (Δ) is set to 100 ms and P30 (δ) by finding a 90-90% intensity difference between the first and last spectra in the power array via the stebpgp1s1d pulse program.

Data is visualized through TopSpin and processed through Bruker Dynamic Center. Diffusion coefficients are calculated from user-defined integrals and hydrodynamic radius is obtained from the Stokes-Einstein equation (equation 3.1).

3.6 Supporting Information

3.6.1 NMR titration spectra

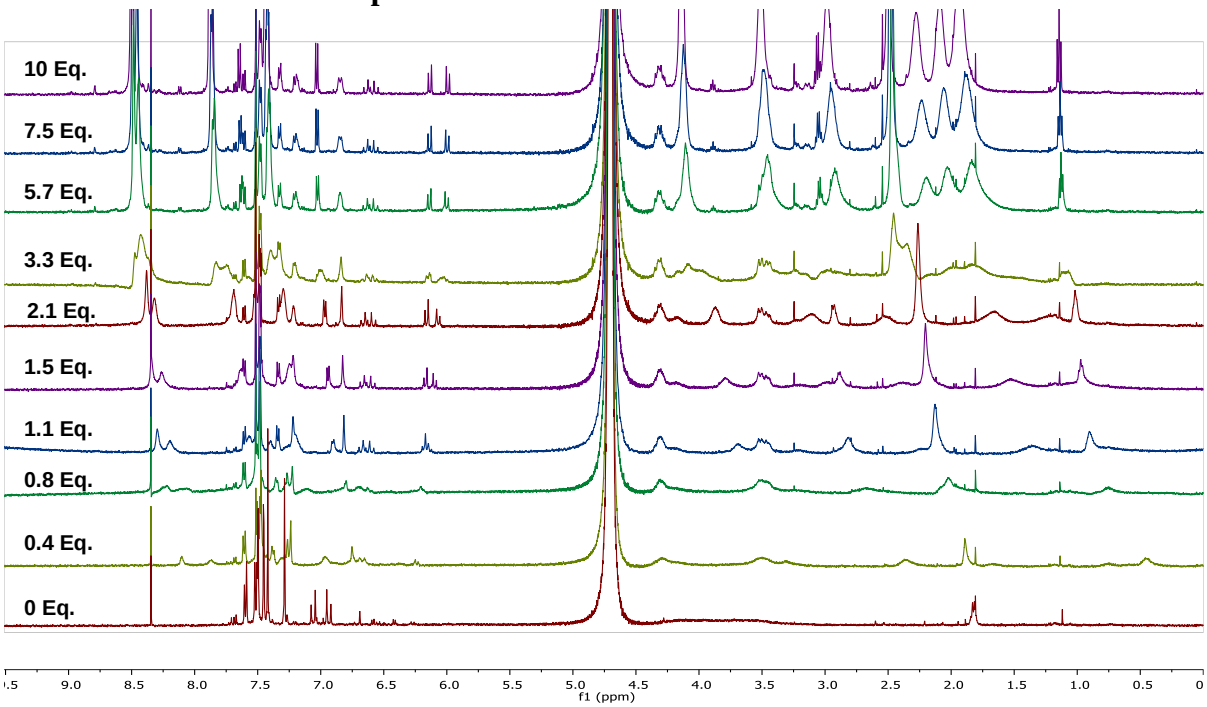

Figure S3.1: ^{1}H NMR titrations of StiCx09 (0.5 mM) with nicotine. The sample was in a deuterated sodium phosphate buffer (75 mM, pD 7.4).

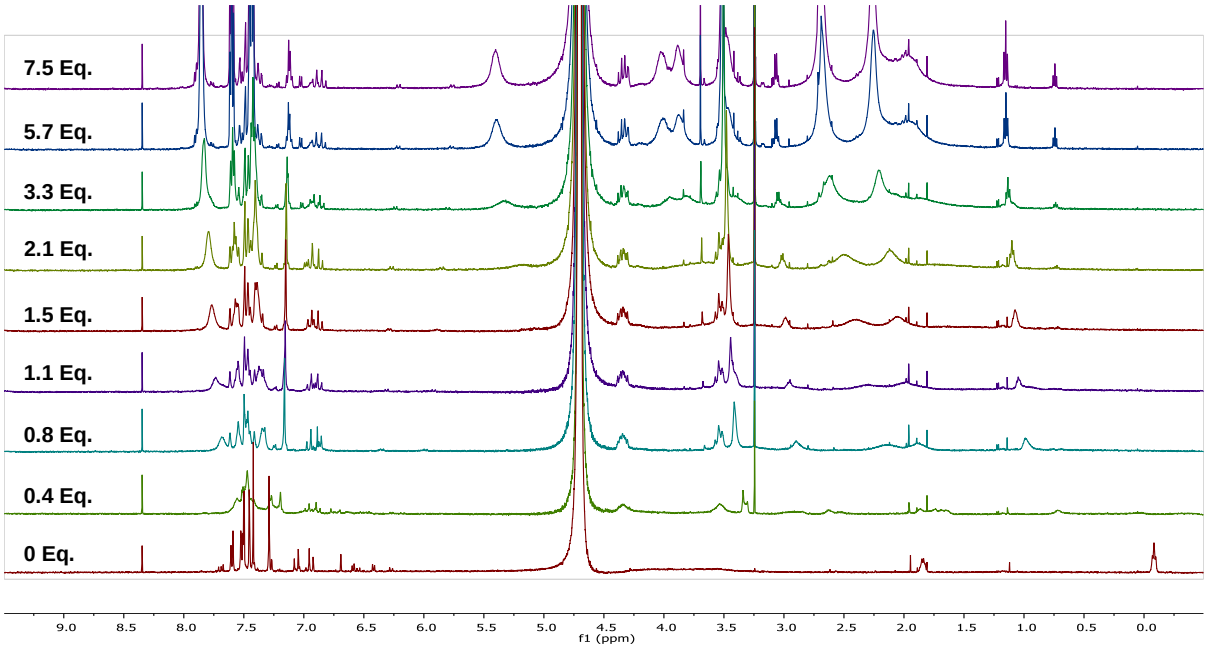

Figure S3.2: ^{1}H NMR titrations of StiCx09 (0.5 mM) with cocaine. The sample was in a deuterated sodium phosphate buffer (75 mM, pD 7.4).

3.6.2 NOESY Spectra

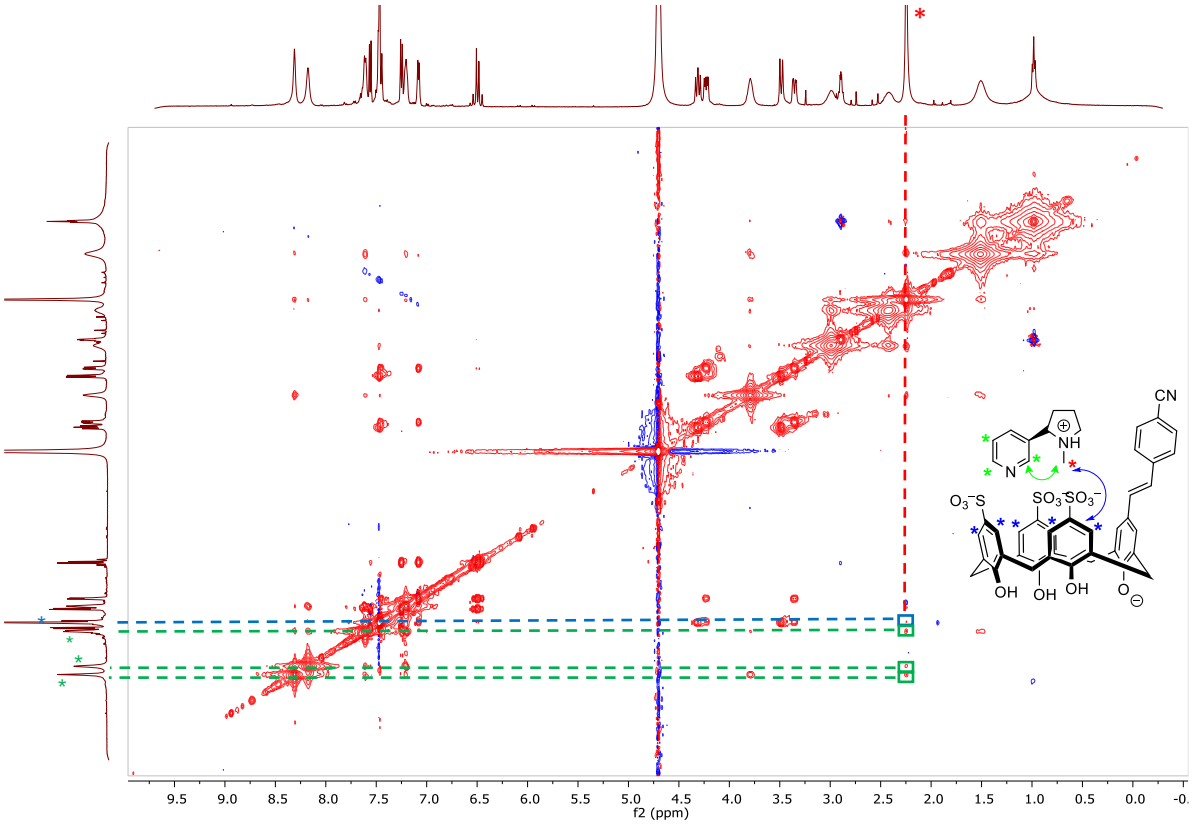

Figure S3.3: NOESY spectra of StiCx09 (7.5 mM) with nicotine. Relevant cross peaks are indicated with dotted lines. The sample was in a deuterated sodium phosphate buffer (75 mM, pD 7.4).

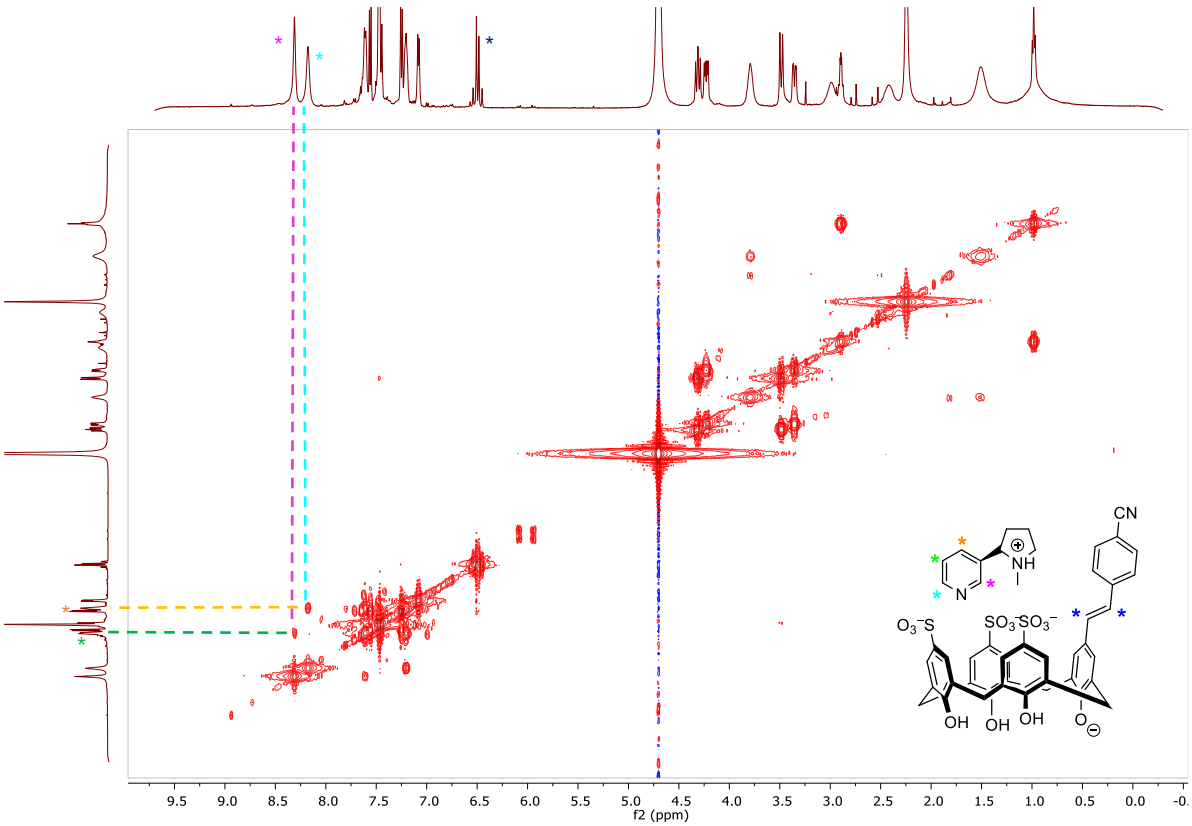

Figure S3.4: COSY spectra of StiCx09 (7.5 mM) with nicotine. Relevant cross peaks are indicated with dotted lines. The sample was in a deuterated sodium phosphate buffer (75 mM, pD 7.4).

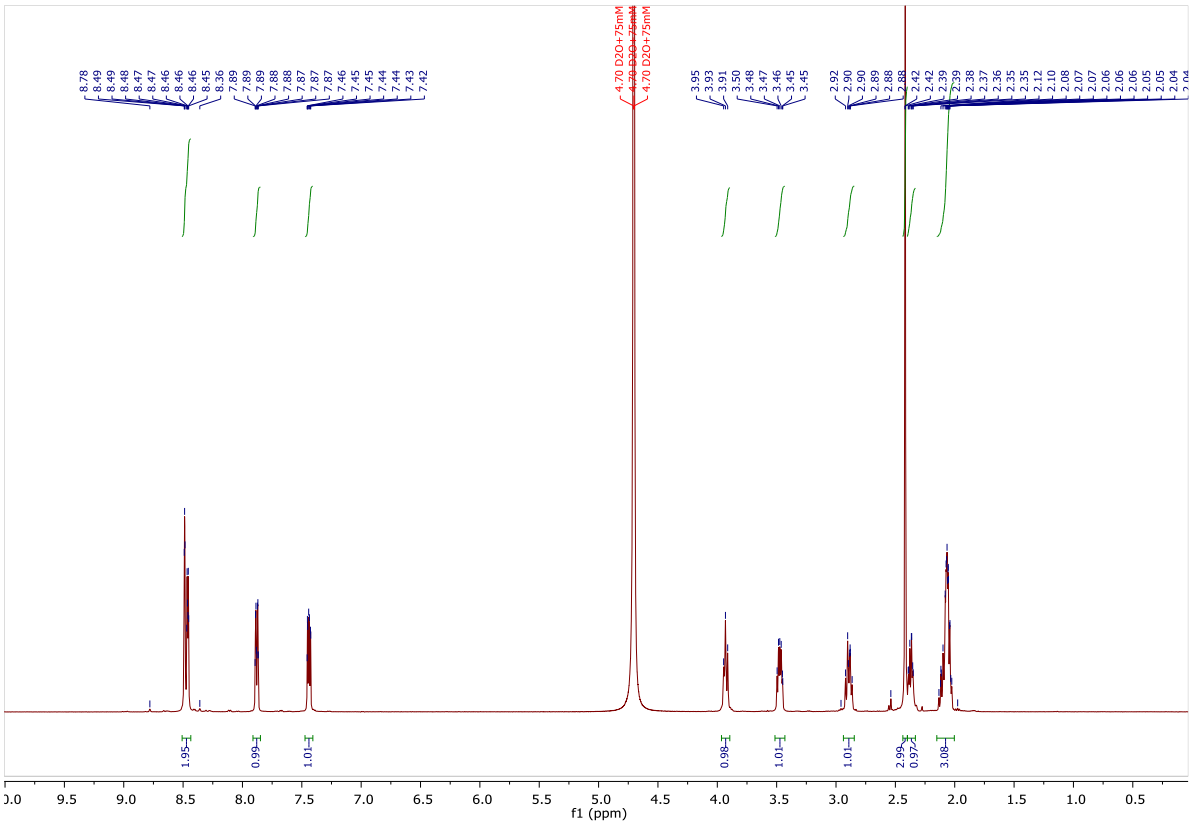

Figure S3.5: [1]H NMR nicotine. The sample was in a deuterated sodium phosphate buffer (75 mM, pD 7.4).

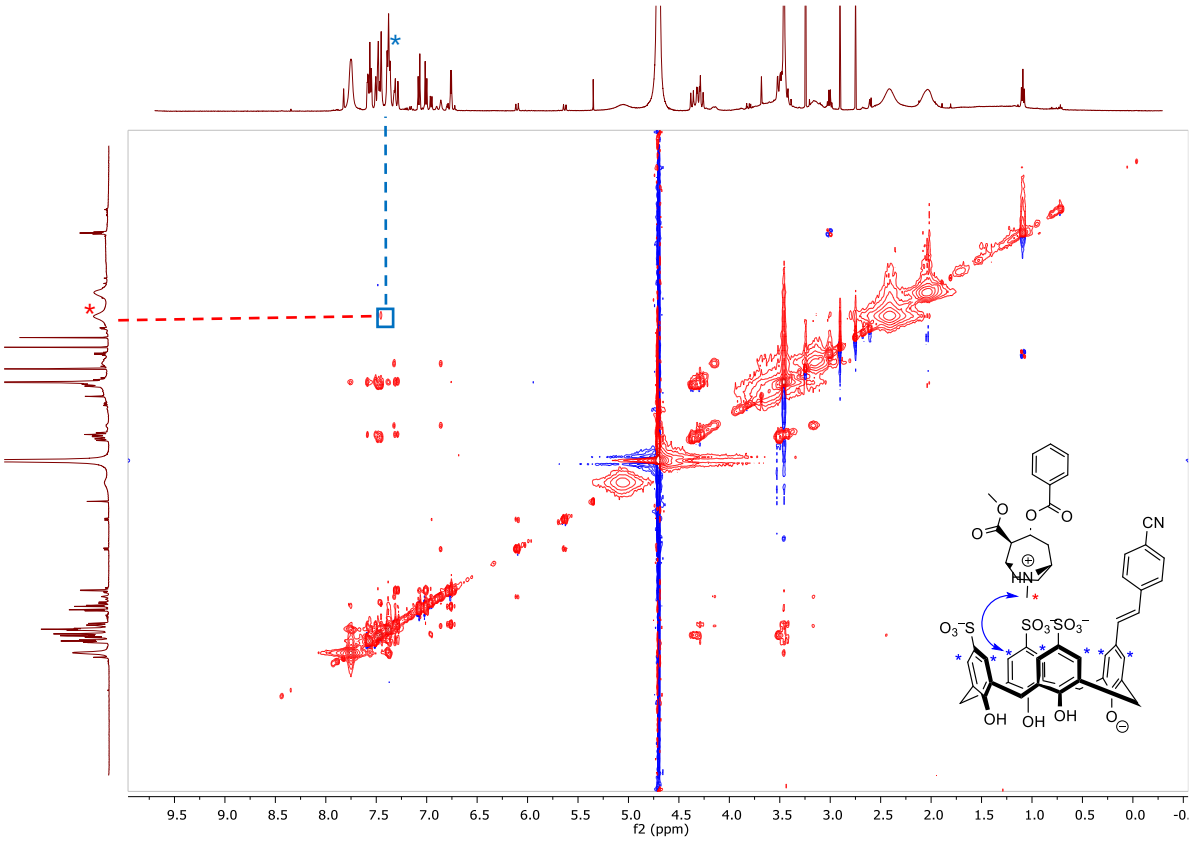

Figure S3.6: NOESY spectra of StiCx09 (7.5 mM) with cocaine. Relevant cross peaks are indicated with dotted lines. The sample was in a deuterated sodium phosphate buffer (75 mM, pD 7.4).

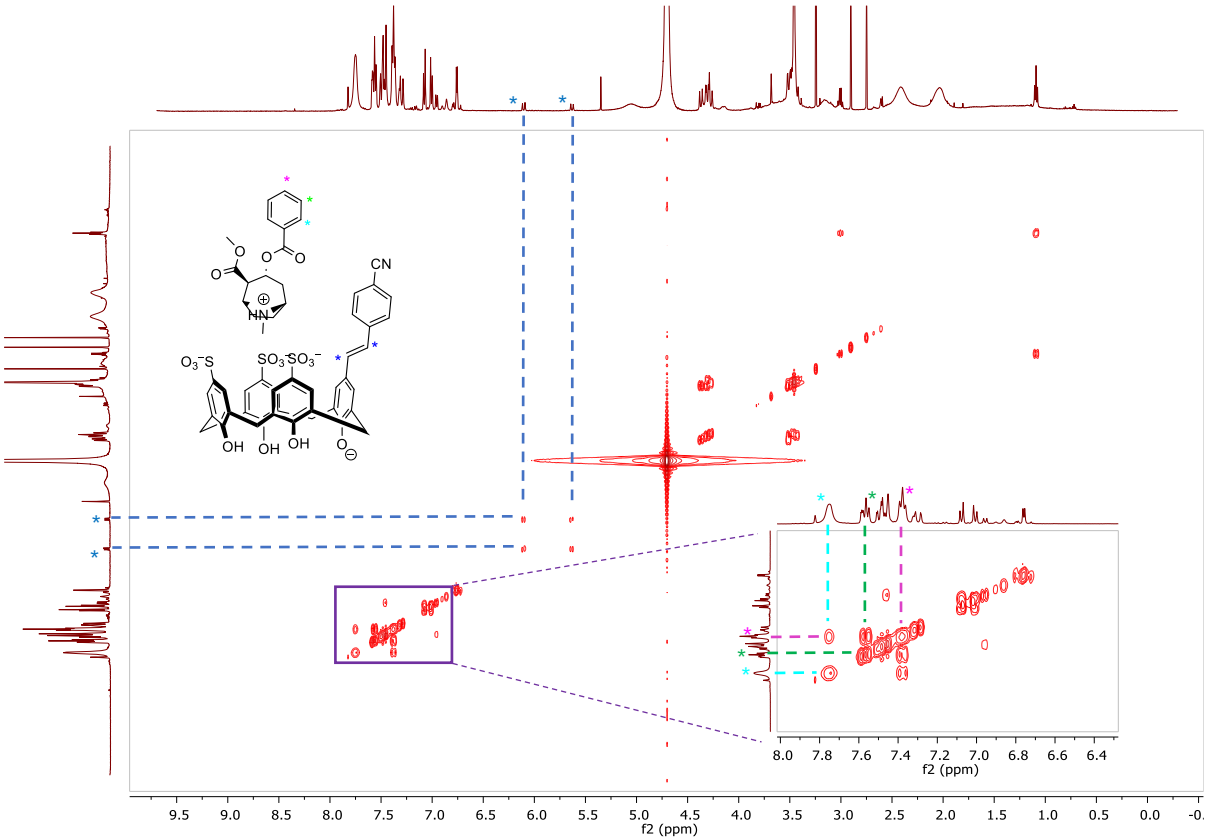

Figure S3.7: COSY spectra of StiCx09 (7.5 mM) with cocaine. Relevant cross peaks are indicated with dotted lines. The sample was in a deuterated sodium phosphate buffer (75 mM, pD 7.4).

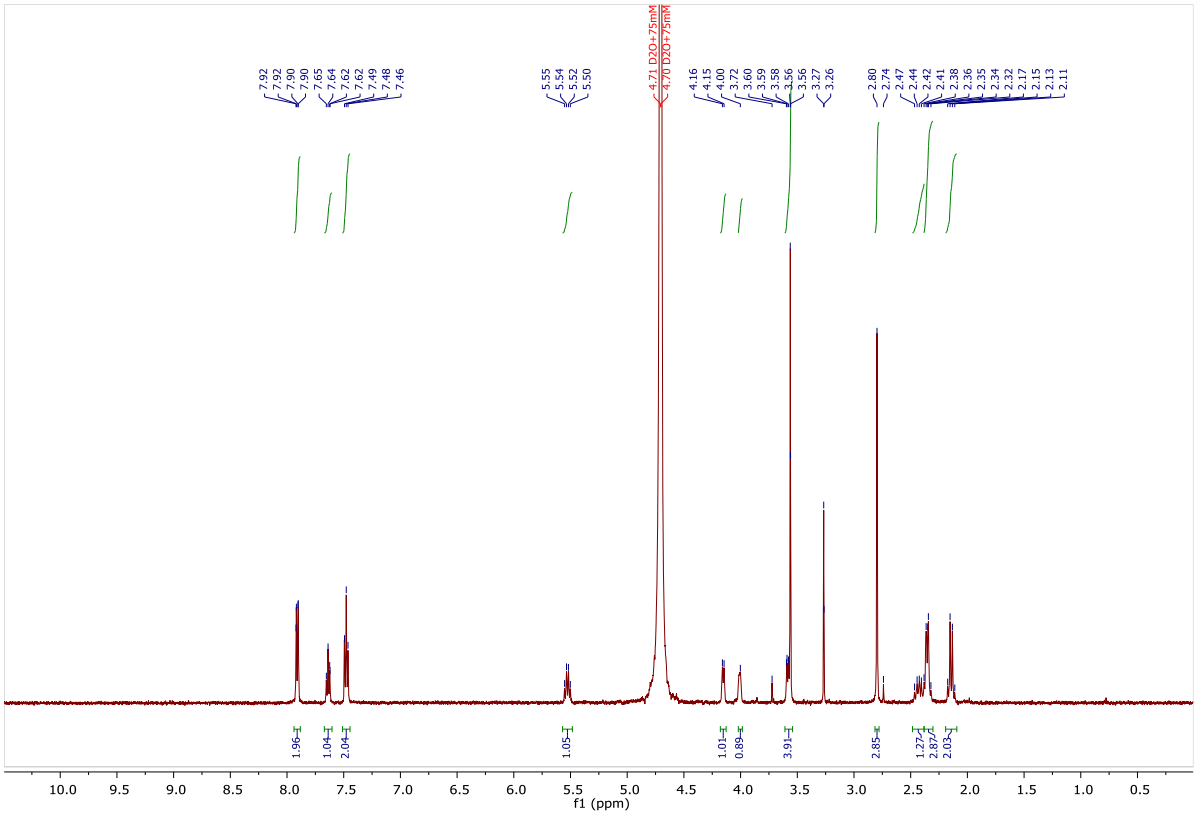

Figure S3.8: ^{1}H NMR nicotine. The sample was in a deuterated sodium phosphate buffer (75 mM, pD 7.4).

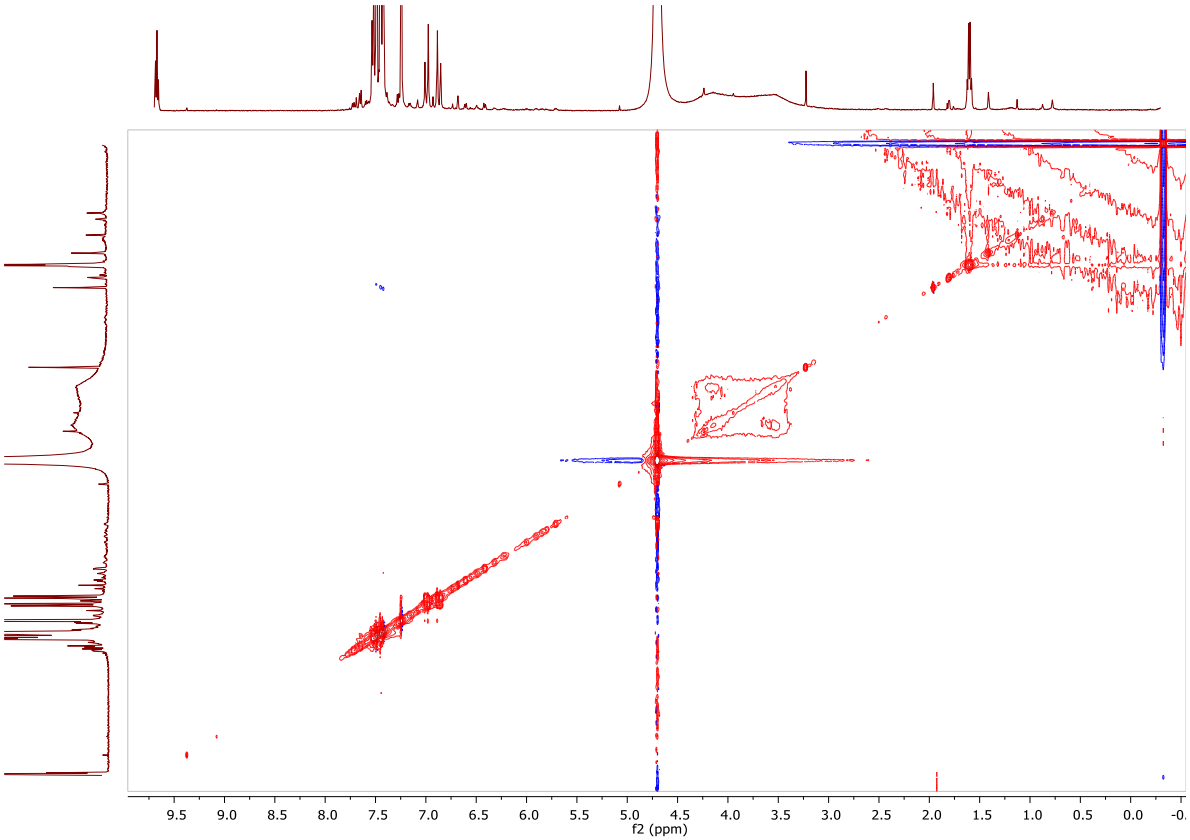

Figure S3.9: NOESY spectra of StiCx09 (7.5 mM) without guest. Lack of cross peaks indicates no dimerization. The sample was in a deuterated sodium phosphate buffer (75 mM, pD 7.4).

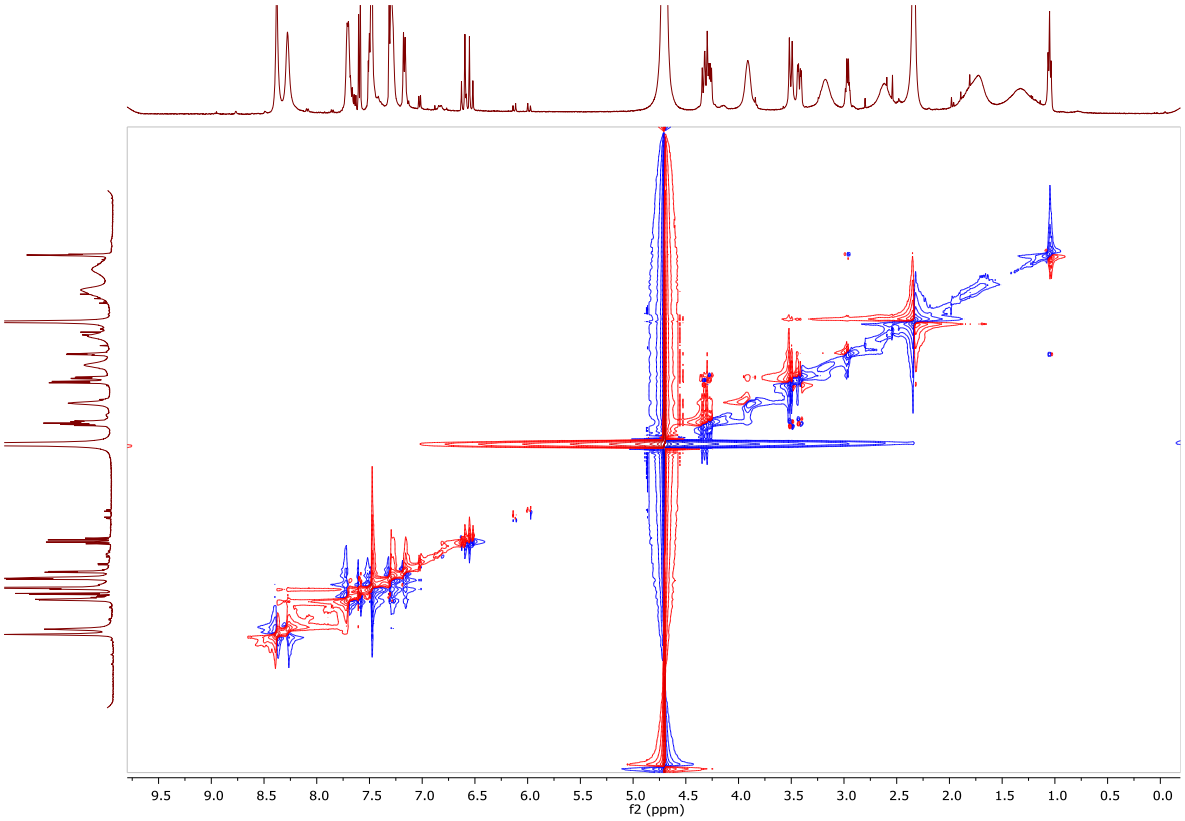

Figure S3.10: ROESY spectra of StiCx09 (7.5 mM) with nicotine. No relevant cross-peaks beyond intramolecular methylene and TEA interactions. The sample was in a deuterated sodium phosphate buffer (75 mM, pD 7.4).

3.6.3 DOSY Experiments

Table S 3.1: DOSY parameters for SitCx09

used γ:	26752 rad/(s*Gauss)
used δ:	0.003 s
used Δ:	0.0999 s
used gradient strength:	variable
Random error estimation of data:	RMS per spectrum (or trace/plane)
Systematic error estimation of data:	worst case per peak scenario
Fit parameter Error estimation method:	from fit using arbitrary y uncertainties
Confidence level:	95%
Used peaks:	peaks from peaklist.xml at spectrum
Used integrals:	area integral
Used Gradient strength:	all values (including replicates) used

Table S3.2: DOSY coefficient results for StiCx09. *Only peaks 1,2,3 and 4 were used for r_h calculations.

Peak name	*F2 [ppm]*	*Io*	*D [m2/s]*	*error*	*errorScale*	*fitInfo*
*1**	*6,9*	*7,03* ± 0.04 x 10^6	*2,8E-10*	*4,0E-12*	*2,0*	*Done*
*2**	*7,0*	*7,68* ± 0.05 x 10^6	*2,7E-10*	*4,6E-12*	*2,0*	*Done*
*3**	*7,3*	*12,96* ± 0.02 x 10^6	*2,7E-10*	*1,2E-12*	*2,0*	*Done*
*4**	*6,6*	*4,37* ± 0.02 x 10^6	*3,0E-10*	*3,9E-12*	*2,0*	*Done*
5	*1,6*	*1,43* ± 0.06 x 10^6	*2,9E-10*	*2,8E-12*	*2,0*	*Done*

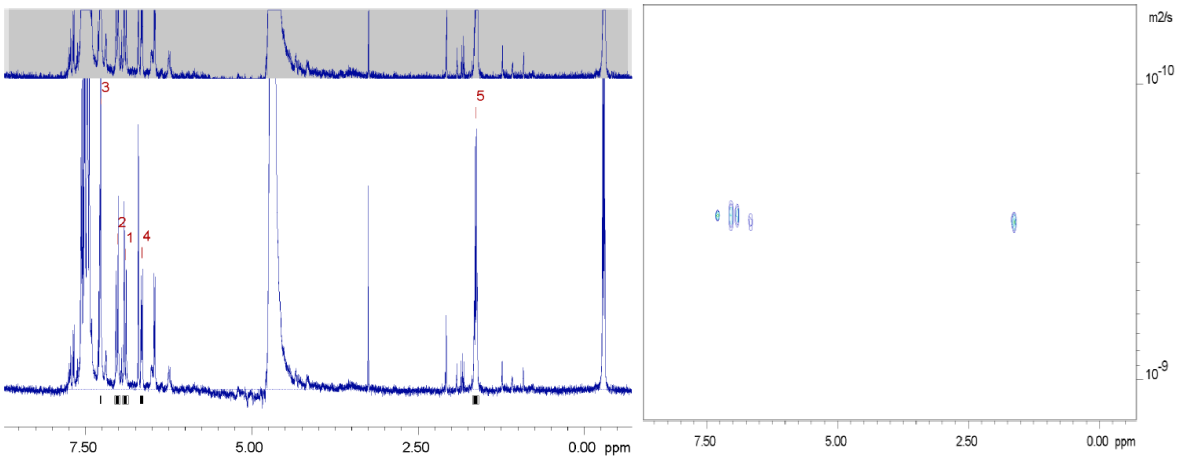

Figure S3.11: [1]H NMR (left) with highlighted integrals and 2D DOSY spectra (right) of StiCx09 used to calculate diffusion coefficients. The sample was in a deuterated phosphate buffer (75 mM, pD 7.4).

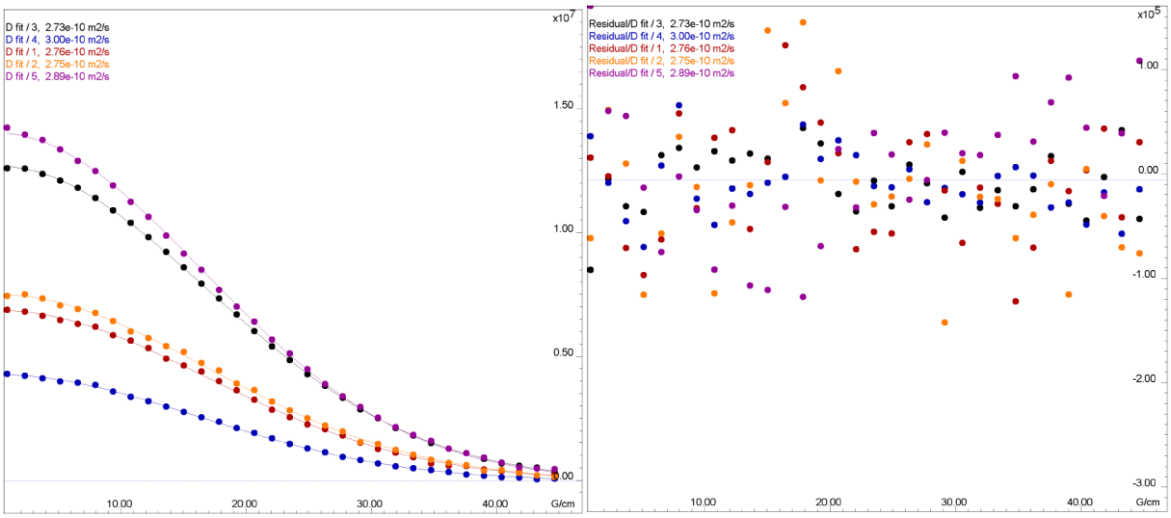

Figure S3.12: 1D DOSY plots of each integral for StiCx09.

Table S3.3: DOSY parameters for StiCx09 + 1 eq. of nicotine

used γ:	26752 rad/(s*Gauss)
used δ:	0.003 s
used Δ:	0.0999 s
used gradient strength:	variable
Random error estimation of data:	RMS per spectrum (or trace/plane)
Systematic error estimation of data:	worst case per peak scenario
Fit parameter Error estimation method:	from fit using arbitrary y uncertainties
Confidence level:	95%
Used peaks:	peaks from peaklist.xml at spectrum
Used integrals:	area integral
Used Gradient strength:	all values (including replicates) used

Table S3.4: DOSY coefficient results for StiCx09 + 1 eq. nicotine. *Only peaks 1 and 2 were used for r_h calculations

Peak name	*F2 [ppm]*	*Io*	*D [m2/s]*	*error*	*errorScale*	*fitInfo*
*1**	*6,5*	*13,94* ± 0.2 x 10^6	*2,4E-10*	*6,1E-12*	*2,0*	*Done*
*2**	*7,1*	*14,8* ± 0.1 x 10^6	*2,4E-10*	*4,0E-12*	*2,0*	*Done*
3	*8,2*	*16,8* ± 0.1 x 10^6	*4,1E-10*	*7,8E-12*	*2,0*	*Done*
4	*3,8*	*17,7* ± 0.3 x 10^6	*3,7E-10*	*1,6E-11*	*2,0*	*Done*

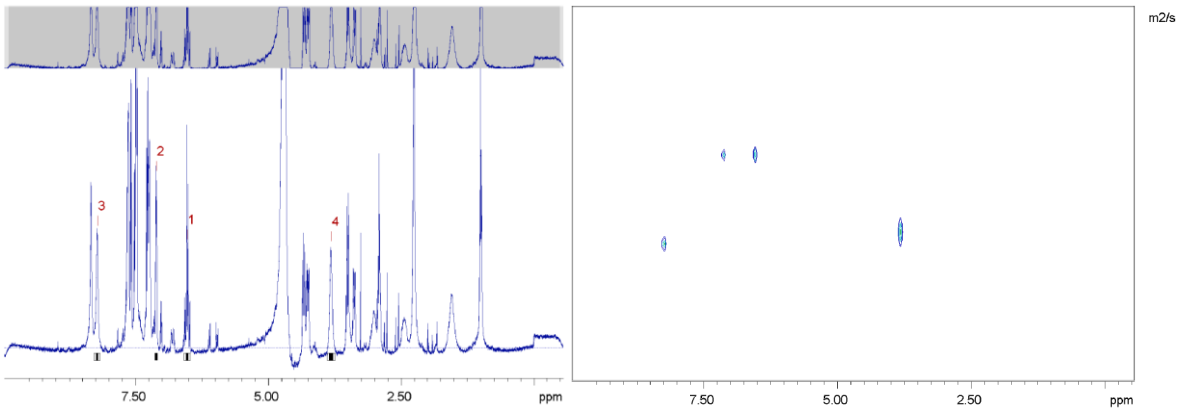

Figure S3.13: ^{1}H NMR (left) with highlighted integrals and 2D DOSY spectra (right) of StiCx09 + nicotine used to calculate diffusion coefficients. The sample was in a deuterated phosphate buffer (75 mM, pD 7.4).

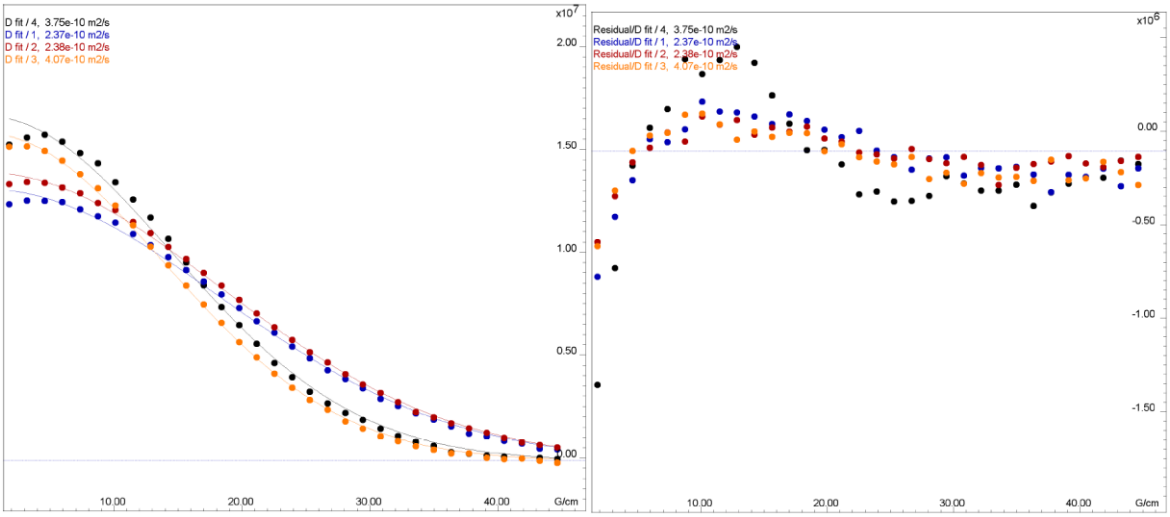

Figure S3.14: 1D DOSY plots of each integral for StiCx09 + nicotine.

Table S3.5: DOSY parameters for StiCx + 1 eq. of cocaine

used γ:	26752 rad/(s*Gauss)
used δ:	0.0026 s
used Δ:	0.0999 s
used gradient strength:	variable
Random error estimation of data:	RMS per spectrum (or trace/plane)
Systematic error estimation of data:	worst case per peak scenario
Fit parameter Error estimation method:	from fit using arbitrary y uncertainties
Confidence level:	95%
Used peaks:	peaks from peaklist.xml at spectrum
Used integrals:	area integral
Used Gradient strength:	all values (including replicates) used

Table S3.6: DOSY coefficient results for StiCx09 + 1 eq. of cocaine. *Only peaks 1 and 2 were used for r_h calculations.

Peak name	*F2 [ppm]*	*Io*	*D [m2/s]*	*error*	*errorScale*	*fitInfo*
*1**	*7,1*	*5,61* ± 0.1 x 10^6	*2,1E-10*	*0*	*2,0*	*Done*
*2**	*7,0*	*5,32* ± 0.1 x 10^6	*2,1E-10*	*0*	*2,0*	*Done*

3	*6,8*	*4,95* ± 0.07 x 10^6	*2,2E-10*	*0*	*2,0*	*Done*
4	*7,7*	*15,88* ± 0.2 x 10^6	*3,2E-10*	*0*	*2,0*	*Done*
5	*2,9*	*5,73* ± 0.04 x 10^6	*9,0E-10*	*0*	*2,0*	*Done*
6	*2,8*	*5,86* ± 0.05 x 10^6	*9,4E-10*	*0*	*2,0*	*Done*
7	*2,0*	*11,33* ± 0.1 x 10^6	*4,1E-10*	*0*	*2,0*	*Done*

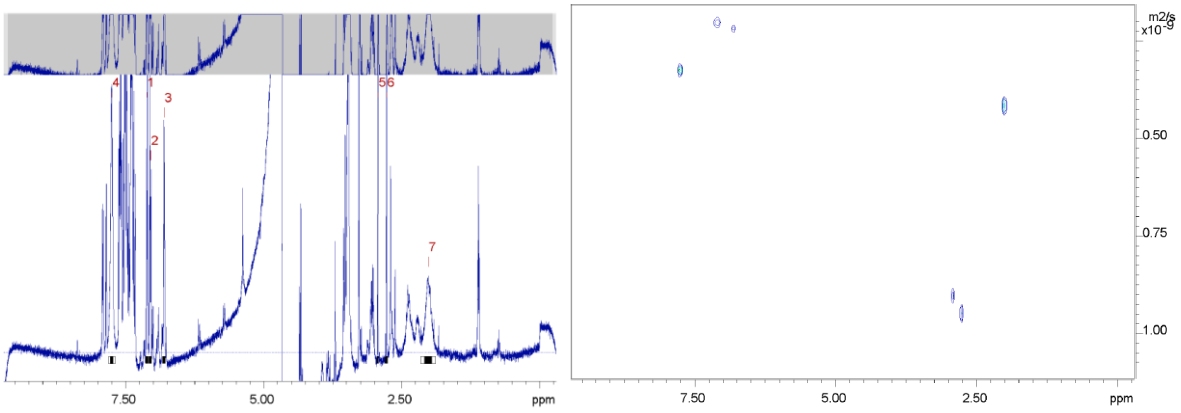

Figure S3.15: ^{1}H NMR (left) with highlighted integrals and 2D DOSY spectra (right) of StiCx09 + cocaine used to calculate diffusion coefficients. The sample was in a deuterated phosphate buffer (75 mM, pD 7.4).

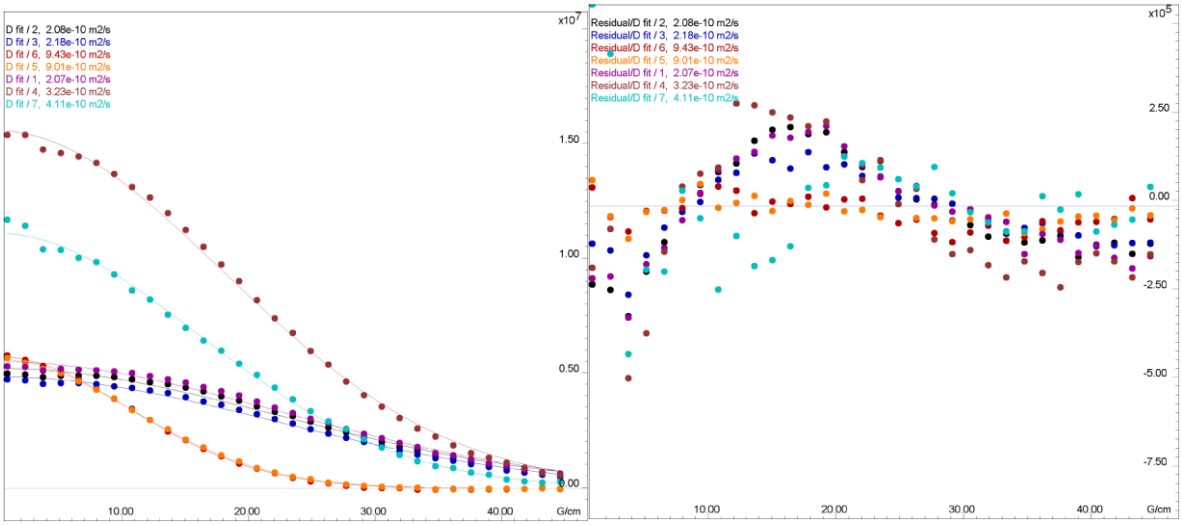

Figure S3.16: 1D DOSY plots of each integral for StiCx09 + cocaine.

Table S3.7: DOSY parameters for nicotine

used γ:	**26752 rad/(s*Gauss)**
used δ:	0.0022 s
used Δ:	0.0999 s
used gradient strength:	variable
Random error estimation of data:	RMS per spectrum (or trace/plane)
Systematic error estimation of data:	worst case per peak scenario
Fit parameter Error estimation method:	from fit using arbitrary y uncertainties
Confidence level:	95%
Used peaks:	peaks from peaklist.xml at spectrum
Used integrals:	area integral
Used Gradient strength:	all values (including replicates) used

Table S3.8: DOSY coefficient results for nicotine.

Peak name	*F2 [ppm]*	*Io*	*D [m2/s]*	*error*	*errorScale*	*fitInfo*
1	*7,5*	*18,66* ± 0.05 x 10^6	*5,4E-10*	*0*	*2,1*	*Done*
2	*7,9*	*18,3* ± 0.07 x 10^6	*5,4E-10*	*0*	*2,1*	*Done*
3	*3,1*	*16,58*± 0.07 x 10^6	*5,5E-10*	*0*	*2,1*	*Done*
4	*2,6*	*52,77* ± 0.06 x 10^6	*5,5E-10*	*0*	*2,1*	*Done*

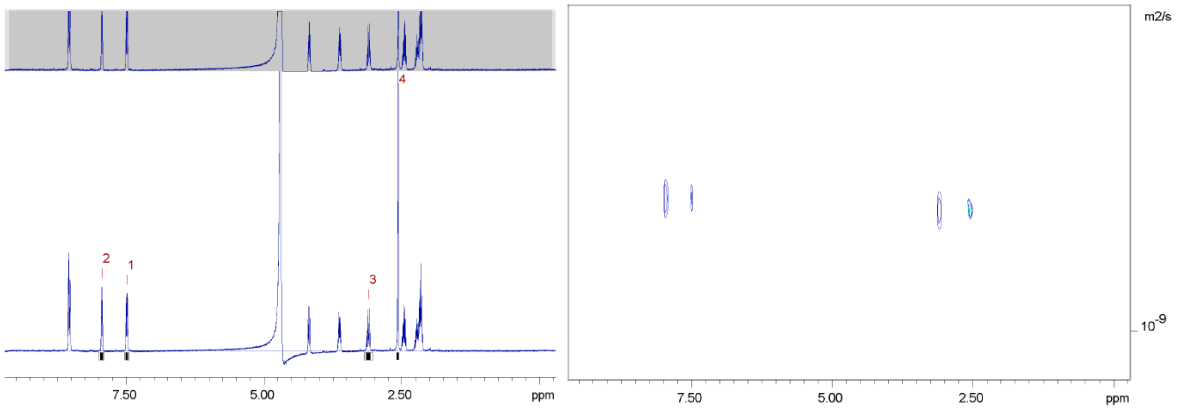

Figure S3.17: ^{1}H NMR (left) with highlighted integrals and 2D DOSY spectra (right) of nicotine used to calculate diffusion coefficients. The sample was in a deuterated phosphate buffer (75 mM, pD 7.4).

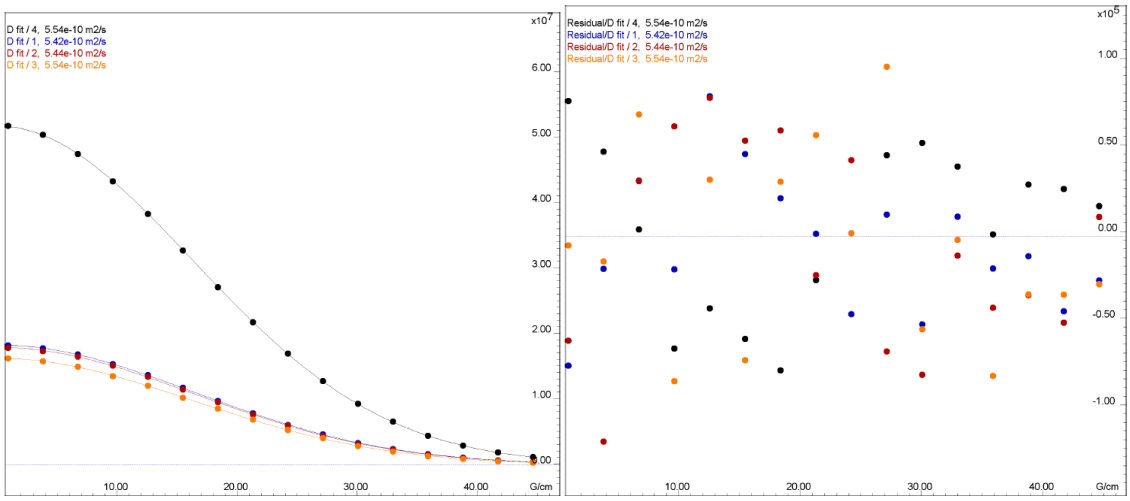

Figure S3.18: 1D DOSY plots of each integral for nicotine.

Table S3.9: DOSY parameters for cocaine

used γ:	**26752 rad/(s*Gauss)**
used δ:	0.0022 s
used Δ:	0.0999 s
used gradient strength:	variable
Random error estimation of data:	RMS per spectrum (or trace/plane)
Systematic error estimation of data:	worst case per peak scenario
Fit parameter Error estimation method:	from fit using arbitrary y uncertainties
Confidence level:	95%
Used peaks:	peaks from peaklist.xml at spectrum
Used integrals:	area integral
Used Gradient strength:	all values (including replicates) used

Table S3.10: DOSY coefficient results for cocaine

Peak name	*F2 [ppm]*	*Io*	*D [m2/s]*	*error*	*errorScale*	*fitInfo*
1	*7,9*	*27,1* ± 0.03 x 10^6	*4,4E-10*	*0*	*2,0*	*Done*
2	*7,5*	*27,18* ± 0.04 x 10^6	*4,4E-10*	*0*	*2,0*	*Done*
3	*2,8*	*35,48* ± 0.03 x 10^6	*4,5E-10*	*0*	*2,0*	*Done*
4	*2,1*	*21,77* ± 0.05 x 10^6	*4,6E-10*	*0*	*2,0*	*Done*

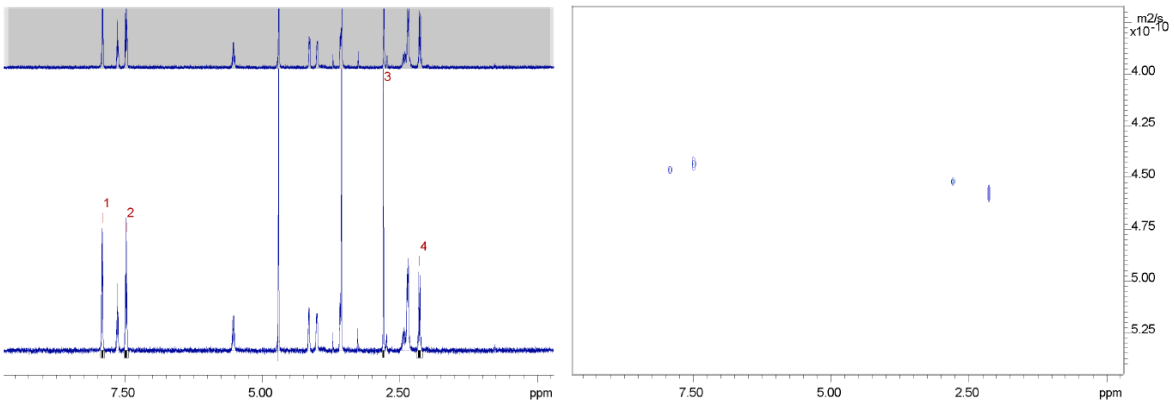

Figure S3.19: ^{1}H NMR (left) with highlighted integrals and 2D DOSY spectra (right) of cocaine used to calculate diffusion coefficients. The sample was in a deuterated phosphate buffer (75 mM, pD 7.4).

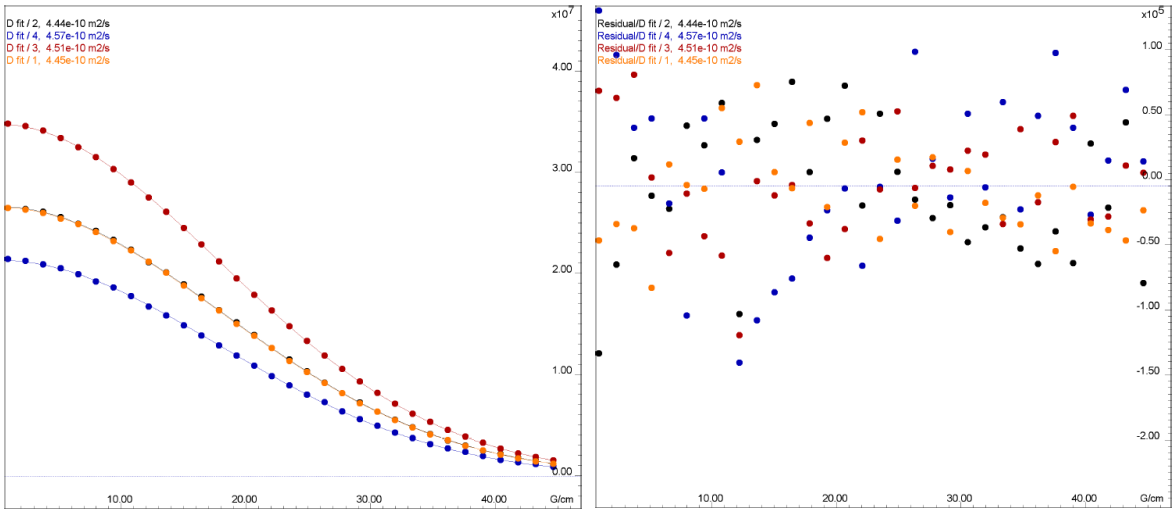

Figure S3.20: 1D DOSY plots of each integral for cocaine.

3.5.4 Control stilbene experiments

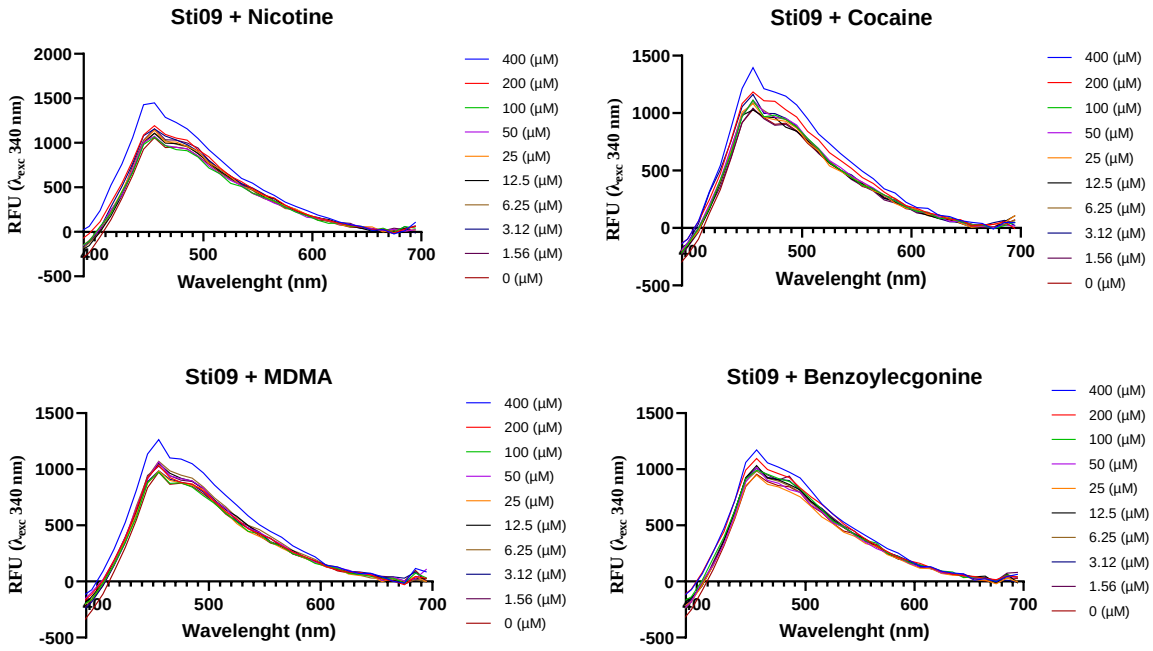

Figure S3.21: Fluorescence titration curves of control Sti09 (8µM) control with nicotine, cocaine, MDMA and benzoylecgonine across a 0-400 µM range. Trials were done in a sodium phosphate buffer (100 mM, pH 7.4).

References

(1) Mako, T. L.; Racicot, J. M.; Levine, M. Supramolecular Luminescent Sensors. *Chem. Rev.* **2019**, *119* (1), 322–477. https://doi.org/10.1021/acs.chemrev.8b00260.

(2) Webber, M. J.; Appel, E. A.; Meijer, E. W.; Langer, R. Supramolecular Biomaterials. *Nat. Mater.* **2016**, *15* (1), 13–26. https://doi.org/10.1038/nmat4474.

(3) Hou, X.; Ke, C.; Bruns, C. J.; McGonigal, P. R.; Pettman, R. B.; Stoddart, J. F. Tunable Solid-State Fluorescent Materials for Supramolecular Encryption. *Nat. Commun.* **2015**, *6* (1), 6884. https://doi.org/10.1038/ncomms7884.

(4) Jayawickramarajah, J.; Wilson, A. J. 5.01 - Volume 5: Supramolecular Medicinal Chemistry and Chemical Biology. In *Comprehensive Supramolecular Chemistry II*; Atwood, J. L., Ed.; Elsevier: Oxford, 2017; p 1. https://doi.org/10.1016/B978-0-12-409547-2.12557-0.

(5) Shumilova, T. A.; Rüffer, T.; Lang, H.; Kataev, E. A. Straightforward Design of Fluorescent Receptors for Sulfate: Study of Non-Covalent Interactions Contributing to Host–Guest Formation. *Chem. – Eur. J.* **2018**, *24* (7), 1500–1504. https://doi.org/10.1002/chem.201704098.

(6) Gu, A.; Wheate, N. J. Macrocycles as Drug-Enhancing Excipients in Pharmaceutical Formulations. *J. Incl. Phenom. Macrocycl. Chem.* **2021**, *100* (1), 55–69. https://doi.org/10.1007/s10847-021-01055-9.

(7) Li, J.-J.; Rong, R.-X.; Yang, Y.; Hu, Z.-Y.; Hu, B.; Zhao, Y.-Y.; Li, H.-B.; Hu, X.-Y.; Wang, K.-R.; Guo, D.-S. Triple Targeting Host–Guest Drug Delivery System Based on Lactose-Modified Azocalix[4]Arene for Tumor Ablation. *Mater. Horiz.* **2023**, *10* (5), 1689–1696. https://doi.org/10.1039/D3MH00018D.

(8) Lagona, J.; Mukhopadhyay, P.; Chakrabarti, S.; Isaacs, L. The Cucurbit[n]Uril Family. *Angew. Chem. Int. Ed.* **2005**, *44* (31), 4844–4870. https://doi.org/10.1002/anie.200460675.

(9) Rekharsky, M. V.; Inoue, Y. Complexation and Chiral Recognition Thermodynamics of 6-Amino-6-Deoxy-β-Cyclodextrin with Anionic, Cationic, and Neutral Chiral Guests: Counterbalance between van Der Waals and Coulombic Interactions. *J. Am. Chem. Soc.* **2002**, *124* (5), 813–826. https://doi.org/10.1021/ja010889z.

(10) Pedersen, C. J. Cyclic Polyethers and Their Complexes with Metal Salts. *J. Am. Chem. Soc.* **1967**, *89* (10), 2495–2496. https://doi.org/10.1021/ja00986a052.

(11) Guo, C.; Sedgwick, A. C.; Hirao, T.; Sessler, J. L. Supramolecular Fluorescent Sensors: An Historical Overview and Update. *Coord. Chem. Rev.* **2021**, *427*, 213560. https://doi.org/10.1016/j.ccr.2020.213560.

(12) Minta, A.; Tsien, R. Y. Fluorescent Indicators for Cytosolic Sodium*. *J. Biol. Chem.* **1989**, *264* (32), 19449–19457. https://doi.org/10.1016/S0021-9258(19)47321-3.

(13) Lee, M. H.; Sessler, J. L.; Kim, J. S. Disulfide-Based Multifunctional Conjugates for Targeted Theranostic Drug Delivery. *Acc. Chem. Res.* **2015**, *48* (11), 2935–2946. https://doi.org/10.1021/acs.accounts.5b00406.

(14) Fernandez, A.; Vermeren, M.; Humphries, D.; Subiros-Funosas, R.; Barth, N.; Campana, L.; MacKinnon, A.; Feng, Y.; Vendrell, M. Chemical Modulation of in Vivo Macrophage Function with Subpopulation-Specific Fluorescent Prodrug Conjugates. *ACS Cent. Sci.* **2017**, *3* (9), 995–1005. https://doi.org/10.1021/acscentsci.7b00262.

(15) Ding, N.; Li, Z.; Tian, X.; Zhang, J.; Guo, K.; Wang, P. Azo-Based near-Infrared Fluorescent Theranostic Probe for Tracking Hypoxia-Activated Cancer Chemotherapy in Vivo. *Chem. Commun.* **2019**, *55* (87), 13172–13175. https://doi.org/10.1039/C9CC06727B.

(16) Bazylevich, A.; Patsenker, L. D.; Gellerman, G. Exploiting Fluorescein Based Drug Conjugates for Fluorescent Monitoring in Drug Delivery. *Dyes Pigments* **2017**, *139*, 460–472. https://doi.org/10.1016/j.dyepig.2016.11.057.
(17) *Cleavable linkers in chemical biology - ScienceDirect*. https://www.sciencedirect.com/science/article/pii/S096808961100597 9?pes=vor#b0050 (accessed 2023-07-27).
(18) Patsenker, L.; Gellerman, G. Fluorescent Reporters for Drug Delivery Monitoring. *Isr. J. Chem.* **2020**, *60* (5–6), 504–518. https://doi.org/10.1002/ijch.201900137.
(19) Gale, P. A.; Twyman, L. J.; Handlin, C. I.; Sessler, J. L. A Colourimetric Calix[4]Pyrrole–4-Nitrophenolate Based Anion Sensor†. *Chem. Commun.* **1999**, No. 18, 1851–1852. https://doi.org/10.1039/A905743I.
(20) Minami, T.; Liu, Y.; Akdeniz, A.; Koutnik, P.; Esipenko, N. A.; Nishiyabu, R.; Kubo, Y.; Anzenbacher, P. Jr. Intramolecular Indicator Displacement Assay for Anions: Supramolecular Sensor for Glyphosate. *J. Am. Chem. Soc.* **2014**, *136* (32), 11396–11401. https://doi.org/10.1021/ja504535q.
(21) Liu, Y.; Hu, C.; A. Serna, J.; Biedermann, F.; A. Levkin, P. Binding Affinity-Based Intracellular Drug Detection Enabled by a Unimolecular Cucurbit[7]Uril-Dye Conjugate. *RSC Chem. Biol.* **2023**. https://doi.org/10.1039/D3CB00131H.
(22) Krämer, J.; Grimm, L. M.; Zhong, C.; Hirtz, M.; Biedermann, F. A Supramolecular Cucurbit[8]Uril-Based Rotaxane Chemosensor for the Optical Tryptophan Detection in Human Serum and Urine. *Nat. Commun.* **2023**, *14* (1), 518. https://doi.org/10.1038/s41467-023-36057-3.
(23) Kumar, N. M.; Gruhs, P.; Casini, A.; Biedermann, F.; Moreno-Alcántar, G.; Picchetti, P. Electrochemical Detection of Drugs via a Supramolecular Cucurbit[7]Uril-Based Indicator Displacement Assay. *ACS Sens.* **2023**, *8* (7), 2525–2532. https://doi.org/10.1021/acssensors.3c00008.
(24) Minaker, S. A.; Daze, K. D.; Ma, M. C. F.; Hof, F. Antibody-Free Reading of the Histone Code Using a Simple Chemical Sensor Array. *J. Am. Chem. Soc.* **2012**, *134* (28), 11674–11680. https://doi.org/10.1021/ja303465x.
(25) Yokoyama, S.; Ito, A.; Asahara, H.; Nishiwaki, N. Anion-Capture-Induced Fluorescence Enhancement of Bis(Cyanostyryl)Pyrrole Based on Restricted Access to a Conical Intersection. *Bull. Chem. Soc. Jpn.* **2019**, *92* (11), 1807–1815. https://doi.org/10.1246/bcsj.20190196.
(26) Zhang, H.; Yang, J.; Liu, Y.-Y.; Song, S.; Ma, J.-F. A Family of Metal–Organic Frameworks with a New Chair-Conformation Resorcin[4]Arene-Based Ligand: Selective Luminescent Sensing of Amine and Aldehyde Vapors, and Solvent-Mediated Structural Transformations. *Cryst. Growth Des.* **2016**, *16* (6), 3244–3255. https://doi.org/10.1021/acs.cgd.6b00213.
(27) Chaudhuri, S.; J. DiScenza, D.; Smith, B.; Yocum, R.; Levine, M. Array-Based Detection of Isomeric and Analogous Analytes Employing Synthetically Modified Fluorophore Attached β-Cyclodextrin Derivatives. *New J. Chem.* **2017**, *41* (23), 14431–14437. https://doi.org/10.1039/C7NJ02968C.
(28) Zhang, Y.; Mollick, S.; Tricarico, M.; Ye, J.; Sherman, D. A.; Tan, J.-C. Turn-On Fluorescence Chemical Sensing through Transformation of Self-Trapped Exciton States at Room Temperature. *ACS Sens.* **2022**, *7* (8), 2338–2344. https://doi.org/10.1021/acssensors.2c00964.
(29) The Huy, B.; Thangadurai, D. T.; Sharipov, M.; Ngoc Nghia, N.; Van Cuong, N.; Lee, Y.-I. Recent Advances in Turn Off-on Fluorescence Sensing Strategies for Sensitive Biochemical Analysis - A Mechanistic Approach. *Microchem. J.* **2022**, *179*, 107511. https://doi.org/10.1016/j.microc.2022.107511.

(30) Yan, C.; Guo, Z.; Chi, W.; Fu, W.; Abedi, S. A. A.; Liu, X.; Tian, H.; Zhu, W.-H. Fluorescence Umpolung Enables Light-up Sensing of N-Acetyltransferases and Nerve Agents. *Nat. Commun.* **2021**, *12* (1), 3869. https://doi.org/10.1038/s41467-021-24187-5.
(31) Verma, A. K.; Noumani, A.; Yadav, A. K.; Solanki, P. R. FRET Based Biosensor: Principle Applications Recent Advances and Challenges. *Diagnostics* **2023**, *13* (8), 1375. https://doi.org/10.3390/diagnostics13081375.
(32) Zhai, D.; Agrawalla, B. K.; Eng, P. S. F.; Lee, S.-C.; Xu, W.; Chang, Y.-T. Development of a Fluorescent Sensor for an Illicit Date Rape Drug – GBL. *Chem. Commun.* **2013**, *49* (55), 6170–6172. https://doi.org/10.1039/C3CC43153C.
(33) Zinke, A.; Ziegler, E. Zur Kenntnis Des Härtungsprozesses von Phenol-Formaldehyd-Harzen, X. Mitteilung. *Berichte Dtsch. Chem. Ges. B Ser.* **1944**, *77* (3–4), 264–272. https://doi.org/10.1002/cber.19440770322.
(34) Gutsche, C. D.; Dhawan, B.; No, K. H.; Muthukrishnan, R. Calixarenes. 4. The Synthesis, Characterization, and Properties of the Calixarenes from p-Tert-Butylphenol. *J. Am. Chem. Soc.* **1981**, *103* (13), 3782–3792. https://doi.org/10.1021/ja00403a028.
(35) Böhmer, V. Calixarenes, Macrocycles with (Almost) Unlimited Possibilities. *Angew. Chem. Int. Ed. Engl.* **1995**, *34* (7), 713–745. https://doi.org/10.1002/anie.199507131.
(36) Iwamoto, K.; Araki, K.; Shinkai, S. Conformations and Structures of Tetra-O-Alkyl-p-Tert-Butylcalix[4]Arenes. How Is the Conformation of Calix[4]Arenes Immobilized? *J. Org. Chem.* **1991**, *56* (16), 4955–4962. https://doi.org/10.1021/jo00016a027.
(37) Fang, P.; Chen, M.; Yin, N.; Zhuang, G.; Chen, T.; Zhang, X.; Du, P. Regulating Supramolecular Interactions in Dimeric Macrocycles. *Chem. Sci.* **2023**, *14* (20), 5425–5430. https://doi.org/10.1039/D3SC00035D.
(38) Kumar, R.; Sharma, A.; Singh, H.; Suating, P.; Kim, H. S.; Sunwoo, K.; Shim, I.; Gibb, B. C.; Kim, J. S. Revisiting Fluorescent Calixarenes: From Molecular Sensors to Smart Materials. *Chem. Rev.* **2019**, *119* (16), 9657–9721. https://doi.org/10.1021/acs.chemrev.8b00605.
(39) Dougherty, D. A. The Cation−π Interaction. *Acc. Chem. Res.* **2013**, *46* (4), 885–893. https://doi.org/10.1021/ar300265y.
(40) Chawla, H. M.; Shukla, R.; Pandey, S. Novel Fluorescein Appended Calix[4]Arenes for Preferential Recognition of Cu2+ Ions. *Tetrahedron Lett.* **2013**, *54* (16), 2063–2066. https://doi.org/10.1016/j.tetlet.2013.02.017.
(41) Maity, D.; Chakraborty, A.; Gunupuru, R.; Paul, P. Calix[4]Arene Based Molecular Sensors with Pyrene as Fluoregenic Unit: Effect of Solvent in Ion Selectivity and Colorimetric Detection of Fluoride. *Inorganica Chim. Acta* **2011**, *372* (1), 126–135. https://doi.org/10.1016/j.ica.2011.01.053.
(42) Zadmard, R.; Akbari-Moghaddam, P.; Darvishi, S. Calix[4]Arene-Based Crab-like Molecular Sensors for Highly Selective Detection of Mercury and Copper Ions. *Supramol. Chem.* **2017**, *29* (1), 17–23. https://doi.org/10.1080/10610278.2016.1161195.
(43) Khan, B.; Shah, M. R.; Ahmed, D.; Rabnawaz, M.; Anis, I.; Afridi, S.; Makhmoor, T.; Tahir, M. N. Synthesis, Characterization and Cu2+ Triggered Selective Fluorescence Quenching of Bis-Calix[4]Arene Tetra-Triazole Macrocycle. *J. Hazard. Mater.* **2016**, *309*, 97–106. https://doi.org/10.1016/j.jhazmat.2016.01.074.
(44) Pathak, R. K.; Dikundwar, A. G.; Row, T. N. G.; Rao, C. P. A Lower Rim Triazole Linked Calix[4]Arene Conjugate as a Fluorescence Switch on Sensor for Zn2+ in Blood Serum Milieu. *Chem. Commun.* **2010**, *46* (24), 4345–4347. https://doi.org/10.1039/C0CC00219D.

(45) Depauw, A.; Kumar, N.; Ha-Thi, M.-H.; Leray, I. Calixarene-Based Fluorescent Sensors for Cesium Cations Containing BODIPY Fluorophore. *J. Phys. Chem. A* **2015**, *119* (23), 6065–6073. https://doi.org/10.1021/jp5120288.
(46) Pathak, R. K.; Dessingou, J.; Hinge, V. K.; Thawari, A. G.; Basu, S. K.; Rao, C. P. Quinoline Driven Fluorescence Turn On 1,3-Bis-Calix[4]Arene Conjugate-Based Receptor to Discriminate Fe3+ from Fe2+. *Anal. Chem.* **2013**, *85* (7), 3707–3714. https://doi.org/10.1021/ac400059w.
(47) Wang, N.-J.; Sun, C.-M.; Chung, W.-S. A Highly Selective Fluorescent Chemosensor for Ag+ Based on Calix[4]Arene with Lower-Rim Proximal Triazolylpyrenes. *Sens. Actuators B Chem.* **2012**, *171–172*, 984–993. https://doi.org/10.1016/j.snb.2012.06.014.
(48) Faye, D.; Lefevre, J.-P.; Delaire, J. A.; Leray, I. A Selective Lead Sensor Based on a Fluorescent Molecular Probe Grafted on a PDMS Microfluidic Chip. *J. Photochem. Photobiol. Chem.* **2012**, *234*, 115–122. https://doi.org/10.1016/j.jphotochem.2012.01.006.
(49) Coleman, A. W.; Jebors, S.; Cecillon, S.; Perret, P.; Garin, D.; Marti-Battle, D.; Moulin, M. Toxicity and Biodistribution of Para-Sulfonato-Calix[4]Arene in Mice. *New J. Chem.* **2008**, *32* (5), 780–782. https://doi.org/10.1039/B718962A.
(50) Paclet, M.-H.; Rousseau, C. F.; Yannick, C.; Morel, F.; Coleman, A. W. An Absence of Non-Specific Immune Response towards Para-Sulphonato-Calix[n]Arenes. *J. Incl. Phenom. Macrocycl. Chem.* **2006**, *55* (3), 353–357. https://doi.org/10.1007/s10847-006-9107-0.
(51) Guo, D.-S.; Liu, Y. Supramolecular Chemistry of P-Sulfonatocalix[n]Arenes and Its Biological Applications. *Acc. Chem. Res.* **2014**, *47* (7), 1925–1934. https://doi.org/10.1021/ar500009g.
(52) Suga, K.; Ohzono, T.; Negishi, M.; Deuchi, K.; Morita, Y. Effect of Various Cations on the Acidity of *p*-Sulfonatocalixarenes. *Supramol. Sci.* **1998**, *5* (1), 9–14. https://doi.org/10.1016/S0968-5677(97)00074-6.
(53) *Parallel Synthesis and Screening of Supramolecular Chemosensors That Achieve Fluorescent Turn-on Detection of Drugs in Saliva | Journal of the American Chemical Society*. https://pubs.acs.org/doi/10.1021/jacs.9b07073 (accessed 2023-08-12).
(54) Zhang, J.; Lan, T.; Lu, Y. Overcoming Major Barriers to Developing Successful Sensors for Practical Applications Using Functional Nucleic Acids. *Annu. Rev. Anal. Chem.* **2022**, *15* (1), 151–171. https://doi.org/10.1146/annurev-anchem-061020-104216.
(55) Peveler, W. J.; Yazdani, M.; Rotello, V. M. Selectivity and Specificity: Pros and Cons in Sensing. *ACS Sens.* **2016**, *1* (11), 1282–1285. https://doi.org/10.1021/acssensors.6b00564.
(56) Tian, J.-H.; Hu, X.-Y.; Hu, Z.-Y.; Tian, H.-W.; Li, J.-J.; Pan, Y.-C.; Li, H.-B.; Guo, D.-S. A Facile Way to Construct Sensor Array Library via Supramolecular Chemistry for Discriminating Complex Systems. *Nat. Commun.* **2022**, *13* (1), 4293. https://doi.org/10.1038/s41467-022-31986-x.
(57) Peveler, W. J.; Algar, W. R. More Than a Light Switch: Engineering Unconventional Fluorescent Configurations for Biological Sensing. *ACS Chem. Biol.* **2018**, *13* (7), 1752–1766. https://doi.org/10.1021/acschembio.7b01022.
(58) Svechkarev, D.; Sadykov, M. R.; Bayles, K. W.; Mohs, A. M. Ratiometric Fluorescent Sensor Array as a Versatile Tool for Bacterial Pathogen Identification and Analysis. *ACS Sens.* **2018**, *3* (3), 700–708. https://doi.org/10.1021/acssensors.8b00025.
(59) Lisa, B.; Jessica, H. Evidence Synthesis - The Opioid Crisis in Canada: A National Perspective. *Health Promot. Chronic Dis. Prev. Can. Res. Policy Pract.* **2018**, *38* (6), 224–233.
(60) Abuse, N. I. on D. *Benzodiazepines and Opioids*. National Institute on Drug Abuse. https://nida.nih.gov/research-topics/opioids/benzodiazepines-opioids (accessed 2023-09-26).
(61) Larocque, A.; Hoffman, R. S. Levamisole in Cocaine: Unexpected News from an Old Acquaintance. *Clin. Toxicol. Phila. Pa* **2012**, *50* (4), 231–241. https://doi.org/10.3109/15563650.2012.665455.

(62) Dasgupta, A. 4 - Combined Alcohol and Drug Abuse: A Potentially Deadly Mix. In *Alcohol, Drugs, Genes and the Clinical Laboratory*; Dasgupta, A., Ed.; Academic Press, 2017; pp 75–88. https://doi.org/10.1016/B978-0-12-805455-0.00004-X.
(63) Koster, R. A.; Alffenaar, J.-W. C.; Greijdanus, B.; VanDerNagel, J. E. L.; Uges, D. R. A. Fast and Highly Selective LC-MS/MS Screening for THC and 16 Other Abused Drugs and Metabolites in Human Hair to Monitor Patients for Drug Abuse. *Ther. Drug Monit.* **2014**, *36* (2), 234. https://doi.org/10.1097/FTD.0b013e3182a377e8.
(64) Komoroski, E. M.; Komoroski, R. A.; Valentine, J. L.; Pearce, J. M.; Kearns, G. L. The Use of Nuclear Magnetic Resonance Spectroscopy in the Detection of Drug Intoxication*. *J. Anal. Toxicol.* **2000**, *24* (3), 180–187. https://doi.org/10.1093/jat/24.3.180.
(65) Andreou, C.; Hoonejani, M. R.; Barmi, M. R.; Moskovits, M.; Meinhart, C. D. Rapid Detection of Drugs of Abuse in Saliva Using Surface Enhanced Raman Spectroscopy and Microfluidics. *ACS Nano* **2013**, *7* (8), 7157–7164. https://doi.org/10.1021/nn402563f.
(66) Li, Z.; Chen, H.; Feng, S.; Liu, K.; Wang, P. Development and Clinical Validation of a Lateral Flow Assay for Urine Fentanyl Screening in the Emergency Department. *Clin. Chem.* **2020**, *66* (2), 324–332. https://doi.org/10.1093/clinchem/hvz023.
(67) Larnder, A.; Saatchi, A.; Borden, S. A.; Moa, B.; Gill, C. G.; Wallace, B.; Hore, D. Variability in the Unregulated Opioid Market in the Context of Extreme Rates of Overdose. *Drug Alcohol Depend.* **2022**, *235*, 109427. https://doi.org/10.1016/j.drugalcdep.2022.109427.
(68) Zhang, X.; Xu, X.; Li, S.; Wang, L.-H.; Zhang, J.; Wang, R. A Systematic Evaluation of the Biocompatibility of Cucurbit[7]Uril in Mice. *Sci. Rep.* **2018**, *8* (1), 8819. https://doi.org/10.1038/s41598-018-27206-6.
(69) Garrido, E.; Pla, L.; Lozano-Torres, B.; El Sayed, S.; Martínez-Máñez, R.; Sancenón, F. Chromogenic and Fluorogenic Probes for the Detection of Illicit Drugs. *ChemistryOpen* **2018**, *7* (5), 401–428. https://doi.org/10.1002/open.201800034.
(70) Kumar, N. M.; Picchetti, P.; Hu, C.; Grimm, L. M.; Biedermann, F. Chemiluminescent Cucurbit[n]Uril-Based Chemosensor for the Detection of Drugs in Biofluids. *ACS Sens.* **2022**, *7* (8), 2312–2319. https://doi.org/10.1021/acssensors.2c00934.
(71) Minami, T.; Esipenko, N. A.; Akdeniz, A.; Zhang, B.; Isaacs, L.; Anzenbacher, P. Jr. Multianalyte Sensing of Addictive Over-the-Counter (OTC) Drugs. *J. Am. Chem. Soc.* **2013**, *135* (40), 15238–15243. https://doi.org/10.1021/ja407722a.
(72) Shcherbakova, E. G.; Zhang, B.; Gozem, S.; Minami, T.; Zavalij, P. Y.; Pushina, M.; Isaacs, L. D.; Anzenbacher, P. Jr. Supramolecular Sensors for Opiates and Their Metabolites. *J. Am. Chem. Soc.* **2017**, *139* (42), 14954–14960. https://doi.org/10.1021/jacs.7b06371.
(73) Zhai, D.; Tan, Y. Q. E.; Xu, W.; Chang, Y.-T. Development of a Fluorescent Sensor for Illicit Date Rape Drug GHB. *Chem. Commun.* **2014**, *50* (22), 2904–2906. https://doi.org/10.1039/C3CC49603A.
(74) Baumes, L. A.; Buaki Sogo, M.; Montes-Navajas, P.; Corma, A.; Garcia, H. A Colorimetric Sensor Array for the Detection of the Date-Rape Drug γ-Hydroxybutyric Acid (GHB): A Supramolecular Approach. *Chem. – Eur. J.* **2010**, *16* (15), 4489–4495. https://doi.org/10.1002/chem.200903127.
(75) Beatty, M. A.; Borges-González, J.; Sinclair, N. J.; Pye, A. T.; Hof, F. Analyte-Driven Disassembly and Turn-On Fluorescent Sensing in Competitive Biological Media. *J. Am. Chem. Soc.* **2018**, *140* (10), 3500–3504. https://doi.org/10.1021/jacs.7b13298.
(76) Liu, Y.; Li, C.-J.; Guo, D.-S.; Pan, Z.-H.; Li, Z. A Comparative Study of Complexation of β-Cyclodextrin, Calix[4]Arenesulfonate and Cucurbit[7]Uril with Dye Guests: Fluorescence

Behavior and Binding Ability. *Supramol. Chem.* **2007**, *19* (7), 517–523. https://doi.org/10.1080/10610270601145444.
(77) Gallo, C.; Thomas, S. S.; Selinger, A. J.; Hof, F.; Bohne, C. Mechanism of a Disassembly-Driven Sensing System Studied by Stopped-Flow Kinetics. *J. Org. Chem.* **2021**, *86* (15), 10782–10787. https://doi.org/10.1021/acs.joc.1c00959.
(78) Morley, J. O.; Morley, R. M.; Docherty, R.; Charlton, M. H. Fundamental Studies on Brooker's Merocyanine. *J. Am. Chem. Soc.* **1997**, *119* (42), 10192–10202. https://doi.org/10.1021/ja971477m.
(79) Lee, Y.-G.; Choi, J.-H. Synthesis of Some Fluorescent Dyes Based on Stilbene Derivatives with Various Substituents and Their Effects on the Absorption Maxima. *Appl. Sci.* **2023**, *13* (9), 5543. https://doi.org/10.3390/app13095543.
(80) Zhang, Y.; Huang, J.; Kong, L.; Tian, Y.; Yang, J. Two Novel AIEE-Active Imidazole/ α-Cyanostilbene Derivatives: Photophysical Properties, Reversible Fluorescence Switching, and Detection of Explosives. *CrystEngComm* **2018**, *20* (9), 1237–1244. https://doi.org/10.1039/C7CE01842H.
(81) Jing, S.; Zheng, C.; Pu, S.; Fan, C.; Liu, G. A Highly Selective Ratiometric Fluorescent Chemosensor for Hg2+ Based on a New Diarylethene with a Stilbene-Linked Terpyridine Unit. *Dyes Pigments* **2014**, *107*, 38–44. https://doi.org/10.1016/j.dyepig.2014.03.023.
(82) Hu, H.; Zhu, M.; Meng, X.; Zhang, Z.; Wei, K.; Guo, Q. Optical Switching and Fluorescence Modulation Properties of Photochromic Dithienylethene Derivatives. *J. Photochem. Photobiol. Chem.* **2007**, *189* (2), 307–313. https://doi.org/10.1016/j.jphotochem.2007.02.020.
(83) Suh, E. H.; Liu, Y.; Connelly, S.; Genereux, J. C.; Wilson, I. A.; Kelly, J. W. Stilbene Vinyl Sulfonamides as Fluorogenic Sensors of and Traceless Covalent Kinetic Stabilizers of Transthyretin That Prevent Amyloidogenesis. *J. Am. Chem. Soc.* **2013**, *135* (47), 17869–17880. https://doi.org/10.1021/ja408230k.
(84) Rafique, S.; Irshad, H.; Majeed, S.; Khadija; Rubab, R.; Imran, M.; Khan, A. M.; Shahzad, S. A. AIEE Active Stilbene Based Fluorescent Sensor with Red-Shifted Emission for Vapor Phase Detection of Nitrobenzene and Moisture Sensing. *J. Photochem. Photobiol. Chem.* **2023**, *437*, 114459. https://doi.org/10.1016/j.jphotochem.2022.114459.
(85) Lentin, I.; Gorbunov, A.; Bezzubov, S.; Nosova, V.; Cheshkov, D.; Kovalev, V.; Vatsouro, I. Shrinkable/Stretchable Bis(Calix[4]Arenes) Comprising Photoreactive Azobenzene or Stilbene Linkers. *Org. Chem. Front.* **2023**, *10* (6), 1470–1484. https://doi.org/10.1039/D2QO01986H.
(86) Lee, J. H.; Jung, S. H.; Lee, S. S.; Kwon, K.-Y.; Sakurai, K.; Jaworski, J.; Jung, J. H. Ultraviolet Patterned Calixarene-Derived Supramolecular Gels and Films with Spatially Resolved Mechanical and Fluorescent Properties. *ACS Nano* **2017**, *11* (4), 4155–4164. https://doi.org/10.1021/acsnano.7b00997.
(87) Jo, J.; Lee, D. Turn-On Fluorescence Detection of Cyanide in Water: Activation of Latent Fluorophores through Remote Hydrogen Bonds That Mimic Peptide β-Turn Motif. *J. Am. Chem. Soc.* **2009**, *131* (44), 16283–16291. https://doi.org/10.1021/ja907056m.
(88) Saltiel, J.; Kumar, V. K. R. Photophysics of Diphenylacetylene: Light from the "Dark State." *J. Phys. Chem. A* **2012**, *116* (43), 10548–10558. https://doi.org/10.1021/jp307896c.
(89) Szyszkowska, M.; Bylińska, I.; Wiczk, W. Influence of an Electron-Acceptor Substituent Type on the Photophysical Properties of Unsymmetrically Substituted Diphenylacetylene. *J. Photochem. Photobiol. Chem.* **2016**, *326*, 76–88. https://doi.org/10.1016/j.jphotochem.2016.03.023.
(90) Krämer, M.; Bunz, U. H. F.; Dreuw, A. Comprehensive Look at the Photochemistry of Tolane. *J. Phys. Chem. A* **2017**, *121* (5), 946–953. https://doi.org/10.1021/acs.jpca.6b09596.

(91) Szyszkowska, M.; Bylińska, I.; Wiczk, W. Variable-Temperature Absorption and Emission Properties of 1,2-Diphenylacetylene and 1,4-Diphenylbuta-1,3-Diyne Derivatives. *J. Photochem. Photobiol. Chem.* **2017**, *348*, 47–56. https://doi.org/10.1016/j.jphotochem.2017.08.012.
(92) Jo, J.; Lee, D. Turn-On Fluorescence Detection of Cyanide in Water: Activation of Latent Fluorophores through Remote Hydrogen Bonds That Mimic Peptide β-Turn Motif. *J. Am. Chem. Soc.* **2009**, *131* (44), 16283–16291. https://doi.org/10.1021/ja907056m.
(93) Ahuja, B. B.; Vigalok, A. Fluorescent Calixarene Scaffolds for NO Detection in Protic Media. *Angew. Chem. Int. Ed.* **2019**, *58* (9), 2774–2778. https://doi.org/10.1002/anie.201813589.
(94) Liang, B.; Dai, M.; Chen, J.; Yang, Z. Copper-Free Sonogashira Coupling Reaction with PdCl2 in Water under Aerobic Conditions. *J. Org. Chem.* **2005**, *70* (1), 391–393. https://doi.org/10.1021/jo048599z.
(95) Gelman, D.; Buchwald, S. L. Efficient Palladium-Catalyzed Coupling of Aryl Chlorides and Tosylates with Terminal Alkynes: Use of a Copper Cocatalyst Inhibits the Reaction. *Angew. Chem. Int. Ed.* **2003**, *42* (48), 5993–5996. https://doi.org/10.1002/anie.200353015.
(96) Al-Saraierh, H.; Miller, D. O.; Georghiou, P. E. Narrow-Rim Functionalization of Calix[4]Arenes via Sonogashira Coupling Reactions. *J. Org. Chem.* **2005**, *70* (21), 8273–8280. https://doi.org/10.1021/jo050488s.
(97) Ahuja, B. B.; Vigalok, A. Fluorescent Calixarene Scaffolds for NO Detection in Protic Media. *Angew. Chem. Int. Ed.* **2019**, *58* (9), 2774–2778. https://doi.org/10.1002/anie.201813589.
(98) Fordham, J. M.; Kollmus, P.; Cavegn, M.; Schneider, R.; Santagostino, M. A "Pool and Split" Approach to the Optimization of Challenging Pd-Catalyzed C–N Cross-Coupling Reactions. *J. Org. Chem.* **2022**, *87* (6), 4400–4414. https://doi.org/10.1021/acs.joc.2c00104.
(99) Rosania, G. R.; Lee, J. W.; Ding, L.; Yoon, H.-S.; Chang, Y.-T. Combinatorial Approach to Organelle-Targeted Fluorescent Library Based on the Styryl Scaffold. *J. Am. Chem. Soc.* **2003**, *125* (5), 1130–1131. https://doi.org/10.1021/ja027587x.
(100) Sharma, V. S.; Vishwakarma, V. K.; Shrivastav, P. S.; Ammathnadu Sudhakar, A.; Sharma, A. S.; Shah, P. A. Calixarene Functionalized Supramolecular Liquid Crystals and Their Diverse Applications. *ACS Omega* **2022**, *7* (50), 45752–45796. https://doi.org/10.1021/acsomega.2c04699.
(101) Daze, K. D.; Ma, M. C. F.; Pineux, F.; Hof, F. Synthesis of New Trisulfonated Calix[4]Arenes Functionalized at the Upper Rim, and Their Complexation with the Trimethyllysine Epigenetic Mark. *Org. Lett.* **2012**, *14* (6), 1512–1515. https://doi.org/10.1021/ol300243b.
(102) Shaurya, A. Design, Synthesis and Evaluation of Calix[4]Arene Based Enrichment Agents for N-Methyl Proteomics. Thesis, 2020. https://dspace.library.uvic.ca/handle/1828/12526 (accessed 2023-10-03).
(103) Doolan, A. M.; Rennie, M. L.; Crowley, P. B. Protein Recognition by Functionalized Sulfonatocalix[4]Arenes. *Chem. – Eur. J.* **2018**, *24* (4), 984–991. https://doi.org/10.1002/chem.201704931.
(104) Hof, F.; Minaker, S.; Daze, K.; Tabet, S.; Ma, M. Method and Array for Identifying Histone-Code-Related Analytes. US9879300B2, January 30, 2018. https://patents.google.com/patent/US9879300B2/zh (accessed 2023-11-07).
(105) Gershon, H.; Gershon, M.; Clarke, D. Effect of N-Halosucinimides on 5-, 7- and 5,7-8-Quinolinol Sulfonic Acids / Herman Gershon, Muriel Gershon, and Donald D. Clark Harding Laboratory, the New York Botanical Garde, Fordham University, Bronx, New York 10458, USA. *Chem. Fac. Publ.* **2007**.

(106) Ogoshi, T.; Umeda, K.; Yamagishi, T.; Nakamoto, Y. Through-Space π-Delocalized Pillar[5]Arene. *Chem. Commun.* **2009**, No. 32, 4874–4876. https://doi.org/10.1039/B907894K.
(107) Bruneau, A.; Roche, M.; Alami, M.; Messaoudi, S. 2-Aminobiphenyl Palladacycles: The "Most Powerful" Precatalysts in C–C and C–Heteroatom Cross-Couplings. *ACS Catal.* **2015**, *5* (2), 1386–1396. https://doi.org/10.1021/cs502011x.
(108) Liang, S.; Hammond, G. B.; Xu, B. Efficient Hydration of Alkynes through Acid-Assisted Brønsted Acid Catalysis. *Chem. Commun.* **2014**, *51* (5), 903–906. https://doi.org/10.1039/C4CC08938C.
(109) Guan, K.; Palmer, D. C. Effects of Trifluoroacetic Acid Concentrations in Mobile Phases on HPLC Retention of Zwitterionic and Weakly Basic Triazole Derivatives. *J. Liq. Chromatogr. Relat. Technol.* **2006**, *29* (3), 415–430. https://doi.org/10.1080/10826070500452077.
(110) Chen, Y.; Mehok, A. R.; Mant, C. T.; Hodges, R. S. Optimum Concentration of Trifluoroacetic Acid for Reversed-Phase Liquid Chromatography of Peptides Revisited. *J. Chromatogr. A* **2004**, *1043* (1), 9–18. https://doi.org/10.1016/j.chroma.2004.03.070.
(111) Iwasaki, R.; Tanaka, E.; Ichihashi, T.; Idemoto, Y.; Endo, K. Semireduction of Alkynes Using Formic Acid with Reusable Pd-Catalysts. *J. Org. Chem.* **2018**, *83* (21), 13574–13579. https://doi.org/10.1021/acs.joc.8b02169.
(112) Li, J.; Hua, R.; Liu, T. Highly Chemo- and Stereoselective Palladium-Catalyzed Transfer Semihydrogenation of Internal Alkynes Affording Cis-Alkenes. *J. Org. Chem.* **2010**, *75* (9), 2966–2970. https://doi.org/10.1021/jo100247a.
(113) Shen, R.; Chen, T.; Zhao, Y.; Qiu, R.; Zhou, Y.; Yin, S.; Wang, X.; Goto, M.; Han, L.-B. Facile Regio- and Stereoselective Hydrometalation of Alkynes with a Combination of Carboxylic Acids and Group 10 Transition Metal Complexes: Selective Hydrogenation of Alkynes with Formic Acid. *J. Am. Chem. Soc.* **2011**, *133* (42), 17037–17044. https://doi.org/10.1021/ja2069246.
(114) Gallo, C.; Thomas, S. S.; Selinger, A. J.; Hof, F.; Bohne, C. Mechanism of a Disassembly-Driven Sensing System Studied by Stopped-Flow Kinetics. *J. Org. Chem.* **2021**, *86* (15), 10782–10787. https://doi.org/10.1021/acs.joc.1c00959.
(115) Nickley, J.; Pesce, A. J.; Krock, K. A Sensitive Assay for Urinary Cocaine Metabolite Benzoylecgonine Shows More Positive Results and Longer Half-lives than Those Using Traditional Cut-offs. *Drug Test. Anal.* **2017**, *9* (8), 1214–1216. https://doi.org/10.1002/dta.2153.
(116) Gozdzialski, L.; Wallace, B.; Noda, I.; Hore, D. Exploring the Use of Infrared Absorption Spectroscopy and Two-Trace Two-Dimensional Correlation Analysis for the Resolution of Multi-Component Drug Mixtures. *Spectrochim. Acta. A. Mol. Biomol. Spectrosc.* **2022**, *282*, 121684. https://doi.org/10.1016/j.saa.2022.121684.
(117) You, L.; Zha, D.; Anslyn, E. V. Recent Advances in Supramolecular Analytical Chemistry Using Optical Sensing. *Chem. Rev.* **2015**, *115* (15), 7840–7892. https://doi.org/10.1021/cr5005524.
(118) *Methods for the determination of limit of detection and limit of ...: Ingenta Connect*. https://www.ingentaconnect.com/content/doaj/09759212/2011/00000002/00000001/art00005 (accessed 2023-10-13).
(119) Jolliffe, I. T.; Cadima, J. Principal Component Analysis: A Review and Recent Developments. *Philos. Trans. R. Soc. Math. Phys. Eng. Sci.* **2016**, *374* (2065), 20150202. https://doi.org/10.1098/rsta.2015.0202.
(120) Malow, R. M.; West, J. A.; Corrigan, S. A.; Pena, J. M.; Criss Lott, W. Cocaine and Speedball Users: Differences in Psychopathology. *J. Subst. Abuse Treat.* **1992**, *9* (4), 287–291. https://doi.org/10.1016/0740-5472(92)90021-F.

(121) Bayer, P.; Matena, A.; Beuck, C. NMR Spectroscopy of Supramolecular Chemistry on Protein Surfaces. *Beilstein J. Org. Chem.* **2020**, *16*, 2505–2522. https://doi.org/10.3762/bjoc.16.203.

(122) Nitsche, C.; Otting, G. NMR Studies of Ligand Binding. *Curr. Opin. Struct. Biol.* **2018**, *48*, 16–22. https://doi.org/10.1016/j.sbi.2017.09.001.

(123) Vinodh, M.; Alshammari, S. G.; Al-Azemi, T. F. Single-Crystal X-Ray Diffraction Analysis of Inclusion Complexes of Triflate-Functionalized Pillar[5]Arenes with 1,4-Dibromobutane and n-Hexane Guests. *Crystals* **2023**, *13* (4), 593. https://doi.org/10.3390/cryst13040593.

(124) Garnett, G. A. E.; Daze, K. D.; Diaz, J. A. P.; Fagen, N.; Shaurya, A.; Ma, M. C. F.; Collins, M. S.; Johnson, D. W.; Zakharov, L. N.; Hof, F. Attraction by Repulsion: Compounds with like Charges Undergo Self-Assembly in Water That Improves in High Salt and Persists in Real Biological Fluids. *Chem. Commun.* **2016**, *52* (13), 2768–2771. https://doi.org/10.1039/C5CC10527G.

(125) Shinkai, S.; Araki, K.; Matsuda, T.; Manabe, O. NMR Determination of Association Constants for Aqueous Calixarene Complexes and Guest Template Effects on the Conformational Freedom. *Bull. Chem. Soc. Jpn.* **1989**, *62* (12), 3856–3862. https://doi.org/10.1246/bcsj.62.3856.

(126) Warmerdam, Z.; Kamba, B.; Shaurya, A.; Sun, X.; Maguire, M.; Hof, F. Calix[4]Arene Sulfonate Hosts Selectively Modified on the Upper Rim: A Study of Nicotine Binding Strength and Geometry. ChemRxiv January 8, 2021. https://doi.org/10.26434/chemrxiv.13542923.v1.

(127) Ede, J. A.; Cragg, P. J.; Sambrook, M. R. Comparison of Binding Affinities of Water-Soluble Calixarenes with the Organophosphorus Nerve Agent Soman (GD) and Commonly-Used Nerve Agent Simulants. *Mol. J. Synth. Chem. Nat. Prod. Chem.* **2018**, *23* (1), 207. https://doi.org/10.3390/molecules23010207.

(128) Groves, P. Diffusion Ordered Spectroscopy (DOSY) as Applied to Polymers. *Polym. Chem.* **2017**, *8* (44), 6700–6708. https://doi.org/10.1039/C7PY01577A.

(129) Atkins, P. W. (Peter W.; De Paula, J. *Atkins' Physical Chemistry*; New York : W.H. Freeman, 2006.

(130) Hajmalek, M.; Khalili, M. S.; Zare, K.; Zabihi, O. Determination of the Acid Dissociation Constants of the P-Sulphonato-Calix[4]Arene. *J. Nanoanalysis* **2014**, *1* (1), 47–51. https://doi.org/10.22034/jna.2014.01.007.

(131) Bain, A. D. Chemical Exchange in NMR. *Prog. Nucl. Magn. Reson. Spectrosc.* **2003**, *43* (3), 63–103. https://doi.org/10.1016/j.pnmrs.2003.08.001.

(132) Sedaghat Doost, A.; Akbari, M.; Stevens, C. V.; Setiowati, A. D.; Van der Meeren, P. A Review on Nuclear Overhauser Enhancement (NOE) and Rotating-Frame Overhauser Effect (ROE) NMR Techniques in Food Science: Basic Principles and Applications. *Trends Food Sci. Technol.* **2019**, *86*, 16–24. https://doi.org/10.1016/j.tifs.2019.02.001.

(133) Manu, V. S.; Olivieri, C.; Veglia, G. Water Irradiation Devoid Pulses Enhance the Sensitivity of 1H,1H Nuclear Overhauser Effects. *J. Biomol. NMR* **2023**, *77* (1), 1–14. https://doi.org/10.1007/s10858-022-00407-y.

(134) Groves, P. Diffusion Ordered Spectroscopy (DOSY) as Applied to Polymers. *Polym. Chem.* **2017**, *8* (44), 6700–6708. https://doi.org/10.1039/C7PY01577A.

(135) Zhegalova, N. G.; He, S.; Zhou, H.; Kim, D. M.; Berezin, M. Y. Minimization of Self-Quenching Fluorescence on Dyes Conjugated to Biomolecules with Multiple Labeling Sites via Asymmetrically Charged NIR Fluorophores. *Contrast Media Mol. Imaging* **2014**, *9* (5), 355–362. https://doi.org/10.1002/cmmi.1585.

(136) Lewis, F. D.; Crompton, E. M. Hydroxystilbene Isomer-Specific Photoisomerization versus Proton Transfer. *J. Am. Chem. Soc.* **2003**, *125* (14), 4044–4045. https://doi.org/10.1021/ja029873e.

(137) Mathew, R.; Kayal, S.; Yapamanu, A. L. Excited State Structural Dynamics of 4-Cyano-4'-Hydroxystilbene: Deciphering the Signatures of Proton-Coupled Electron Transfer Using Ultrafast Raman Loss Spectroscopy. *Phys. Chem. Chem. Phys.* **2019**, *21* (40), 22409–22419. https://doi.org/10.1039/C9CP02923K.

(138) Bilal, S. M.; Kayal, S.; Sanju, K. S.; Adithya Lakshmanna, Y. Femtosecond Time-Resolved Raman Spectroscopy Reveals Structural Evidence for Meta Effect in Stilbenols. *J. Phys. Chem. A* **2018**, *122* (19), 4601–4608. https://doi.org/10.1021/acs.jpca.7b12339.

(139) Lewis, F. D.; Sinks, L. E.; Weigel, W.; Sajimon, M. C.; Crompton, E. M. Ultrafast Proton Transfer Dynamics of Hydroxystilbene Photoacids. *J. Phys. Chem. A* **2005**, *109* (11), 2443–2451. https://doi.org/10.1021/jp044942s.

(140) *1D NOESY made easy | NMR Facility - Chemistry Department*. https://chemnmrlab.uchicago.edu/2021/03/10/1d-noe_1/ (accessed 2024-01-25).